



National Library
of Canada

Acquisitions and
Bibliographic Services Branch

395 Wellington Street
Ottawa, Ontario
K1A 0N4

Bibliothèque nationale
du Canada

Direction des acquisitions et
des services bibliographiques

395, rue Wellington
Ottawa (Ontario)
K1A 0N4

Your file - Votre référence

Our file - Notre référence

NOTICE

The quality of this microform is heavily dependent upon the quality of the original thesis submitted for microfilming. Every effort has been made to ensure the highest quality of reproduction possible.

If pages are missing, contact the university which granted the degree.

Some pages may have indistinct print especially if the original pages were typed with a poor typewriter ribbon or if the university sent us an inferior photocopy.

Reproduction in full or in part of this microform is governed by the Canadian Copyright Act, R.S.C. 1970, c. C-30, and subsequent amendments.

AVIS

La qualité de cette microforme dépend grandement de la qualité de la thèse soumise au microfilmage. Nous avons tout fait pour assurer une qualité supérieure de reproduction.

S'il manque des pages, veuillez communiquer avec l'université qui a conféré le grade.

La qualité d'impression de certaines pages peut laisser à désirer, surtout si les pages originales ont été dactylographiées à l'aide d'un ruban usé ou si l'université nous a fait parvenir une photocopie de qualité inférieure.

La reproduction, même partielle, de cette microforme est soumise à la Loi canadienne sur le droit d'auteur, SRC 1970, c. C-30, et ses amendements subséquents.

Canada

UNIVERSITY OF ALBERTA

MODELLING THE MAGNETIC EFFECTS OF
DISTRIBUTED MAGNETOSPHERIC CURRENTS

BY



ERIC DONOVAN

A thesis submitted to the Faculty of Graduate Studies and Research in partial fulfillment of the requirements for the degree of Doctor of Philosophy in Physics.

Department of Physics

Edmonton Alberta

Fall 1993



National Library
of Canada

Acquisitions and
Bibliographic Services Branch

395 Wellington Street
Ottawa, Ontario
K1A 0N4

Bibliothèque nationale
du Canada

Direction des acquisitions et
des services bibliographiques

395, rue Wellington
Ottawa (Ontario)
K1A 0N4

Your file - Votre référence

Our file - Notre référence

The author has granted an irrevocable non-exclusive licence allowing the National Library of Canada to reproduce, loan, distribute or sell copies of his/her thesis by any means and in any form or format, making this thesis available to interested persons.

L'auteur a accordé une licence irrévocable et non exclusive permettant à la Bibliothèque nationale du Canada de reproduire, prêter, distribuer ou vendre des copies de sa thèse de quelque manière et sous quelque forme que ce soit pour mettre des exemplaires de cette thèse à la disposition des personnes intéressées.

The author retains ownership of the copyright in his/her thesis. Neither the thesis nor substantial extracts from it may be printed or otherwise reproduced without his/her permission.

L'auteur conserve la propriété du droit d'auteur qui protège sa thèse. Ni la thèse ni des extraits substantiels de celle-ci ne doivent être imprimés ou autrement reproduits sans son autorisation.

ISBN 0-315-88203-4

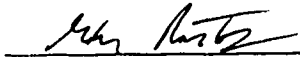
Canada

June 10, 1993

To Whom It May Concern

This letter is to give permission to **Mr. Eric Frank Donovan** to use the Figure presented in Figure 1 of his thesis, which I published in

Rostoker, G., Magnetospheric substorms as a signature of the solar-terrestrial interaction, in *Ionospheric Structure and Variability on a Global Scale and Interactions With Atmosphere and Magnetosphere*, ed. by L. Bossy and R.W. Schunk, p.2 , AGARD-CP-441, Neury Sur Seine, France, 1989.

A handwritten signature in black ink, appearing to read "Gordon Rostoker", written over a horizontal line.

Gordon Rostoker

JGR—Journal of Geophysical Research

The editors of JGR welcome original scientific contributions on the physics and chemistry of the earth, its environment, and the solar system. Papers on space physics, aeronomy, planetary atmospheres, and exterior planetary magnetism are published monthly in the blue-covered JGR. Four copies of the typescript should be submitted to

George L. Siscoe, JGR
Department of Atmospheric Sciences
UCLA
Los Angeles, California 90024
(213) 825-9378

Editor's Assistant: Ted Feliciello

Papers on the physics and chemistry of the solid earth, planetology, geodesy, geothermics, and material's science related to stated geophysical problems are published monthly in the red-covered JGR; papers should be submitted to Thomas J. Ahrens, California Institute of Technology. Papers on the physics and chemistry of the atmosphere, the hydrosphere, the air-sea interface, the oceans, and the ocean basins are published monthly in the green-covered JGR; papers should be submitted to Gabriel Csanady, WHOI. Information for contributors may be obtained from the AGU publications office.

Editor

George L. Siscoe (1977-1981)

Associate Editors

Space Physics

M. Ashour-Abdalla	F. W. Perkins, Jr.
James L. Burch	T. A. Potemra
W. C. Feldman	M. H. Rees
C. K. Goertz	Arthur D. Richmond
T. W. Hill	Raymond G. Roble
Thomas E. Holzer	Gordon Rostoker
Marcia Neugebauer	Robert W. Schunk
John F. Noxon	I. A. Stewart
Sidney L. Ossakow	Richard S. Stolarski
Chung Park	Darrell F. Strobel

Editorial Staff

Publications Manager: Judy C. Holoviak.
Editorial Services Supervisor: Mary J. Scroggins.
Production Supervisor: Vicki Sullivan. *Copy Editors:* P. Bell, E. Garrison, P. Knox, L. LaMacchia, T. Thomas, M. Thor, and S. Whelan. *Editorial Proofreader:* A. Olinger. *Production Staff:* M. Dulin.

AGU Office. Address all correspondence to the appropriate department at the American Geophysical Union, 2000 Florida Avenue, N.W., Washington, D.C. 20009. Phone (202) 462-6903.

Publication Charge Policy. The page charge income received for JGR helps support rapid publication, allows more pages per volume, and makes possible the low subscription rates which result in a circulation of over 5000 issues, about half going to libraries, where wider distribution is affordable.

For full typeset articles (regardless of length) the publication charge is \$90 per page for papers on which copyright is transferred to AGU. For summaries (for which the full paper is placed on microfiche) there is no publication charge for the first two pages but a charge of \$120 for each additional page plus a \$15 deposit charge for each 96 pages placed on microfiche. When the page charge is honored, 100 reprints are supplied without further charge.

For the blue-covered and red-covered sections there is no page charge for papers for which authors have prepared final typewritten copy according to AGU specifications and have transferred copyright to AGU. The author's institution is encouraged to purchase reprints of these papers; the income from reprints adds to the support received from page charges.

Foldouts and color figures may be published if they are necessary to the proper presentation of material. The additional cost for these services must be borne by the author. Check with the AGU reprint department for current prices.

Microform Publication. Authors are encouraged to submit concise papers. To reduce publication expense and still allow for complete reporting of work, AGU provides a microfiche deposit service to its authors. In addition to original papers for which summaries have been published in the journal, materials well suited to micropublication include lengthy mathematical derivations, tables of data, computer printouts, and appendices. Photographs with a wide tonal range are not suitable for microfiche. Detailed information on preparing copy for microfiche is available from the AGU editorial office. Additional material is incorporated in the microform editions of the journal, and therefore is a part of the archived literature. Material published in microform can be ordered by individuals at a nominal cost from the AGU business office.

Subscriptions. AGU members may subscribe to JGR in printed or microfiche editions for their personal use at the regular annual rate of \$30 for the blue-covered section, \$20 for the red-covered section, and \$15 for the green-covered section. Student may subscribe at reduced rates. Subscriptions for libraries, reading rooms, and other multiple-use institutions are available at special rates. Contact AGU for details. Single issues are \$15 each.

Changes of Address and Claims. Send address changes to AGU circulation department; allow 5 weeks advance notice. Claims for missing issues will not be honored because of insufficient notice of address change. Loss in mail unless claimed within 90 days for U.S.A. and 150 days for other countries from last day of month of publication, or such reasons as 'missing from files.'

Copyright. Permission is granted to use short quotations from this journal and figures and tables for publication in scientific books and journals. We request that the source be cited appropriately. The appearance of the code at the bottom of the first page of an article in this journal indicates the copyright owner's consent that copies of the article may be made for personal or internal use or for the personal or internal use of specific clients. This consent is given on the condition that the copier pay the stated per copy fee through the Copyright Clearance Center, Inc. for copying beyond that permitted by Section 107 or 108 of the U.S. Copyright Law. This consent does not extend to other kinds of copying, such as copying for general distribution, for advertising or promotional purposes, for creating new collective works, or for resale. Articles published prior to 1978 are subject to the same provisions. The reproduction of multiple copies and the use of articles or extracts for commercial purposes require the consent of the author and specific permission from AGU.

The blue-covered section, JGR—Space Physics (USPS 132170), is published monthly by the American Geophysical Union 2000 Florida Avenue, N.W. Washington, D. C. 20009.

Second class postage paid at Washington, D. C. and additional offices.

Copyright © 1979 by the American Geophysical Union.

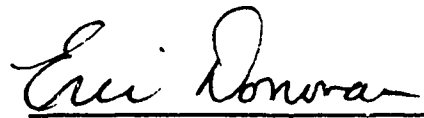
University of Alberta

Release Form

Name of Author: Eric Donovan
Title of Thesis: Modelling the Magnetic Effects of Distributed
Magnetospheric Currents
Degree: Doctor of Philosophy
Year This Degree Granted: 1993

Permission is hereby granted to the University of Alberta to reproduce single copies of this thesis and to lend or sell such copies for private, scholarly or scientific research purposes only.

The author reserves all other publication and other rights in association with the copyright in the thesis, and except as hereinbefore provided neither the thesis nor any substantial proportion thereof may be printed or otherwise reproduced in any material form whatever without the author's written permission.

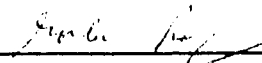


Eric Donovan
Department of Physics
University of Alberta
Edmonton, Alberta
T6G 2J1
Canada

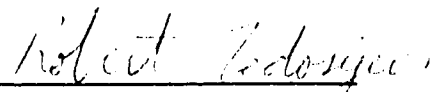
10 June 1993

UNIVERSITY OF ALBERTA
FACULTY OF GRADUATE STUDIES AND RESEARCH

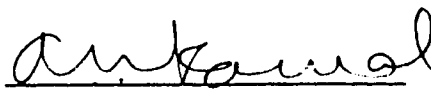
The undersigned certify that they have read, and recommend to the Faculty of Graduate Studies and Research for acceptance, a thesis entitled "Modelling the Magnetic Effects of Distributed Magnetospheric Currents" submitted by Eric Donovan in partial fulfillment of the requirements for the degree of Doctor of Philosophy in Physics.




G. Rostoker, Supervisor




R. Fedosejevs



A. N. Kamal

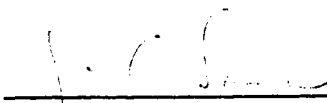


A. T. Y. Lui



W. Rozmus

June 7, 1993



J. C. Samson

Abstract

This dissertation deals with the testing, development and use of global models of the magnetospheric magnetic field. I applied novel tests to existing magnetic field models and identified shortcomings of those models. These results were my motivation for developing a new technique for the representation of the magnetic effects of distributed magnetospheric currents.

I perform tests on the Tsyganenko 1987 and 1989 (T87 and T89) models. I use an ionospheric electric potential model, in conjunction with the T87 and T89 models, to infer magnetospheric plasma convection patterns. I assess the validity of magnetic field mappings obtained using the Tsyganenko models by comparing these inferred convection patterns with *in situ* measurements of plasma bulk flow velocity. I also examine the topology of magnetic field lines traced using the T89 magnetic field model. As well, I compare expected magnetospheric currents with the Tsyganenko model currents. One important conclusion I reach is that the T87 and T89 magnetic field models do not adequately represent the effects of the large scale field-aligned currents or the cross-tail current, including closure on or near the magnetopause.

I model the magnetic effects of the field-aligned and transverse currents by summing the magnetic fields due to a large number of cylindrical current elements of finite length and radius. Using the T87 model, modified to include the effects of field-aligned currents, I show that the equatorial crossing points of central plasma sheet field lines stretching 15 or more Earth radii down the magnetotail can be shifted more than 10 Earth radii away from the noon-midnight meridian and that this result depends on how the field-aligned current circuit is closed in the magnetosphere. Using the magnetic fields due to model Chapman-Ferraro, ring, and neutral sheet currents, I develop a new magnetic field model for the nightside magnetosphere. The model field is fit to average values of the lobe and neutral sheet magnetic field strengths.

Acknowledgements

I would like to thank Gordon Rostoker for his friendship, support and generosity: Gordon's kindness and enthusiasm are an inspiration to me. From him, I learned a great deal about how science is done, about space science in general and how to present my work. John Samson has always been encouraging and persistently asked challenging and relevant questions. This prepared me to deal competently with questions at conferences and from referees. I am also grateful to John for taking the time to set up an enlightening course on wave propagation in nonuniform media.

I have benefited both personally and professionally from the lively interaction with everyone in the space physics group. Hamid Al Nashi, Karen Apps, Anna Belehaki, Sherwood Botsford, Jo-Anne Brown, Sarah Derr, Jeff Candy, Martin Connors, Frances Fenrich, Przemek Frycz, Abdelhaq Hamza, Barry Harrold, Brian Jackel, Steven Kidd, Terry Kolber, William Liu, Sandy MacAulay, John Manuel, Robert Rankin, Wojciech Rozmus, Susan Skone, Beth Tooley, Chris Wei and Baolin Xu all helped to make this a wonderful place for me to be.

I am also indebted to several members of the space physics group for the following reasons. Brian Jackel provided me with a coded version of the T89 model and helped with the development of my model of the magnetic effects of field-aligned currents. Martin Connors produced the Viking images in figures 57 and 58. Sherwood Botsford and Martin dealt with hundreds of computer problems for me. John Manuel provided the Mathematica routines that I used to produce the two dimensional vector plots and three dimensional plots of curves in this thesis. John and Martin discussed my work with me for countless hours. Susan Skone provided the footpoints that I used for the mappings illustrated in figures 59-62.

As well, Susan produced the plots shown in these figures. Karen Apps helped with some of the intricacies of IDL. On two occasions, Beth Tooley prepared camera ready copy and figures when I was short of time. Sandy MacAulay gave me useful hints on fitting functions to data. Abdelhaq Hamza and Sandy spent time during the last few months discussing MHD with me, which was great preparation for my defense. Finally, when I was rapidly losing perspective a few days before my defense, Przemek Frycz dragged me away from my books and taught me how to play table tennis.

I am grateful to David Stern for his interest in my work and taking the time on many occasions to discuss magnetic field modelling in general and my work in particular. Carl Pfitzer provided me with a useable model of the magnetic effects of the Chapman-Ferraro currents. I appreciate the encouraging and thought-provoking comments of my external examiner, Anthony Lui.

Eric Sigveldson, Roger Millard, Mary Hay, Gordon Hay, Steven Spear, Rob Baker and Loretta Salé helped me come to grips with some fluid dynamics problems. Our river expeditions have been an important part of my life in Alberta and were always a great way to refresh my mind.

My mother, Mary Thornbury, has been supportive and encouraging throughout my student life. I am especially grateful to her and her husband, Jack Livesey, for providing me with a great place to get away to. Loretta Salé has been a wonderful friend over the last four years. She has helped me through some difficult times and contributed to many happy and memorable ones.

Table of Contents

	page
1. Introduction	1
The Auroral Ionosphere	3
Magnetospheric Morphology and Phenomenology	4
Coordinate Systems	6
Geomagnetic Activity and Magnetospheric Substorms	9
The Concept of a Magnetic Field Line	12
A Review of Relevant Observations	13
Table 1	21
Figures	22
Relevant Magnetospheric Physics	27
The Magnetopause	28
The Large-Scale Magnetospheric Electric Field	29
Magnetospheric Currents	34
2. Time-Independent Magnetospheric Magnetic Field Models	40
Empirical Magnetospheric Magnetic Field Models: A Brief Review	41
The Magnetic Field due to Sources Inside the Earth	42
The Magnetic Field due to Distributed Intramagnetospheric and Magnetopause Currents: Three Types of Empirical Magnetospheric Magnetic Field Models	45
Testing Global Models of the Magnetospheric Magnetic Field	52
T87 Cross-Tail Current	54
T87 Field-Aligned Current	58
Flare T87 and T89 CPS Field Lines	63

T89 Equatorial B_z in the Noon-Midnight Meridian	67
Figures	71
Rationale for the Development of New Modelling Techniques	86
3. Modelling the Magnetic Effects of Magnetospheric Currents	89
Example Uses	96
Figures	101
Elements of a Global Model: Transverse Currents	109
Model Ring Current	109
Model Cross-Tail Current With Closure	110
Figures	114
Elements of a Global Model: Field-Aligned Currents	122
Figures	130
4. Applications	143
Effects of Field-Aligned Currents on Mappings	143
Figures	146
A New Global Model	151
Figures	159
Mapping During An Individual Event	161
Figures	165
5. Discussion	171
Bibliography	178

List of Tables

table	page
1. CPS plasma velocities	21

List of Figures

figure	page
1. Schematic diagram of the magnetosphere	22
2. <i>Heppner and Maynard</i> [1987] ionospheric potential model	23
3. Average properties of the lobe and neutral sheet magnetic fields	24
4. TRIAD satellite measurement of the eastward component of the magnetic field due to extra-terrestrial currents	25
5. The ionospheric footprints of the Region I and Region II field-aligned current systems	26
6. Contours of constant model J_y and J_z evaluated on the plane $X_{\text{gsm}} = -25R_E$. $J_y = 0$ contours	71
7. Cross-tail current line traces for the T87 $Kp = 3$ model projected in the $X_{\text{gsm}} = -25R_E$ plane	72
8. Contours of constant magnetic field strength for the T87 $Kp = 3$ model on the $X_{\text{gsm}} = -25R_E$ plane	73
9. Flare of field lines for the T87 $Kp = 3$ model in the vicinity of the solar wind-magnetosphere interface	74
10. Field-aligned component of the T87 $Kp = 3$ model current on the $X_{\text{gsm}} = -6.73R_E$ plane	75
11. Field-aligned component of the T87 $Kp = 3$ model current on the $X_{\text{gsm}} = -25R_E$ plane	76
12. Field-aligned current along a model field line	77
13. Flare angle of $Kp = 4$ versions of the T87 and T89 model magnetic fields at $X_{\text{gsm}} = -8 R_E$	78
14. Flare angle of $Kp = 4$ versions of the T87 and T89 model magnetic fields at $X_{\text{gsm}} = -15 R_E$	79

15.	<i>Heppner and Maynard</i> [1987] ionospheric electric potential pattern A prepared using code described in <i>Rich and Maynard</i> [1989]	80
16.	Contours of constant inferred potential in the equatorial plane for the $Kp=4$ versions of the T87 and T89 models and <i>Heppner and Maynard</i> [1987] ionospheric convection pattern A	81
17.	X_{gsm} component of the inferred convection velocity in the equatorial plane for the $Kp=4$ versions of the T87 and T89 models	82
18.	T89 B_z distribution in the model neutral sheet for $Kp = 0$ and a dipole tilt of 16°	83
19.	Regions of negative B_z in the the T89 model neutral sheet for various dipole tilts	84
20.	Magnetic field lines traced using the T89 $Kp = 0$ model with dipole tilts of 16° and 32°	85
21.	The function $f_1(\rho, z)$ for $\rho=0,1,2$, and 3	101
22.	Current and magnetic field line traces for a type I current element	102
23.	The function $g_2(\rho, z)$ for $z = 0$, $a = 4$ and three values of γ	103
24.	The function $f_2(\rho, z)$ for two values of D	104
25.	Current line traces for a type II current element	105
26.	Electric current vectors for a circuit constructed with three type I current elements	106
27.	Extraneous current in the example circuit	107
28.	Magnetic field due to two current sheets	108
29.	Location of current elements used to build up the model ring current ..	114
30.	Northward component of magnetic field in the equatorial plane due to three model ring currents	115

31.	Magnetic field intensity in the equatorial plane due to a terrestrial dipole and model ring current	116
32.	Current flow paths for the model cross-tail current system	117
33.	Model magnetic field magnitude on the surface $X_{\text{gsm}} = -25R_E$	118
34.	Model magnetic field magnitude on the surface $X_{\text{gsm}} = -25R_E$	119
35.	Flare of model magnetic field lines near the magnetopause	120
36.	Model magnetic field strength near the magnetopause	121
37.	View from above the north pole showing a locus of points used as footprints of the model night-side Region I and II currents	130
38.	One closure path of field-aligned currents used in this study	131
39.	One closure path of field-aligned currents used in this study	132
40.	Current sheet thickness as a function of distance from the Earth	133
41.	Vector plots showing the perturbation magnetic field due to the model field-aligned current system	134
42.	The eastward perturbation magnetic field at TRIAD altitude and 2100 hours MLT due to the model field-aligned current	135
43.	Magnetic field due to the model field-aligned current system $6.63 R_E$ from the Earth's centre at 0300 hours MLT	136
44.	Magnetic field due to the model field-aligned current system $6.63 R_E$ from the Earth's centre at 0125 hours MLT	137
45.	The expected and model maximum values of the azimuthal magnetic field due to a model field-aligned current system as a function of distance from the Z_{gsm} axis	138
46.	Magnetic perturbation due to added field-aligned and closure currents on the surface $X_{\text{gsm}} = -15R_E$	139

47.	Magnetic perturbation due to added field-aligned and closure currents on the surface $X_{\text{gsm}} = -15R_E$	140
48.	Equatorial B_z in noon-midnight meridian due to added field-aligned and closure currents	141
49.	Equatorial B_z at $X_{\text{gsm}} = -15R_E$ due to added field-aligned and closure currents	142
50.	Shift in latitude and longitude of the footprints of field lines traced towards the Earth from points on a curve at geosynchronous distance and 0300 hours MLT	146
51.	Shift in latitude and longitude of the footprints of field lines traced towards the Earth from points on a curve at geosynchronous distance and 0125 hours MLT	147
52.	Maximum local time shift of the ionospheric footprint of magnetic field lines traced from points at 0300 hours MLT on a surface $6.63 R_E$ from the Earth's centre	148
53.	Projections in the XY_{gsm} plane of field lines traced using the T87 $Kp = 2$ model modified to include the magnetic effects of field-aligned and closure currents	149
54.	Projections in the XY_{gsm} plane of field lines traced using the T87 $Kp = 2$ model modified to include the magnetic effects of field-aligned and closure currents	150
55.	Magnetic field values in the neutral sheet according to the global model and the empirical function of <i>Rostoker and Skone</i> [1993]	159
56.	Lobe field strength according to the global model and the empirical function of <i>Slavin et al.</i> [1993]	160
57.	Viking satellite image of auroral oval at 0114:47 UT on April 3, 1976 ...	165
58.	Viking satellite image of auroral oval at 0116:07 UT on April 3, 1976 ...	166
59.	Auroral oval boundaries mapped to the gsm equatorial plane using the T87 model	167
60.	Auroral oval boundaries mapped to the gsm equatorial plane using the T89 model	168

61.	Auroral oval boundaries mapped to the gsm equatorial plane using the new model	169
62.	Locus of points from the border of the bright feature in figure 58 mapped to the equatorial plane using the T87, T89 and the new model	170

List of Abbreviations

CPS	central plasma sheet
gse	geocentric solar ecliptic coordinate system
gsm	geocentric solar magnetospheric coordinate system
HLBL	high-latitude boundary layer
IGRF	international geomagnetic reference field
IMF	interplanetary magnetic field
LLBL	low-latitude boundary layer
MHD	magnetohydrodynamic(s)
MLT	magnetic local time
PSBL	plasma sheet boundary layer
R_E	1 Earth radius
sm	solar magnetic coordinate system
T87,T89	Tsyganenko 1987,1989 model

1. Introduction

In an attempt to explain perturbations in the geomagnetic field *Chapman and Ferraro* [1930] suggested that charged particles moving outwards from the sun are deflected by the Earth's magnetic field. Their idea was that the differential motion of the deflected electrons and positive ions would cause a current layer to form on a boundary enclosing a region of space around the Earth that is a cavity in the particle stream. The magnetic field due to these currents would both add to the magnetic field within the cavity and shield the interplanetary medium from the terrestrial magnetic field. Inhomogeneities in the particle stream would lead to variations in the surface currents which in turn would lead to magnetic fluctuations within the cavity. Chapman and Ferraro's initial idea has been demonstrated to be essentially correct although the nature of the interplanetary medium is somewhat different than they envisaged.

Chapman and Ferraro [1930] suggested that the charged particles originated in clouds ejected sporadically from the sun. Their hypothesis was that when one of these ejected clouds passed across the Earth the current layer would be present and at other times it would be absent. As well, in their initial work they assumed that the interplanetary medium did not contain any appreciable magnetic field. It is now known that there is magnetic field and an ever-present flow of charged particles in the interplanetary medium. This flow of charged particles is called the solar wind and is comprised of coronal plasma which has been heated, causing it to expand rapidly outwards through the solar system [*Parker*, 1958]. Typical solar wind particle number densities and flow speeds and interplanetary magnetic field (IMF) magnitudes near the Earth's orbit are $10^7/\text{m}^3$, 400 km/sec and 6 nT, respectively [*Parks*, 1991]. *In situ* magnetic field measurements have confirmed

that the current layer first predicted by *Chapman and Ferraro* [1930] is a persistent feature of the terrestrial environment [*Ness et al.*, 1964]. This current layer is a boundary between the solar wind and the region of space surrounding the Earth known as the magnetosphere.

The term magnetosphere was first used by *Gold* [1959] to denote “the region above the ionosphere in which the magnetic field of the Earth has a dominant control over the motions of gas and fast charged particles”. The ionosphere is the part of the Earth’s upper atmosphere where charged particles are present in “quantities sufficient to affect the propagation of radio waves” [*Rishbeth and Garriott*, 1969]. Today, it is appropriate to define the magnetosphere as the region of space surrounding the Earth, bounded at its base by the ionosphere and in outer space by the solar wind. By convention, the boundary between the magnetosphere and the solar wind is called the magnetopause. The interaction of the solar wind with the magnetosphere compresses the magnetospheric magnetic field on the day-side and stretches it out to great distances from the Earth on the night-side forming a structure called the magnetotail.

Models of the magnetic field due to magnetospheric currents are used in virtually every area of magnetospheric study. This thesis is a description of my efforts to understand the shortcomings of previously developed magnetic field models and to develop a new one. The introduction is a review of magnetospheric terminology, observations that shed light on both current systems and trends in the average magnetic field and some of the basic theory that has been developed to understand magnetospheric current systems. In chapter two, I deal with previously developed magnetic field models and identify some of their shortcomings. The material in this chapter formed the basis of my decision to develop a new magnetic field model.

Chapters three and four are an outline of the method that I used to construct a global magnetospheric magnetic field model and my use of that model, respectively. I conclude the thesis with a discussion (chapter 5) of why this work is important and what future work needs to be done to improve the model I have developed.

Throughout this thesis, I use the term “distributed magnetospheric currents”. I have borrowed this term from *Olson* [1974], who used it to describe volume filling electric currents distributed throughout the magnetosphere: I use it here with the same meaning.

The Auroral Ionosphere

I begin with a brief discussion about the high-latitude ionospheric current systems (*Rishbeth and Garriott* [1969] provide an introductory review of ionospheric physics.). My purpose here is to define terms that are used later in this thesis. In the Earth’s ionosphere, electrons are magnetized while positive ions are collision dominated. Consequently, electrons and ions respond differently to an applied electric field and an applied electric field will cause ionospheric currents to flow. It is often useful to treat transverse (flowing perpendicular to the ambient magnetic field) and parallel electric currents and fields separately. Furthermore, the great mobility of charged particles along the magnetic field means that in the ionosphere the parallel electric field is significantly smaller than the transverse electric field and in discussions of ionospheric physics the term “electric field” is used rather than “transverse electric field”. A transverse current parallel to the applied electric field is called a Pederson current, while one perpendicular to it is called a Hall current. The part of the ionosphere in which most of the transverse currents flow is restricted in altitude from ~ 100 km to ~ 150 km. In the auroral regions, electric

fields that exist as a consequence of magnetospheric dynamics drive large-scale latitudinally localized current systems known as the auroral electrojets. In the dawn and dusk sectors of the auroral ionosphere the electrojet currents are predominantly westward and eastward, respectively. The auroral electrojets are coincident with the auroral ovals, the roughly oval shaped regions encircling both geomagnetic poles where visual aurora are present. The average auroral ovals extend over $\sim 5^\circ$ in latitude with equatorward edges located $\sim 23^\circ$ from each magnetic pole. The regions poleward of the auroral ovals are called the polar caps.

Magnetospheric Morphology and Phenomenology

Space scientists have identified different magnetospheric regions using the properties of the ambient plasma and local magnetic field topology and strength. Figure 1 is a schematic illustration of the Earth's magnetosphere showing its division into these regions. In the following paragraphs, I briefly define and describe the primary magnetospheric regions.

The magnetopause is the current layer that forms the boundary between the magnetosphere and the solar wind. These currents serve to shield the interplanetary medium from the magnetospheric magnetic field (and vice-versa) and deflect the solar wind plasma around the magnetosphere. The thickness of the current layer is on the order of 10^6 m [Russell and Elphic, 1978]. The solar wind is super-sonic and super-Alfvénic [Siscoe, 1987] relative to the magnetosphere. Consequently, a magnetohydrodynamic shock front, called the bow shock, forms in the solar wind upstream of the magnetosphere. As the solar wind passes through the bow shock, it is both heated and slowed to subsonic and sub-Alfvénic velocities [Spreiter and Alksne, 1969]. The region between the bow shock and the magnetopause is termed

the magnetosheath and contains shocked solar wind plasma flowing nearly parallel to the magnetopause (except around the sub-solar point). Immediately inside the magnetopause is a boundary layer containing plasma that is magnetosheath-like in both composition and velocity [Lundin, 1988]. The existence of this boundary layer is evidence that some solar wind particles and momentum cross the magnetopause and enter the magnetosphere. This boundary layer is divided into regions. These are the high- and low-latitude boundary layers (HLBL and LLBL) which are threaded by open and closed magnetic field lines, respectively [Eastman *et al.*, 1976]. The HLBL is also referred to as the plasma mantle [Rosenbauer *et al.*, 1975; Lundin 1988].

Inside the boundary layers, within the magnetotail, there are two primary regions, the lobes and the central plasma sheet (CPS), which are separated by the plasma sheet boundary layer (PSBL). The CPS is threaded by closed magnetic field lines and populated by a plasma of both solar wind and ionospheric origin [Peterson *et al.*, 1981]. Typically, plasma number densities within the CPS are ~ 0.1 to 1 cm^{-3} , ion temperatures range from ~ 1 to $\sim 7 \text{ keV}$ and the ion temperatures are greater than those of the electrons by a factor of ~ 3 [Frank, 1985]. On the other hand, the lobes are threaded by open magnetic field lines and are populated by a very tenuous plasma ($< 0.01 \text{ cm}^{-3}$), in comparison to that in the CPS [Frank, 1985]. Particles in the lobe are of both solar wind and ionospheric origin [Peterson *et al.*, 1984]. Lobe particles of solar wind origin likely enter through the cusps, which are regions on the magnetospheric boundary where the magnetic field just inside the magnetosphere is weak. The PSBL is threaded by closed magnetic field lines and is identified as a separate region from the CPS by the presence of field-aligned beams of fast ions [Lui *et al.*, 1977; DeCoster and Frank, 1979]. In the

heart of the CPS is the neutral sheet, which separates the northern and southern magnetospheric hemispheres. The CPS encircles the Earth, its inner edge merges smoothly with the ring current which is a nearly azimuthally symmetric current carried by geomagnetically trapped energetic particles.

Coordinate Systems

A number of coordinate systems are used in the space science community. The need for more than one arises mainly because the dominant source of the magnetic field is different in different magnetospheric regions. Consequently, data obtained from observations in one region are often better ordered in a coordinate system chosen particularly for that region. As well, theoretical studies are often better formulated in one coordinate system or another, depending on what particular physical process and magnetospheric region is being investigated.

I use three coordinate systems: (1) geographic; (2) geocentric solar magnetospheric (herein referred to as gsm); (3) solar magnetic (herein referred to as sm). In the following paragraphs, I describe these three systems and briefly outline the procedure to convert from one coordinate system to another. I indirectly use a fourth system, the geocentric solar ecliptic (gse) system, when discussing the direction of the IMF; however, I limit my use of this coordinate system to stating whether the IMF Z_{gse} component is positive or negative. Generally, the inner product of the IMF and the magnetospheric magnetic field immediately inside the magnetopause at the subsolar point will be positive (negative) if the IMF Z_{gse} component is positive (negative). If the IMF Z_{gse} component is positive or negative then the IMF is said to be pointing northward or southward, respectively. Two technical reviews on the topic of geophysical coordinate systems and how to transform from any given

system to any other system have been given by *Russell* [1971] and *Hapgood* [1992]. The information presented here is derived primarily from Russell's review paper.

The geographic coordinate system is Earth-fixed (i.e., it rotates with the Earth). Typically, a location in the geographic system is specified in terms of spherical coordinates. These are longitude (measured positive eastward from the Greenwich meridian, which corresponds to longitude= $\phi=0$), latitude (measured positive northward from the rotational equator, which corresponds to latitude= $\lambda=0$) and radial distance from the Earth's centre. A cartesian geographic coordinate system is typically defined so that the Z -axis is the Earth's rotational axis (with north being positive) and the positive X -axis passes through the Greenwich meridian. The geographic coordinate system is useful for the interpretation of near-Earth observations. In this region, the Earth's magnetic field is the dominant magnetic field, and obtaining estimates of the Earth's magnetic field at a given location from standard models (see chapter 2) requires knowledge of where that location is in geographic coordinates. As well, meaningful comparisons of simultaneous ionospheric and ground-based observations from several different instruments are only possible if the locations of the observed phenomena are known, relative to one another. This is most easily accomplished by expressing results in terms of geographic coordinates.

The gsm coordinate system is defined as follows: the X_{gsm} axis is the sun-Earth line (positive towards the sun) and the Z_{gsm} -axis is chosen so that the Earth's dipole axis is in the $Y_{\text{gsm}} = 0$ plane. The positive Z_{gsm} direction is chosen so that the angle between the geographic positive Z -axis and the positive Z_{gsm} direction is less than 90° . For this purpose, the Earth's dipole axis is chosen so that it is parallel to the terrestrial dipole moment as derived from the IGRF magnetic field model

(see chapter 2). The gsm coordinate system is used primarily in the magnetotail region. As I pointed out above, the magnetotail aligns itself with the solar-wind flow relative to the Earth. On average, the solar wind flow direction is aberrated $\sim 4^\circ$ from the sun-Earth line due to the orbital motion of the Earth. Thus, on average the magnetotail is nearly aligned with ($\sim 4^\circ$ off parallel to) the X_{gsm} -axis.

The sm coordinate system is defined so that the Z_{sm} axis is parallel to the Earth's dipole axis and the sun-Earth line is in the $Y_{\text{sm}} = 0$ plane. As in the gsm coordinate system, the positive Z_{sm} direction is chosen so that the angle between the geographic positive Z direction and the positive Z_{sm} direction is less than 90° . The sm equatorial plane (i.e., the $Z_{\text{sm}} = 0$ plane) is perpendicular to the Earth's dipole axis. In the inner magnetosphere, the dominant contribution to the magnetic field is that of the terrestrial dipole. That field, in turn, governs the motion of charged particles in the region. Hence, it is in the inner magnetosphere that the sm coordinate system is most often used. In the following sections, I will use the term magnetic local time (MLT). In this thesis, I use the term to refer to the longitude in the SM coordinate system expressed in hours, with 1200 hours MLT corresponding to local noon (i.e., the sun directly overhead). As well, the MLT increases eastward.

Transformation matrices must be defined in order to convert a vector expressed in one system into one expressed in another. To convert between the three coordinate systems above, one need only know the sun-Earth and Earth's dipole directions in geographic coordinates. The Earth's dipole direction in geographic coordinates is readily obtained from the IGRF terrestrial magnetic field model described in chapter 2. A prescription for determining the position of the sun in geographic coordinates is given by both *Russell [1971]* and *Hapgood [1992]*.

When the terrestrial dipole is oriented perpendicular to the sun-Earth line, then the sm and gsm coordinate systems as defined above are the same. In general, the dipole tilt angle is defined to be the angle the sun-Earth line makes with the sm equatorial plane. It is also the angle between the Z_{gsm} and Z_{sm} axes. Thus, when the dipole is perpendicular to the sun-Earth line, the dipole tilt angle is zero. The dipole direction is roughly 11° from the geographic Z -axis which is, in turn, 67.5° from the plane of the Earth's orbit around the sun. Consequently, the dipole tilt angle can range from 33.5° towards the sun to 33.5° away from the sun.

Geomagnetic Activity and Magnetospheric Substorms

The energy that drives magnetospheric currents and plasma motions, as well as the auroral electrojets, is derived from the solar wind. Variations within the solar wind, the magnetosphere and the ionosphere lead to variations in the rate at which solar wind energy enters the magnetosphere and in how that energy is both stored and dissipated. The variability of this solar wind-magnetosphere interaction lead researchers to develop methods of quantifying magnetospheric activity. Attempts to understand how solar wind energy enters the magnetosphere and, more importantly, the details of how that energy is dissipated, lead directly to the concept of the magnetospheric substorm.

Geomagnetic indices have been developed and used to quantify magnetospheric activity. The three indices that I refer to in this thesis are Kp , AE and Dst , each of which is determined from magnetic perturbations measured on the surface of the Earth. They are only indicators of magnetospheric activity insofar as the currents that lead to the magnetic perturbations are themselves good indicators of magnetospheric activity. Roughly speaking, the Kp index is calculated by averaging the

maximum magnetic perturbations from thirteen magnetometers located at mid-latitudes (i.e., subauroral). Kp is calculated for each of eight three-hour intervals every day. AE is an estimate, based on auroral zone magnetic field measurements, of the sum of the maximum perturbed magnetic fields due to auroral electrojets at the dawn and dusk sides. The Dst index is an estimate of the magnetic perturbation due to the ring current (defined below). *Rostoker* [1972] reviewed how these indices are obtained from magnetometer data and some of the potential dangers of using them as “instantaneous” indicators of magnetospheric activity.

Although the division is somewhat arbitrary, it is useful to think of solar wind energy entering the magnetosphere as being comprised of two components, one contributing to what is called the directly driven system and the other consisting of energy that is stored in the magnetospheric magnetic field [*Rostoker et al*, 1987]. Energy contributing to the directly driven system is (after time delay of up to a few minutes) dissipated in the auroral ionosphere (via Joule heating) or causes an increase in the geomagnetically trapped particle densities and/or energies in the inner magnetosphere. The large-scale electric field that drives the ionospheric currents that cause the Joule heating also drives the auroral electrojets. Consequently, the AE index is often used as a measure of directly driven system activity [e.g., *Rostoker et al.*, 1988]. Energy that is stored shows up predominantly in the form of an increase in the lobe magnetic field strength. Changes in solar wind properties can lead to changes in the driven system and the beginning of or an increase of the rate of energy storage or a sudden release of that stored energy. The storage and release of that energy is referred to as the loading-unloading process.

The driven system and the loading-unloading processes are part of the magnetospheric substorm process, although it is the latter that researchers are usually

referring to when the term magnetospheric substorm is used. More specifically, the loading-unloading process consists of three phases. The first is the growth phase during which energy is being stored [McPherron, 1970]. The second and third are the expansive and recovery phases which were originally defined in terms of a sequence of changes in the visible aurora [Akasofu, 1964; McPherron, 1991] and are, essentially, periods of episodic release of the stored energy [Kisabeth and Rostoker, 1974].

The substorm is one of the most actively studied magnetospheric phenomena. One reason for this great interest is the belief, on the part of most researchers, that the key to understanding magnetospheric dynamics in general lies in understanding the way that the magnetospheric system responds to changes in both the rate and way that energy enters that system. In spite of this great interest, or perhaps because of it, a number of remarkably different theories have been developed that purport to explain part, or all, of the substorm process [Lui, 1991]. One way that one substorm theory differs from another lies in what physical processes are invoked in those theories to explain why, at some particular time, the stored energy is suddenly released. During the expansive phase, for example, a current wedge forms [Clauer and McPherron, 1974]. A wedge consists of field-aligned current flowing from the magnetosphere into the ionosphere that diverts (through the ionosphere) into field-aligned current flowing out to the magnetosphere. Where the field-aligned current originates in the magnetosphere and what physical processes lead to its generation are hotly debated questions [e.g., Birn and Hones, 1981; Rostoker and Eastman 1987; Goertz and Smith 1989; Lui et al., 1990]. One way to answer, at least in part, questions such as where, in the magnetosphere, the currents that form the substorm current wedge are generated, is through “magnetic field mapping”. The

reasoning is that, if we knew where the magnetic field lines go in the magnetosphere, then this could help us determine which theories are possibly correct and which are definitely not correct [Samson *et al.*, 1992].

The Concept of a Magnetic Field Line

In this thesis, a magnetic field line is defined to be a parameterized curve in space ($\vec{R}(s)$) that is the solution of the following equation:

$$\frac{d\vec{R}}{ds} = \frac{\vec{B}(\vec{R})}{|\vec{B}(\vec{R})|} \quad (1)$$

At all points along this curve the magnetic field is tangent to the curve. As well, the parameter s is a measure of distance along the field line from some (arbitrarily) specified zero point on the field line. A field line is identified by a point in space through which it passes. If this point is stationary and the magnetic field is time independent then the field line does not move. On the other hand, the point defining the field line can be moving. For instance, this point could be the location of a specified parcel of plasma. Hence, although the definition of a field line that I have adopted here is a purely mathematical one, field lines defined in this way can move.

Within the context of magnetospheric physics, researchers often refer to “open” and “closed” magnetic field lines. A field line is said to be open if it extends outside of the magnetospheric system, into the solar wind. On the other hand, a field line is said to be closed if it can be traced from the ionosphere, through the magnetosphere, back to the ionosphere in the opposite hemisphere.

A Review of Relevant Observations

I have used the results from a wide range of magnetospheric and ionospheric experiments in producing the work presented in this thesis. In this section, I review the results of relevant experimental work. I begin with a review of *in situ* measurements of ionospheric electric fields and CPS plasma convection velocities. Next, I summarize observations of the magnetic perturbations associated with large scale field-aligned current systems. Finally, I outline observations upon which our picture of the large scale transverse currents in the magnetosphere is based. Throughout this thesis, I will use acronyms to identify various spacecraft. Details about the spacecraft in question are obtainable from the references.

The empirical model of the ionospheric electric potential developed by *Heppner and Maynard* [1987] is based on the combined electric field data sets of the OGO 6 and DE 2 polar orbiting satellites. The data are represented by polar plots of ionospheric electric equipotentials for several ranges of IMF direction and level of geomagnetic activity as quantified by the Kp index. Figure 2 is a contour plot of ionospheric electric equipotentials obtained from the Heppner-Maynard model appropriate for periods of positive IMF B_y and geomagnetic activity levels in the range $3+ < Kp < 4-$. The figure is a reproduction of Figure 1 of *Heppner and Maynard* [1987]. In their paper, and in chapter 2 of my thesis, this ionospheric electric potential pattern is referred to as potential model A of Heppner and Maynard.

Studies by *Huang and Frank* [1986] and *Baumjohann et al.* [1989] show that typical CPS velocities in the region $-20 R_E < X_{gsm} < -10 R_E$ are normally earthward and below 100 km/sec. I provide a summary of plasma flow properties in the CPS derived from the ISEE 1 satellite data set in Table 1. The data in this

table are from a study of CPS convection velocities by *Rostoker et al.* [1988]. The flows are broken down into four categories of magnetospheric activity. *Rostoker et al.* [1988] based their classification of the activity level on the properties of a time series of one minute AE values. One activity level was termed “a quiet magnetosphere” and corresponded to $AE < 100$ nT and nearly constant in time. The other three levels corresponded to different states of the directly driven system as indicated by trends in the AE time series. If the AE index was steadily increasing or decreasing in time the activity level was described as “growth” and “decay” of the directly driven system, respectively. If AE was greater than 100 nT and roughly constant in time the activity level was described as “steady” behavior of the driven system. In all cases they restricted their attentions to times when $AE < 400$ nT. *Rostoker et al.* [1988] determined the convection velocity as a function of distance from the noon-midnight meridian, grouping their results in ranges of Y_{gsm} ($Y_{gsm} < -10 R_E$, $-10 R_E < Y_{gsm} < 10 R_E$, $Y_{gsm} > 10 R_E$). They found similar distributions of plasma convection velocities in each of the three bins. Thus, the only measurement of the dependence of convection velocity on distance from the noon-midnight meridian that uses a large number of *in situ* observations indicates no measurable variation with Y_{gsm} .

Sergeev and Lennartsson [1988] used ISEE 1 satellite data to determine the plasma convection velocity in the CPS on two well separated days. In each case, the measurements lasted several hours. One measurement was made when the satellite was close to the noon-midnight meridian and the other when the satellite was about $10 R_E$ from the noon-midnight meridian. On the basis of these two measurements, they concluded that the convection velocity is persistently much larger near the centre than at the flanks of the CPS. Due to the very small number of observations

used in their study and the inherent variability of the magnetospheric electric field, even on time scales of several hours or more [Mozer, 1971], their conclusions should be regarded as speculative rather than definitive.

Early plasma measurements by *Hones et al.* [1972] and *Eastman et al.* [1976] established that the LLBL contains tailward flowing plasma on closed field lines and that the plasma motion was predominantly perpendicular to the ambient magnetic field direction. The boundary between the CPS and the LLBL is, therefore, a convection reversal. A convection reversal has also been identified in the PSBL [Orsini et al., 1984]. It follows from the discussion in the next section that convection reversals are also electric field reversals. Taken together, the electric field reversals at the inner edge of the LLBL, in the PSBL and the ionosphere are evidence for a connection, along magnetic field lines, between the LLBL and the ionosphere, through the PSBL. In fact, *Rostoker and Boström* [1976] deduced that there is an electric field reversal in the PSBL (prior to any direct observational evidence for that electric field reversal) on the basis of their belief that the LLBL is topologically connected with the PSBL along magnetic field lines.

The existence of the magnetotail was inferred by *Ness* [1965] on the basis of IMP 1 satellite magnetic field measurements. His observations indicated that the magnetic field within the magnetotail was, predominantly, aligned with the sun-Earth direction, pointing towards (away from) the Earth above (below) the equatorial region. This magnetic field configuration indicated that there must be a cross-tail current separating the two magnetospheric lobes [Williams and Mead, 1965]. The lobe magnetic field varies with magnetic activity and solar wind conditions, typically becoming larger with both increasing activity [Behannon, 1968] and more southward IMF [Coroniti and Kennel., 1972]. More recently, *Slavin et al.*

[1985] used ISEE 3 magnetometer data to demonstrate that the average lobe field strength falls off roughly as $|X_{\text{gsm}}|^{-0.53}$ for $X_{\text{gsm}} < -20 R_{\text{E}}$. Using ISEE 1 data, *Nakai et al.* [1991] showed that the average lobe field strength varies as $R^{-1.20}$ for $10 R_{\text{E}} < R < 22.6 R_{\text{E}}$, where R is the distance from the Earth's centre. The average lobe field strengths given by these relationships are plotted in Figure 3a.

Within the CPS, the magnetic field strength is lower than that of the lobes. For instance, particle and field measurements have shown that the sum of the magnetic and thermal pressures (i.e., $P + B^2/(2\mu_0)$) are roughly the same, at any instant, in the CPS and the lobes [*Baumjohann and Paschmann, 1990*]. In comparison to that in the lobe and CPS, the neutral sheet magnetic field strength is small. The magnetic field in the neutral sheet is typically perpendicular to the plane of the neutral sheet and represents magnetic flux crossing the equatorial region from the southern CPS to the northern CPS. In what follows, I use B_z to indicate the neutral sheet magnetic field (positive northward). Here, the z direction strictly means perpendicular to the neutral sheet; however, especially for times of small dipole tilts, this is essentially the Z_{gsm} direction.

Fairfield [1986] used measurements from the IMP 6, 7, and 8 spacecraft to determine the character of B_z in the neutral sheet at distances from the Earth ranging from 10 to 40 R_{E} . He found that while there were observations of negative B_z in the region of the neutral sheet, the average value of B_z in the neutral sheet was clearly positive. Furthermore, his results indicated that the neutral sheet magnetic field is larger, by roughly 1 or 2 nT, at the flanks (i.e., at larger $|Y_{\text{gsm}}|$) than near the centre of the magnetotail. For distances between 20 and 40 R_{E} away from the Earth, he found that the average value was between 1 and 2 nT. Furthermore, in an earlier study, *Fairfield* [1979] showed that for IMP 6 magnetic field measurements

made between 20 and 33 R_E from the Earth in the tail, B_z was on average positive in the neutral sheet and decreased, on average, with increasing distance from the neutral sheet. Thus the average B_z values in the actual neutral sheet should be somewhat larger than those obtained by Fairfield. More recently, *Rostoker and Skone* [1993] developed a functional representation of the neutral sheet magnetic field dependence on X_{gsm} . They used only magnetic field values from times when it was verifiable that the satellite was in the neutral sheet. Their B_z values are somewhat larger than those obtained by *Fairfield* [1986].

Early *in situ* magnetic field measurements in the inner magnetosphere confirmed the existence of a nearly azimuthally symmetric (about the Earth's dipole axis) ring current carried by geomagnetically trapped charged particles [*Smith et al.*, 1960]. On average, its magnetic signature is consistent with a westward current of 2 or 3 R_E radial extent, consisting of a total current on the order of 1 or 2 MA [*Smith et al.*, 1960; *Akasofu and Chapman* 1961; *Frank* 1971]. The radial extent of and total current carried by the ring current vary considerably with magnetospheric activity. The radial extent of the ring current is a function of the magnetic field topology and recent (on a scale of tens of hours) magnetic activity and solar wind conditions [*Lyons and Williams*, 1984]. The total current carried by the ring current typically increases (by a factor of two or more) during substorms [*Williams* 1985; *Lui et al.*, 1987]. The total current decays to its "quiet-time" or "prestorm" value on a time scale of tens of hours [*Lyons and Williams*, 1984].

As well as the cross-tail and ring currents, there are currents that flow along the magnetic field direction from the magnetosphere to the ionosphere and vice versa. The best information available about the field-aligned current distribution comes from satellite measurements of magnetic perturbations in the top-side ionosphere

a few hundred km above the Earth's surface. Early studies using the TRIAD satellite [e.g., *Zmuda and Armstrong, 1974; Yasuhara et al., 1975; Iijima and Potemra, 1976*] elucidated the average distribution of field-aligned currents in the top-side ionosphere. There is field-aligned current flowing either into or out of the ionosphere throughout most of the region coincident with the visual auroral oval. Data from a TRIAD satellite pass, showing magnetic perturbations, from which the existence of these currents is inferred, is included here in Figure 4. In most local time zones there are two well-defined regions of field-aligned current, which *Iijima and Potemra [1978]* called the Region I and Region II currents. The poleward part of the auroral zone contains the Region I currents, whereas the equatorward part contains the Region II currents. On the dawn side, the Region I currents flow downward into the ionosphere and the Region II currents flow upward out of the ionosphere. On the dusk side, the directions of the currents are reversed. A diagram showing the statistically determined locations of the Region I and Region II current systems is included here as Figure 5. At TRIAD altitudes (~ 800 km), the magnitude of the eastward perturbation of the magnetic field between the two current sheets is typically between 100 and 500 nT, although values in excess of 1000 nT are occasionally observed [*Zmuda and Armstrong, 1974*]. The amount of current flowing in the Region I current system was generally found to be somewhat larger than that in the Region II system [*Yasuhara et al., 1975*], although near midnight the linear current density (or total current per unit of longitudinal angle) of the two current sheets is nearly equal [*Iijima and Potemra, 1978*]. Typical values for the amount of current in the dawn and dusk northern hemisphere Region I current systems are roughly 1.5 MA for quiet times ($|AL| < 100$ nT) and 2.5 MA for more active times ($|AL| > 100$ nT), and typical current densities range

from 0.5 to 1 $\mu\text{A}/\text{m}^2$ [Iijima and Potemra, 1978]. Near midnight, the ionospheric closure between the Region I and II currents is via north-south flowing Pederson currents [Senior *et al.*, 1982], but the field-aligned currents are always accompanied by an electric field that drives significant Hall currents [e.g., Rostoker and Boström, 1976]. Away from midnight, it is not possible for the Region I and II currents to be closed entirely by meridional currents, because of their unequal linear current densities [Kamide *et al.*, 1976; Senior *et al.*, 1982].

There have been numerous attempts to use particle and field measurements to determine where, in the magnetosphere, field-aligned currents are generated. Statistical pictures of the divergence of the equatorial current [e.g., Roelof, 1989; Zanetti *et al.*, 1991] and magnetic field data from individual satellite passes through the current sheets [e.g., Kelley *et al.*, 1986] support the view that the Region II currents are generated in the near-Earth CPS and ring current regions. Low-altitude electric field, magnetic field and particle precipitation measurements indicate that the Region I currents flow on closed field lines and that the ionospheric convection reversal is either embedded within [e.g., Rostoker, 1991] or at the poleward boundary of the current layer [e.g., Smiddy *et al.*, 1980]. This supports the view that the Region I currents flow to the outer magnetosphere through the PSBL in which an electric field reversal has been observed [Orsini *et al.*, 1984]. Currents of Region I sense have been observed in the PSBL via their magnetic signature [e.g., Fairfield, 1973; Ohtani *et al.*, 1988].

Based on numerous satellite passes through the magnetopause, researchers have built up an empirical picture of what the overall shape of the magnetospheric boundary is. Early studies indicated that the subsolar point (essentially the intersection between the magnetopause and the sun-Earth line) is typically around

10 R_E from the Earth, although this distance varies significantly with solar wind parameters [*Ness et al.*, 1964]. *Formisano et al.* [1979] determined that the magnetopause is centred on the sun-Earth line (aberrated slightly due to the Earth's motion across the solar wind direction) and is nearly circular in cross section (east-west extent within 10% of that in north-south direction). *Sibeck et al.* [1991] developed an empirical model of the radial distance of the magnetopause from the sun-Earth line based on the locations of ~ 1800 satellite magnetopause crossings. They derived functions describing the average magnetopause radius (perpendicular to the sun-earth line) for ranges of both solar wind pressure and IMF northward component.

Table 1. CPS plasma bulk velocities (in km/sec) over the range $-10 R_E < X_{gsm} < -23 R_E$ for different types of magnetospheric substorm activity (see text).

Phase of the Substorm	$-20 < Y_{gsm} < -10$	$-10 < Y_{gsm} < 10$	$10 < Y_{gsm} < 20$
Quiet (AE < 100 and steady)	17 (321)	10 (261)	Insufficient data
Driven System Growth (AE < 400)	16 (162)	11 (259)	37 (55)
Steady Driven System (AE < 400)	19 (455)	22 (524)	25 (537)
Driven System Decay (AE < 400)	24 (246)	20 (303)	24 (110)
Code	v (n)	X-component of bulk flow velocity vector (positive earthwards) followed by the number of data points from which the averaged flow vectors are obtained	

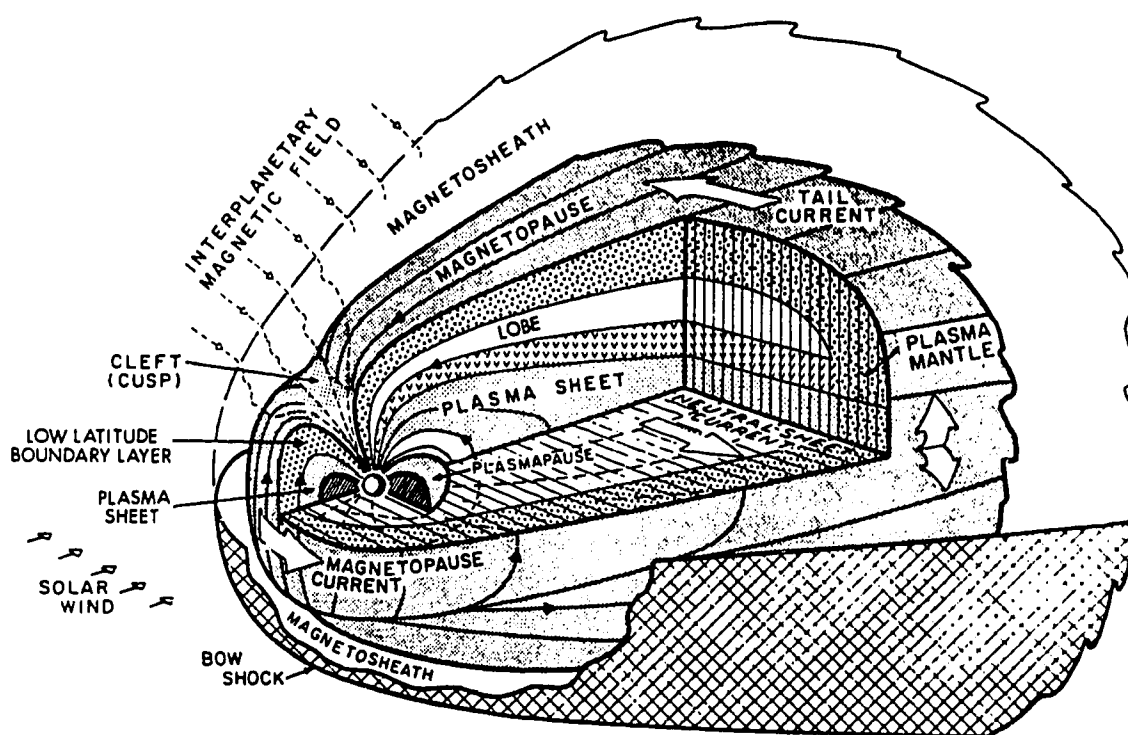


Figure 1. Schematic diagram of the magnetosphere. (Originally published by Rostoker [1989]).

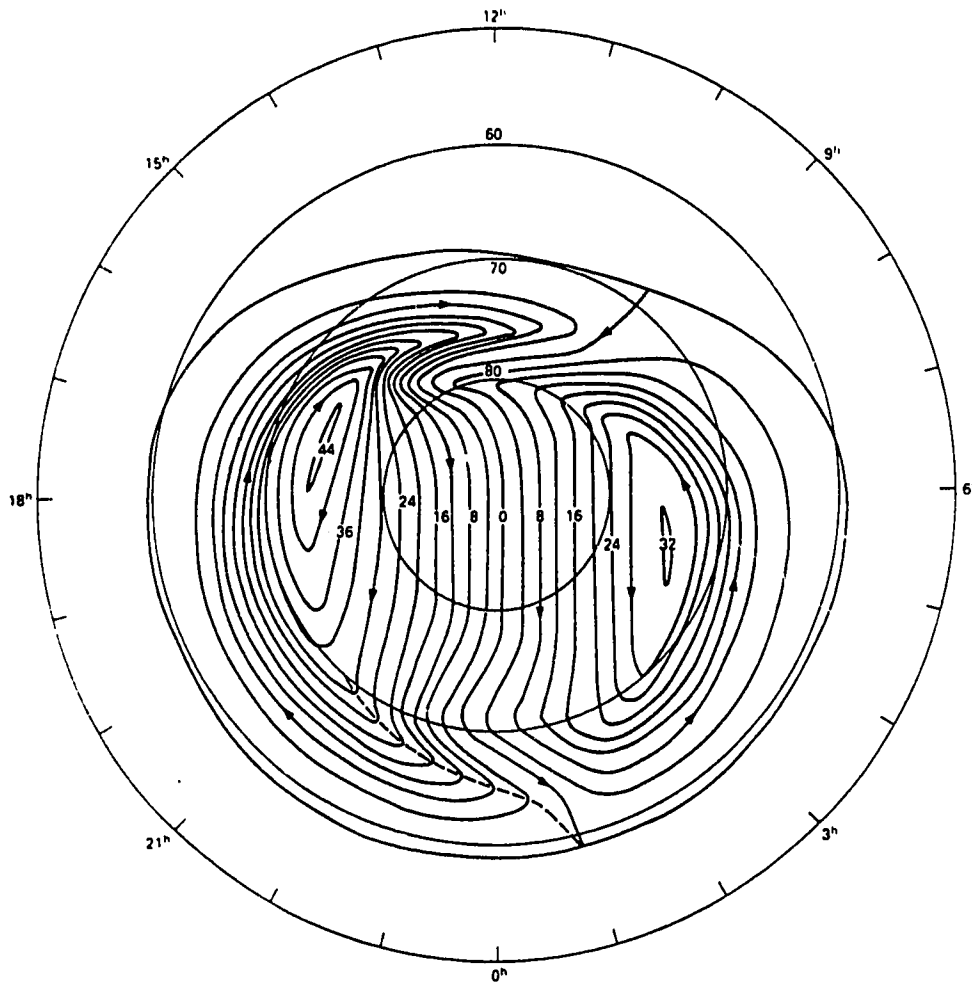


Figure 2. *Heppner and Maynard* [1987] ionospheric electric potential model A. The contours are separated by 4 kV. This is Figure 1 from *Heppner and Maynard* [1987] and is reproduced here without modification. The dashed curve near midnight indicates the location of the “Harang discontinuity” according to *Heppner and Maynard* [1987]. For a description of the Harang discontinuity see the paper by *Heppner* [1972] in which the term was first used.

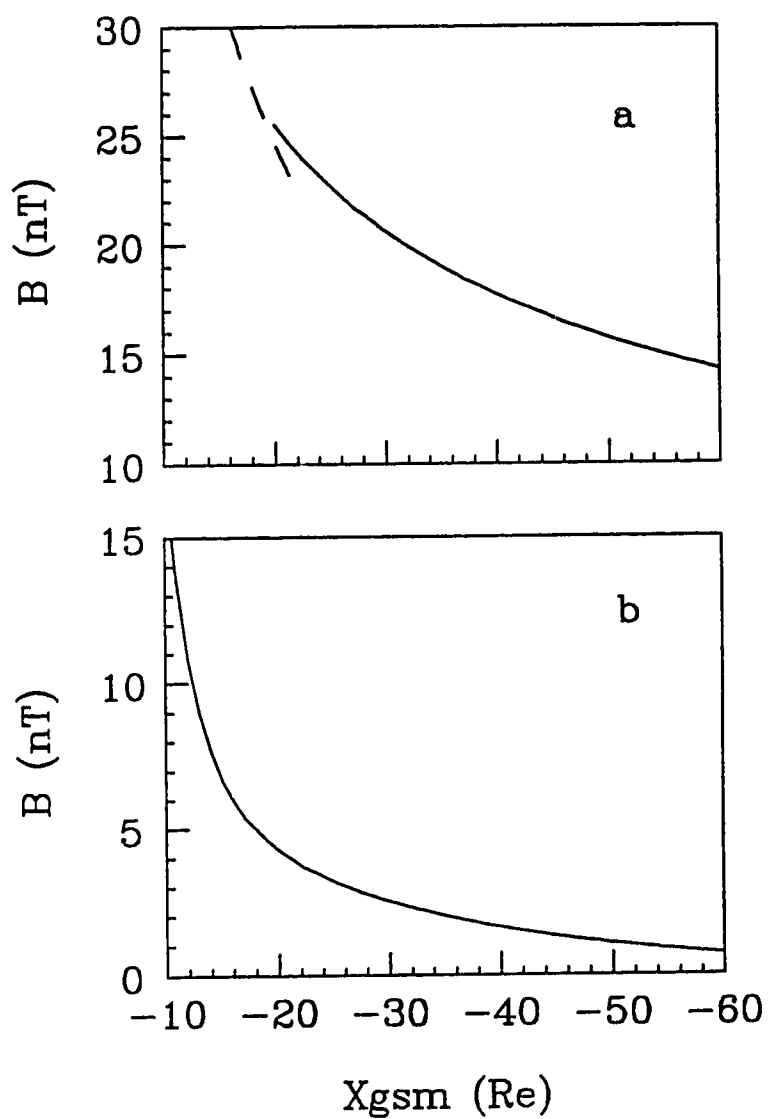


Figure 3. Average properties of the lobe and neutral sheet magnetic fields: (a) average lobe field strength for $X_{gsm} < -20 R_E$ [Slavin *et al.*, 1985] (solid curve) and $10 R_E < R < 22.6 R_E$ [Nakai *et al.*, 1991] (dashed curve); (b) average neutral sheet B_z for $-10 R_E > X_{gsm} > -60 R_E$ [Rostoker and Skone, 1993].

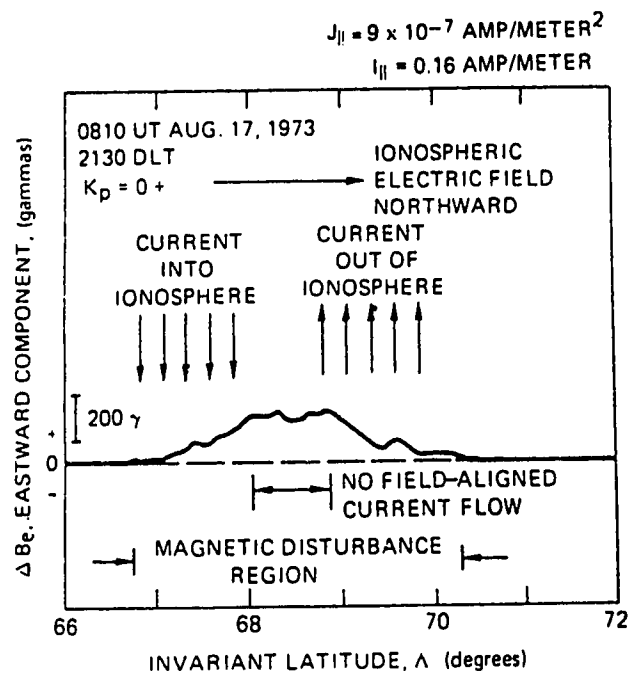


Figure 4. TRIAD satellite measurement of the eastward component of the magnetic field due to extra-terrestrial currents. The currents thought to be responsible for the magnetic perturbation are illustrated on the figure. The vertical scale is in nT. This is Figure 2 from *Zmuda and Armstrong [1974]* and is reproduced here without modification.

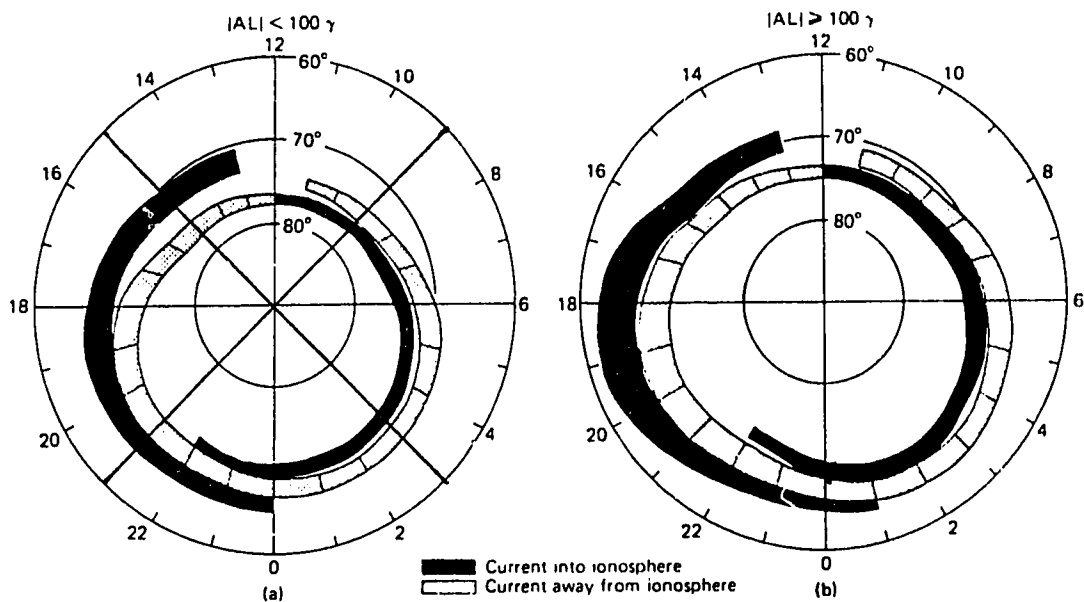


Figure 5. The ionospheric footprints of the Region I (poleward) and Region II (equatorward) field-aligned current systems for weakly disturbed ($|AL| < 100 \text{ nT}$) and more active ($|AL| > 100 \text{ nT}$) conditions. These results summarize TRIAD satellite observations. This is Figure 13 from *Iijima and Potemra [1978]* and is reproduced here without modification.

Relevant Magnetospheric Physics

In this section, I discuss the following from a theoretical perspective: (1) how one would calculate the magnetopause location; (2) why there is a magnetospheric electric field; (3) why it is expected that both transverse and field-aligned currents flow in the magnetosphere. The work presented in this thesis is aimed at furthering our understanding of the average magnetospheric magnetic field configuration. As such, time dependent effects are not a consideration. I begin, then, with the time independent, ideal magnetohydrodynamic (MHD) equations and Ampere's law:

$$\vec{\nabla} \cdot \vec{J} = 0 \quad (2)$$

$$\rho_m \vec{V} \cdot \vec{\nabla} \vec{V} = -\vec{\nabla} \cdot \tilde{P} + \vec{J} \times \vec{B} \quad (3)$$

$$\vec{E} + \vec{V} \times \vec{B} = 0 \quad (4)$$

$$\vec{\nabla} \times \vec{B} = \mu_o \vec{J} \quad (5)$$

Here, ρ_m and V are the plasma mass density and velocity, respectively, and

$$\tilde{P} = P_{\perp} \tilde{I} + (P_{\parallel} - P_{\perp}) \hat{b} \hat{b} \quad (6)$$

is the gyrotropic pressure tensor, where \tilde{I} is the identity matrix and \hat{b} is the unit vector in the direction of the magnetic field [e.g., *Siscoe*, 1983]. These equations provide a reasonable description of many steady state magnetospheric processes;

however, it is important to remember that violations of the conditions that must be assumed for the proper use of these equations lead to some of the most interesting, and still essentially steady-state, magnetospheric phenomena. These include the existence of the cross-tail current and magnetic merging [Speiser, 1970], as well as the transport of momentum from the magnetosheath into the LLBL [Miura, 1984].

The Magnetopause

In most theoretical studies aimed at finding the location of the magnetopause for a given set of solar wind parameters, the magnetopause is treated as though it is an interface through which no magnetic flux and no charged particles will cross. The standard approach is to balance total pressure within the magnetosheath just outside the magnetopause with that in the magnetosphere just inside the magnetopause. Assuming time independent MHD applies within the magnetosheath and inside the magnetosphere, this pressure balance can be expressed mathematically as

$$\frac{B_o^2}{2\mu_o} + P_o^2 = \frac{B_i^2}{2\mu_o} + P_i^2 \quad (7)$$

where the “gas pressure” P includes the thermal and dynamic pressures and the subscripts o and i stand for outside and inside, respectively [Schindler and Birn, 1978]. In the magnetosheath the magnetic pressure is typically small in comparison to the gas pressure while just inside the magnetopause the opposite is true [cf. Siscoe, 1987]. It turns out that, even though the magnetosheath plasma is by no means cold, the gas pressure P is very nearly proportional to the dynamic pressure of the solar wind gas if there was no shock front upwind of the magnetosphere

[Spreiter *et al.*, 1966]. Here, I will use K to denote that constant of proportionality. Assuming the magnetic field is exactly zero in the magnetosheath, then the currents on the magnetopause shield the external region from magnetic field due to sources within the magnetosphere. Assuming that magnetic field is due that of the Earth (B_{terr}), the magnetic field just inside the boundary is given by

$$B_i = 2fB_{\text{terr}} \quad (8)$$

If the magnetopause was a planar surface the value of f would be 1. If it was an Earth centred sphere, f would be 1.5. In general, f is a number that indicates how the curvature of the magnetopause effects the contribution to the total magnetic field due to the shielding currents and it will be between 1 and 1.5. Of course, the shielded magnetic field is not that due only to the Earth; however, an Earth centred dipole field is the only magnetic field for which this problem has been solved. Ultimately, the problem is to solve

$$\frac{(2fB_{\text{terr}})^2}{2\mu_0} = K\rho_{\text{sw}}V_{\text{sw}}^2\cos^2(\Psi) \quad (9)$$

where ρ_{sw} and V_{sw} are the solar wind mass density and speed, respectively, and Ψ is the angle between the solar wind direction and the normal to the magnetopause surface.

The Large Scale Magnetospheric Electric Field

Of course, the magnetopause is not an impenetrable barrier. If magnetic flux and solar wind particles could not cross this surface, the magnetosphere would not

be a very interesting region of space. In this section, I will briefly discuss how two processes, which are essentially violations of ideal MHD, lead to the presence of a large scale magnetospheric electric field. These two processes are referred to as “magnetic reconnection” and “viscous interaction”. The assumption here is that ideal MHD applies throughout the magnetosphere and in the solar wind, but not at its outer boundary. Assuming ideal MHD applies, the existence of an electric field implies plasma convection (equation 4). Furthermore, the plasma convection velocity is perpendicular to the electric field. Electrostatic equipotentials, then, are plasma streamlines. In the ionosphere, equipotentials are streamlines for particles that are magnetized. In the lower ionosphere this applies to the electrons only while in the upper ionosphere this applies to both electrons and ions [cf. *Rishbeth and Garriott, 1969*].

One theory that was formulated to explain magnetospheric convection was put forth by *Axford and Hines* [1961], who invoked a process they called “a viscous-like interaction”. The term viscous interaction refers to one or more processes that occur in the vicinity of the low-latitude magnetopause that lead to a transfer of magnetosheath momentum across the magnetopause and into the low-latitude boundary layer. In a collisionless plasma, this viscous interaction is presumably due to the action of instabilities on, or near, the magnetopause. One candidate for this is the Kelvin-Helmholtz instability which simulations have shown can occur in the LLBL and can lead to momentum transport from the magnetosheath into the LLBL [*Miura, 1984; Manuel 1992*]. In this scenario, LLBL plasma is forced to move in the antisunward direction and return Earthward through the CPS. The streamlines are equipotentials that, when mapped to the ionosphere (assuming $\vec{E} \cdot \vec{B} = 0$), are qualitatively the same as those shown in Figure 2 [*Axford and Hines, 1961*]. The

defining features of convection driven in this way are the existence of the LLBL (i.e., antisunward flow on closed field lines) and relative insensitivity of convection in that region to changes in the IMF.

Intense currents and regions of large magnetic field energy can arise as a consequence of the motion of plasma in a magnetic field: this is particularly true in regions that separate distinct plasma populations. The Earth's magnetopause is the boundary between the magnetospheric and solar wind plasma populations. As I pointed out above, magnetopause currents arise as a consequence of the motion of the solar wind plasma relative to the magnetosphere. It has been suggested that a process called magnetic reconnection can occur at the boundary between regions containing plasma if the magnetic field in one region is oppositely directed to that in the other and if the plasma in both regions is convecting towards the boundary (see the review by *Sonnerup* [1979] and references therein). In this process, oppositely directed magnetic fields in the interface region add, resulting in a region of low or zero magnetic field strength. Magnetic energy convected into this "reconnection region" with the plasma is converted into kinetic energy of the plasma that in turn jets out of the reconnection region along the boundary separating the two plasma populations. One consequence of this process is a magnetic field component perpendicular to the boundary between the two plasma populations *outside* of the reconnection region. In turn, this means that magnetic field lines extend from one plasma region into the other. *Dungey* [1961] suggested that magnetic reconnection takes place in the region of the Earth's magnetopause. In this scenario, reconnection occurs at a location on the magnetopause that depends on the orientation of the IMF [e.g., *Toffoletto and Hill*, 1986]. One natural consequence of magnetic reconnection at the magnetopause would be the existence of open mag-

netospheric magnetic field lines. If a region of space within the magnetosphere is threaded by open magnetic field lines, then there will be a finite electric field in that magnetospheric region simply because the solar wind plasma is moving (see equation 4). Consequently, there is an electric potential difference applied across the region within the magnetosphere. Thus, assuming that magnetic field lines threading the polar caps are open (there is ample evidence for this [*Lyons and Williams, 1984*]), magnetic reconnection is indirectly the “cause” of the cross-polar cap potential drop. This cross-polar cap potential drop leads to an ionospheric convection pattern qualitatively like that shown in Figure 2 of *Dungey [1961]*. The defining features of magnetospheric convection arising as a consequence of magnetic reconnection at the magnetopause are a strong dependence of convection on the IMF, no LLBL and an electric field parallel to the surface of the magnetopause [*Sonnerup, 1979*].

It is generally accepted that both magnetic reconnection and viscous interaction are important processes driving magnetospheric convection. The existence of the LLBL and the presence of a cross-polar cap potential even when solar wind conditions are unfavorable for reconnection (i.e., prolonged northward IMF) are well documented [*Eastman et al., 1976; Reiff et al., 1981*]. The strong dependence of convection on the IMF is also well documented [*Doyle and Burke, 1983*]. The correlation between the IMF and the cross-polar cap potential led many researchers to conclude that magnetic reconnection is the only process occurring at the magnetopause that leads to large-scale magnetospheric convection [e.g., *Azford, 1969*]; however, a more reasonable conclusion would be that viscous interaction could be responsible for as much as $\sim 20\%$ of the cross-polar cap potential during times of southward IMF and perhaps all of it during times of prolonged northward IMF

(see section by Rostoker in *Wolf et al. [1986]*).

Above, I reviewed observations of plasma convection in the CPS that showed no noticeable dependence of the average convection velocity on Y_{gsm} . There are reasons to suspect that if there is a dependence on Y_{gsm} then the convection velocity in the centre of the tail should be lower than near the flanks of the tail. In a steady state, the convection electric field can be thought of in terms of the distribution of space charge. Assuming ideal MHD applies, using Gauss' law and $\vec{E} = \vec{B} \times \vec{V}$, the space charge can be expressed as

$$\rho_c = \epsilon_o(\mu_o \vec{V} \cdot \vec{J} - B\Omega) \quad (10)$$

Here, Ω is the field-aligned vorticity. The dawn to dusk directed convection electric field in the magnetotail (discussed above) indicates regions of positive and negative space charge on the dawn and dusk flanks, respectively. Considering only the second term in parenthesis in equation 10, the existence of these regions of space charge is consistent with the direction of the magnetic field and that of the vorticity at the dawn and dusk flanks of the CPS. The $\vec{V} \cdot \vec{J}$ term in equation 10 is usually neglected in discussions of magnetospheric space charge. In fact, there are regions in the CPS where one might expect the product $\vec{V} \cdot \vec{J}$ to be large enough for this term to be significant. For instance, on the dawn and dusk sides of the near-Earth CPS, this term gives negative and positive space charge, respectively. We can think of this space charge as a shielding charge, reducing the magnitude of the cross-tail electric field in the central part of the CPS. In global magnetospheric simulations, the convection electric field is either uniformly distributed across the CPS or weaker in the middle than at the flanks of the CPS [*C. Mobarry, private communication*].

Magnetospheric Currents

An expression for the component of the current that is perpendicular to the magnetic field (\vec{J}_\perp) can be obtained from the MHD equation for stress balance. This standard approach is outlined in *Vasyliunas* [1984]. Using

$$\frac{1}{B^2} (\vec{B} \times (\vec{J} \times \vec{B})) = \vec{J}_\perp \quad (11)$$

the transverse current can be extracted from the momentum balance equation:

$$\vec{J}_\perp = \frac{\vec{B} \times \vec{\nabla} P_\perp}{B^2} + \frac{P_\parallel - P_\perp}{B^2} \vec{B} \times [(\hat{b} \cdot \vec{\nabla}) \hat{b}] + \frac{\rho_m}{B^2} \vec{B} \times (\vec{V} \cdot \vec{\nabla} \vec{V}) \quad (12)$$

This expression may also be obtained by calculating the currents due to the differential motions of electrons and ions in the spatially varying magnetic and electric fields. The standard approach is to express the current in terms of the guiding centre motions (i.e., gradient and curvature drifts) as well as gyration of the particles about their guiding centres: the result is the same [*Parker*, 1957]. I will assume, for the sake of clarity, that the pressure is isotropic. This assumption is often justifiable on both experimental and theoretical grounds [*Hill and Voigt*, 1992]. In this case, the second term in equation 12 is zero, and the current is the sum of two contributions. These are due to the first and third terms and are commonly referred to as the diamagnetic and inertial currents, respectively [e.g., *Sato*, 1982]. Throughout most of the CPS and in the ring current region, the inertial current is small relative to the diamagnetic current, and can be neglected while in the LLLB and outer CPS the opposite is true [*Sato*, 1982].

The ring current is carried by geomagnetically trapped particles. In the ring current region, there is a peak in the plasma pressure. Further from the Earth, the pressure gradient points towards the Earth. Closer to the Earth, the opposite is true. The outer ring current then is westward while the inner ring current is eastward.

Under the above assumptions, in the CPS there is only one contribution to the cross-tail current. This is the diamagnetic current that flows from dawn to dusk at the interfaces between the CPS and the lobes (i.e., both north and south). Near the neutral sheet, however, the radius of curvature of the field lines can be small in comparison to the gyroradii of at least some of the ions. For these ions, the guiding centre approximation is not valid. "Non-adiabatic" drifts of these particles can cause currents that are not described by ideal MHD.

Speiser [1970] showed that non-adiabatically drifting ions in the vicinity of the neutral sheet can carry a current. That this is true can be seen by envisioning a plane of zero magnetic field (i.e., a neutral sheet) separating two regions of oppositely directed uniform magnetic field. Charged particles will undergo simple gyrational motion while in the region of uniform magnetic field. Charged particles in the vicinity of the neutral sheet may pass through the neutral sheet. For example, if the region is filled with a monoenergetic gas made up of one type of ion, half of the ions that are within two gyroradii of the neutral sheet will cross it during their orbit. The orbit of any particle that passes through the neutral sheet will be a serpentine path, the particle undergoing part of a gyration first on one side of the sheet, then the other and so on. The net motion of the particle is parallel to the neutral sheet and perpendicular to the background magnetic field. Ions will move in the opposite direction as electrons and therefore a current will flow.

The momentum balance equation does not contain any information, directly, about the parallel component of the field-aligned current; however, using the current continuity equation, information about the divergence of the field-aligned current can be obtained by taking the divergence of the transverse current that, in turn, was obtained from the momentum balance equation. Following the derivation of *Hasegawa and Sato*, [1979] and *Sato* [1982],

$$\vec{\nabla} \cdot \vec{J}_{\parallel} = -\vec{\nabla} \cdot \vec{J}_{\perp} \quad (13)$$

and

$$\vec{\nabla} \cdot \vec{J}_{\parallel} = \frac{2}{B} \vec{J}_{\perp} \cdot \vec{\nabla} B - \rho_m \vec{V} \cdot \vec{\nabla} \frac{\Omega}{B} \quad (14)$$

where I have neglected a term containing the product of the inertial current and the fractional gradient in the plasma density. The ionospheric footprint of the Region II currents is equatorward of that of the Region I currents. Observations outlined above are consistent with the Region I currents being generated in the outer CPS and LLBL. On the other hand, the Region II currents originate in the inner magnetosphere. Thus, the first and second terms on the right hand side of equation 14 are models for the generation of the Region II and Region I currents, respectively.

Using a similar approach, *Vasyliunas* [1970] derived an expression for the field-aligned current at the ionospheric end of a flux tube:

$$J_{\parallel i} = \frac{B_i}{2B_{\text{eq}}^2} \vec{B}_{\text{eq}} \cdot (\vec{\nabla} V_i \times \vec{\nabla} P_{\text{eq}}) \quad (15)$$

where

$$V(s) = \int_{eq}^s \frac{ds'}{B(s')} \quad (16)$$

Here, V_i is $V(s_i)$, and s_i is the distance, along the magnetic field, from the equator to the ionosphere. As well, quantities subscripted with *eq* and *i* are the values of those quantities determined at the equatorial and ionospheric ends of the flux tube, respectively. A complete derivation of equation 15, which is now referred to as “the Vasyliunas equation”, is given by *Heinemann and Pontius* [1990]. The equation is derived by assuming $\vec{J} \times \vec{B} = \vec{\nabla} P$, extracting $\vec{\nabla} \cdot \vec{J}_{\parallel}$ from that equation, assuming $J_{\parallel} = 0$ at the magnetospheric equator and obtaining $J_{\parallel i}$ from $\vec{\nabla} \cdot \vec{J}_{\parallel}$ by using the divergence theorem. It turns out that there is no need to integrate all the way along the flux tube to the ionosphere: the field-aligned current as a function of distance (s) along a field line can be obtained in exactly the same fashion [*Schindler and Birn*, 1978]. The use of the simplified stress balance equation limits the applicability of this equation to the inner magnetosphere where inertial effects are likely not important. Therefore, the Vasyliunas equation is usually taken to be an equation describing only the Region II current system.

Stern [1988] pointed out that, provided the simplified MHD stress balance condition $\vec{J} \times \vec{B} = \vec{\nabla} P$ holds, then the field-aligned current flowing out of the ionospheric end of a flux tube, as given by the Vasyliunas equation, can be determined completely from the magnetic field. Stern’s idea was to use the Vasyliunas equation, in conjunction with a model magnetic field, to infer field-aligned current densities. If the magnetic field configuration is consistent with $\vec{J} \times \vec{B} = \vec{\nabla} P$, then the field-aligned current obtained from applying the Vasyliunas equation will be the same

as that obtained from Ampere's law; however, magnetic field models do not, in general, satisfy even this simple stress balance condition [*Walker and Southwood, 1982*].

It should be recognized that equations 14 and 15 are statements of consistency. For instance, the second term on the right hand side of equation 14 is a mathematical statement to the effect that if there is a gradient in the field-aligned vorticity in the direction of the plasma velocity, then field-aligned currents are generated. It is interesting to explore what physical processes lead to the generation of these field-aligned currents.

The physical mechanisms leading to the generation of the large-scale field-aligned currents are by no means completely understood even though a great deal of theoretical work along these lines has been carried out. For example, from equation 10, it is clear that if there is field-aligned vorticity then there is a net space charge. Increasing the vorticity in a region, or convecting it in, will lead to an increase in space charge in that region. *Sato [1982]* showed that it is possible, through diffusion of vorticity into the LLBL from the solar wind and the subsequent discharging of the excess charge through the ionosphere, to support a steady state Region I current system.

In spite of the observational and theoretical studies I have discussed in this chapter, there remains uncertainty about where Region I currents are generated and how field-aligned currents close. For instance, *Stern [1983]* has shown that it is possible for large scale field-aligned currents of Region I sense to be produced throughout the CPS. As well, flux conservation considerations, applied to *Iijima and Potemra's [1978] results*, indicate that the boundary between the night-side Region I and II currents is roughly 20 R_E away from the Earth [*S. Skone, private*

communication]. The coupling, or closure, of the Region I and Region II currents through the magnetosphere is also not well understood. For instance, it is not clear whether results indicating a meridional connection between the Region I and Region II currents [*Ohtani et al.*, 1990] and an azimuthal connection between the dawn and dusk Region II currents [e.g., *Roelof*, 1989, *Zanetti et al.*, 1991] apply to part (i.e. the substorm expansion phase associated part), or all, of the field-aligned current circuit.

2. Time Independent Magnetospheric Magnetic Field Models

One of the main problems in space physics is that of magnetosphere-ionosphere coupling, which relates directly to how particles, electromagnetic waves and electrostatic waves make their way from the outer magnetosphere to the ionosphere and vice versa. More specifically, much attention has been given to the identification of the magnetospheric sources of auroral particles and the large scale field-aligned currents. Knowledge of the average, typical and time-dependent topology of the magnetospheric magnetic field is of fundamental importance to our understanding of both of these phenomena.

Static magnetic field models are an important tool in magnetospheric physics. Several methods are used to develop these models. One is to solve, either numerically or analytically, the equations that are thought to govern the system. Another approach is to measure the magnetic field at locations throughout the magnetosphere and to develop analytical magnetic field models that fit, as closely as possible, these measurements. A third technique is to use a simple field model that corresponds to a clearly specified current system. Models developed using these approaches are referred to as physical, empirical or *ad hoc*, respectively.

An important use of these models is mapping, along magnetic field lines, from the ionosphere to the magnetosphere and vice versa. These mappings require a magnetic field model that is as realistic as is presently possible. Due to this requirement, virtually all mappings are carried out using empirical models [e.g., *Lopez et al.*, 1990; *Elphinstone et al.*, 1991; *Pulkkinen et al.*, 1991] although some studies involve the use of an existing empirical model that has been modified by the addition of an *ad hoc* model field [e.g., *Pulkkinen*, 1991]. Empirical models have also been used in attempts to provide a more global perspective of magnetosphere-

ionosphere coupling [e.g., *Stern and Alexeev*, 1988; *Birn et al.*, 1991]. Furthermore, these models have been used to provide a “realistic” magnetic field in theoretical studies. For instance, *Erickson and Wolf* [1980] and *Kivelson and Spence* [1988] have used empirical models in attempts to address the question of the stability of the magnetotail and the possibility of “steady-state” magnetospheric convection.

Empirical Magnetospheric Magnetic Field Models: A Brief Review

An empirical magnetospheric magnetic field model typically consists of a sum of vector functions

$$\vec{B}_{\text{model}}(\vec{R}) = \sum_{i=1}^N \vec{f}_i(\lambda_i^1, \dots, \lambda_i^{M_i}; \vec{R}) \quad (17)$$

where the individual functions (\vec{f}_i) are chosen to represent the contribution to the magnetic field due to terrestrial sources and various extra-terrestrial sources including the ring current, cross-tail current, magnetopause currents and field-aligned currents. The constants λ_i^j are selected so that the model satisfies either appropriate boundary conditions or a chosen criterion of “best fit” to a large data base of magnetic field measurements. As well, some basic physical constraints (such as $\vec{\nabla} \cdot \vec{B}_{\text{model}} = 0$) are usually imposed on the model. Due to the complicated nature of the magnetospheric current system, the real challenge in the development of realistic models is the selection of the functions, \vec{f}_i .

Generally, the model field is separated into a contribution due to sources inside the Earth ($\vec{B}_{\text{terr}}(\vec{R})$) and sources external to the Earth ($\vec{B}_{\text{ext}}(\vec{R})$):

$$\vec{B}_{\text{model}}(\vec{R}) = \vec{B}_{\text{terr}}(\vec{R}) + \vec{B}_{\text{ext}}(\vec{R}) \quad (18)$$

Furthermore, the field due to extraterrestrial sources is typically separated into contributions due to the ring current, Chapman-Ferraro currents, cross-tail current (with closure on the magnetopause) and field-aligned currents (with closure in the magnetosphere and in the ionosphere):

$$\vec{B}_{\text{ext}}(\vec{R}) = \vec{B}_{\text{rc}}(\vec{R}) + \vec{B}_{\text{cf}}(\vec{R}) + \vec{B}_{\text{ct}}(\vec{R}) + \vec{B}_{\text{fa}}(\vec{R}) \quad (19)$$

These divisions are somewhat arbitrary. As discussed in the introduction, both the Chapman-Ferraro currents and the closure of the cross-tail current are *magnetopause* currents. Furthermore, at least some of the closure of the field-aligned currents through the magnetosphere is, in fact, part of the cross-tail and ring current systems. As well, the ring and cross-tail currents overlap in the inner magnetosphere. One motivation for breaking up the external field (and hence magnetospheric currents) in this way is to force the currents associated with each of the four contributing magnetic fields to be divergence free. That is, the currents consistent with each of these magnetic fields can be constructed out of closed circuits.

The Magnetic Field due to Sources Inside the Earth

Work aimed at the development of accurate models of the Earth's magnetic field has been carried out for centuries. Indeed, it was Carl Friedrich Gauss who first developed the mathematical representation for the terrestrial magnetic field and who, with Wilhelm Weber, founded a worldwide network of magnetic observatories with the objective of estimating the coefficients in the spherical harmonic expansion below (see the historical review by *Stern* [1989]). Any realistic magnetospheric magnetic field model must contain a contribution due to the terrestrial magnetic

field. Therefore, while their development is a research area quite separate from the development of magnetospheric models, a brief review of the topic of terrestrial magnetic field models is appropriate here. The thorough technical review on the subject of modelling the terrestrial magnetic field given by *Langel* [1987] is the primary source of the information presented in the following two paragraphs.

The magnetic field due to sources within the Earth is curl free in regions of interest here. As such, it is typically modelled using the gradient of a scalar function

$$\vec{B}_{\text{terr}} = -\vec{\nabla}\phi_{\text{terr}} \quad (20)$$

where, since $\vec{\nabla} \cdot \vec{B}_{\text{terr}} = 0$,

$$\nabla^2\phi_{\text{terr}} = 0 \quad (21)$$

everywhere above the Earth's surface. The scalar potential, being a solution of Laplace's equation, can be expressed as an infinite series of spherical harmonics:

$$\phi_{\text{terr}}(r, \theta, \phi) = a \sum_{n=1}^{\infty} \sum_{m=0}^n (g_n^m \cos(m\phi) + h_n^m \sin(m\phi)) \left(\frac{a}{r}\right)^{n+1} P_n^m(\theta) \quad (22)$$

where $P_n^m(\theta)$ is the Schmidt quasi-normalized associated Legendre function [e.g., *Langel* 1987]. A number of empirical models consisting of truncated versions of the series in equation 22 have been developed. The coefficients g_n^m and h_n^m are selected by fitting the model magnetic field to a large data base of measurements from ground based and plane and satellite borne magnetometers. Complications arise because the terrestrial field, and hence the appropriate coefficients, are slowly

varying in time. The most commonly used of these models is the International Geomagnetic Reference Field (IGRF) model (see *IAGA Commission 2 Working Group 4* [1969]). The order (n) of the published model is limited by uncertainty in the measurements, the computational difficulty involved in extracting accurate coefficients from the data and data coverage. The IGRF model is updated on a 5 year basis. Currently, the order of the most recent version of the model is $n = 10$ [*IAGA Division V*, 1991]. The published IGRF model provides a magnetic field value in geographic coordinates. In geographic coordinates, the polar angle θ is the colatitude and the azimuthal angle ϕ is the longitude (East).

Often, it is enough or even preferable to use an Earth centred dipole magnetic field as a model of the terrestrial magnetic field. One dipole magnetic field model can be obtained by truncating the IGRF model at $n = 1$:

$$\vec{B}_{\text{terr}} = -\vec{\nabla} \frac{a^3}{r^2} (g_1^0 \cos \theta + (g_1^1 \cos \phi + h_1^1 \sin \phi) \sin \theta) \quad (23)$$

This is the magnetic field of an Earth centred magnetic dipole with dipole moment \vec{m} given in cartesian geographic coordinates by

$$(m_x, m_y, m_z) = a^3(g_1^1, h_1^1, g_1^0) \quad (24)$$

The strength of the IGRF dipole was $\sim 31225 \text{ nT R}_E^3$ in 1945 and $\sim 30435 \text{ nT R}_E^3$ in 1985 [*IAGA Division V*, 1991].

*The Magnetic Field due to Distributed Intramagnetospheric
and Magnetopause Currents:
Three Types of Empirical Magnetospheric Magnetic Field Models*

There has been a variety of techniques used to model the magnetic effects of magnetospheric current systems. In this section, I will briefly review some of these techniques. As well, I will describe three previously developed empirical magnetic field models, those of *Olson and Pfitzer* [1974], *Mead and Fairfield* [1975] and *Tsyganenko* [1987]. Each of these models have been extensively used in space physics research and have been, at least in their time, considered to be “state of the art”.

The magnetic field due to the Earth’s ring current can be modelled in a number of ways. For instance, *Akasofu and Chapman* [1961] developed a model of an azimuthally symmetric ring current by examining the guiding centre and gyration motions of trapped particles in a dipole field. Their model relies on knowledge of the particle energy and pitch angle distributions in the equatorial plane. The magnetic field is calculated by applying the Biot-Savart law. The $\vec{J} \times \vec{B}$ force, obtained using their model current and the dipole magnetic field, was consistent with the forces due to pressure gradients in the plasma from which they determine the currents. The same is not true if the perturbed magnetic field (i.e., that of the model ring current and the dipole) is used. *Akasofu et al.* [1961] carried this calculation to second order, using particle motions in the perturbed magnetic field to calculate new currents, from which a new magnetic field is determined.

The approach of *Akasofu et al.* [1961] is satisfying from the point of view of self consistency of the perturbed magnetic field and the particles that carry the current; however, this approach is computationally intensive, especially if the

perturbed magnetic field is due to a more realistic terrestrial field, the ring current as well as the magnetopause, tail and field-aligned currents. *Olson* [1974] uses a set of elliptical, infinitesimally thin current loops to model the ring current. The magnetic field due to these current loops is calculated by direct Biot-Savart law integration. The method is better than that of *Akasofu and Chapman* [1961] from the standpoint of computational efficiency; however, the current density is either infinite or zero and the magnetic field becomes infinite in the vicinity of the wire loops. Thus, stress balance considerations cannot be addressed with this model. As well, the evaluation of the magnetic field due to even this simple current configuration was too computationally demanding in 1974 for this direct integration model to be used. Pragmatism has led to a different approach: often, a modeller will use a simple azimuthally symmetric function to represent the ring current magnetic field. The function is chosen so that the current flow lines are concentric circles in the magnetic equatorial (i.e., sm system) plane, with most of the current between ~ 5 and $\sim 8 R_E$ from the Earth. For example, *Tsyganenko* [1987] uses the following function to model the ring current magnetic field (in sm cylindrical coordinates) for $Kp = 0$:

$$(B_\rho, B_\phi, B_z) = \frac{C(3\rho z, 0, 2Z^2 - \rho^2 + 214.7)}{(\rho^2 + Z^2 + 107.3)^{\frac{5}{2}}} \quad (25)$$

Here, C is a constant and ρ and Z are in R_E . While this approach is very “user friendly”, there is no hope of satisfying stress balance considerations with such a simple function. For instance, examining the curl of the model magnetic field above, the associated current is everywhere westward while, in reality, stress balance dictates that there must be an inner ring current which is eastward.

Models of the magnetic field due to the Chapman-Ferraro currents generally fall into one of three categories. The first of these involves the use of the method of images. The magnetic field due to an image dipole that is parallel to and of equal, or larger strength than the terrestrial dipole is added to the magnetic field of the terrestrial dipole. *Chapman and Ferraro [1930]* added the magnetic field of a dipole of equal strength to the terrestrial dipole. In this case, the plane half way between the dipoles and normal to the line joining the dipoles has zero magnetic flux crossing it. This plane is the “magnetopause” in their model. *Hones [1963]* used an image dipole with a dipole moment 28 times that of the Earth, located $28 R_E$ in the sunward direction. The sum of the image and terrestrial dipole fields results in a “magnetosphere” that is roughly ellipsoidal in shape (see Figure 1 in *Hones [1963]*), roughly $30 R_E$ in length and with a subsolar point $7.5 R_E$ from the Earth. Here, the term magnetosphere refers to the cavity that contains all magnetic field lines that can be traced back to the Earth. In this model, the magnetic field due to the Chapman-Ferraro currents is just the magnetic field, within the magnetosphere, due to the image dipole. This approach is computationally efficient and will give a reasonable magnetic field due to Chapman-Ferraro currents in the vicinity of the Earth (see, for example, *Lui [1978]*); however, the shape of the model “magnetopause” is completely dictated by the choice and location of the image dipole and is not, in any way, determined by the interaction of the solar wind with the magnetospheric magnetic field.

A second technique to model the magnetic effects of the Chapman-Ferraro currents is to prescribe a magnetospheric boundary and use the fact that the magnetic field inside the boundary due to the Chapman-Ferraro currents is curl-free and therefore can be expressed as the derivative of a scalar potential that is a solution of

Laplace's equation. The appropriate potential is found by solving Laplace's equation with the Neumann boundary condition. That is, the component of the total field normal to the magnetopause (zero for a closed magnetosphere) is stipulated, which in turn gives the component of the magnetic field due to Chapman-Ferraro currents normal to the magnetopause. The primary difficulty with this approach is developing a model with a realistic magnetopause surface: in practice, solutions have been obtained in cavities bounded by magnetopauses with some standard cross-section. For example, *Voigt* [1981] used this approach to develop a model of the magnetic field due to Chapman-Ferraro currents on a model magnetopause consisting of a hemisphere on the dayside and an infinite cylinder on the nightside. The scalar potential is expressed in terms of spherical harmonics on the dayside and Bessel functions on the night side. *Stern* [1985] uses a magnetopause that is a paraboloid of revolution. The scalar potential is expanded in terms of parabolic harmonics. Again, this approach is capable of giving reasonable magnetic field values throughout the inner magnetosphere. It too, however, leads to model magnetopauses that are not realistically shaped. For instance, *Voigt's* [1981] nightside magnetopause is a non-flaring cylinder, while theoretical [e.g., *Coroniti and Kennel*, 1972] and empirical studies [e.g., *Sibeck et al.*, 1991] indicate that the magnetotail must flare.

The third technique in general use to model the magnetic effects of the Chapman-Ferraro currents is to use the Biot-Savart law to calculate them directly. This approach has been used by a number of researchers and involves the selection of a magnetopause surface, determination of currents on that surface and the evaluation of the Biot-Savart law integral. The advantage of this approach is the ability to select a magnetopause surface by applying some physical condition or condi-

tions at that surface. For instance *Mead and Beard* [1964] determined this surface by balancing solar wind dynamic pressure with magnetic field pressure just inside the boundary. To start with, they estimate this magnetic pressure by assuming the magnetic field strength just inside the boundary is twice the component of the dipole field parallel to the boundary. The surface current density is then determined by assuming the magnetic field just outside the surface is zero. The next step is to repeat the procedure, using the sum of the terrestrial dipole and magnetopause current magnetic fields to estimate the field strength just inside the magnetopause to determine a “second” surface and so on. The ultimate criterion, one which *Mead and Beard* [1964] claim is extremely well met after only several iterations, is that the magnetic field outside of the magnetosphere due to magnetopause currents and the terrestrial dipole is small compared to that due to the dipole alone. More recently, *Olson* [1969] used the approach of *Mead and Beard* [1964], in conjunction with an improved method of evaluating the Biot-Savart law integral, to calculate the magnetic field due to the Chapman-Ferraro currents for situations where the terrestrial dipole is not perpendicular to the solar wind direction.

Models of the magnetic field due to the cross-tail current usually involve evaluation of the Biot-Savart law integral for current distributions that match, as closely as is reasonable, the actual cross-tail current distribution. The real limitation here is the inability to evaluate the Biot-Savart law integral for all but the simplest current systems. *Olson* [1974] models the cross-tail current system with a large number of “D” shaped infinitesimally thin current loops. Using two “D” shaped elements, one element of a theta shaped current is constructed. The tail field is due to a large number of these theta shaped current elements. This approach leads to a current free lobe, realistic lobe field variation with distance down tail and in

the model region corresponding to the CPS, except in the vicinity of the current elements, where the magnetic field becomes infinite. *Tsyganenko* [1987] uses two steps to model the magnetic field due to the cross-tail currents. The first is to evaluate the Biot-Savart law integral to determine the magnetic field due to three current sheets that extend infinitely in the dawn-dusk direction and in the antisunward direction. The current sheets are in the equatorial plane and $30 R_E$ above and below the equatorial plane (the sheets at $\pm 30 R_E$ are included to avoid infinities in the northward component of the magnetic field and represent the closure current on the magnetopause). The current sheets are of finite thickness and the current density peaks in the equatorial plane and falls off monotonically with distance from it. The currents flow parallel to the Y_{gsm} direction. Their inner edge is roughly $3 R_E$ from the Earth. The dawn-dusk (Y_{gsm}) component of the magnetic field due to these sheets is zero. As well, the X_{gsm} and Z_{gsm} components are independent of Y_{gsm} . To allow for finite B_y and to limit the effects of these currents in the Y_{gsm} direction, the magnetic field is multiplied by a taper function:

$$f(Y_{gsm}) = \frac{1}{\pi} \left(1 + \left(\frac{Y_{gsm}}{\Delta y} \right)^2 \right)^{-1} \quad (26)$$

Here Δy is about 1/2 the dawn-dusk scale size of the cross-tail tail current system and is $\sim 15 R_E$. The final model field is then

$$\vec{B}_{ct} = f(Y_{gsm})(B_x^{\circ}(X_{gsm}, Z_{gsm}), 0, B_z^{\circ}(X_{gsm}, Z_{gsm})) \quad (27)$$

where \vec{B}° is the magnetic field due to the infinite sheets. This model of the tail current magnetic field has advantages and, as I show below, several disadvantages.

As I discussed above, a global empirical magnetospheric magnetic field model is intended to represent the magnetic effects of all intramagnetospheric and magnetopause currents. In this paragraph I describe three such models, each of which have been extensively used by the space physics community. *Olson and Pfitzer* [1974] used the ring, cross-tail and magnetopause current models of *Olson* [1969,1974] discussed above to model the total magnetospheric magnetic field. The model parameters were adjusted so that the model field fits, as closely as possible, a data base of *in situ* measurements. They then used the “wire model” to calculate the magnetic field at a large number of points within the magnetosphere. A vector field, each component of which is an expansion of polynomials in cartesian gsm coordinates was then fit to the wire model magnetic field values. This vector field is the final “Olson-Pfitzer” model. This model does not allow for various activity levels or for dipole orientations not parallel to the Z_{gsm} axis. *Mead and Fairfield* [1975] avoided the difficulties associated with the wire model approach by least squares fitting a data base to a vector field, the components of which are, again, polynomials. Their data set consisted of $\sim 12,000$ IMP magnetic field measurements, each measurement an average of the satellite magnetometer output over $1/2 R_E$ of the satellite path. They derived four models from data in four different activity ranges (as quantified by Kp). These four models also include a dependence on dipole tilt. *Tsyganenko* [1987] fit the sum of his model ring and cross-tail current magnetic fields as well as a vector polynomial function to a data set consisting of $\sim 37,000$ *in situ* magnetic field measurements. The data are from IMP and HEOS satellites. Again, each measurement is an average along $1/2 R_E$ of the satellite track. Six models were derived by binning the data in six different activity ranges (again activity as quantified by Kp). As well, the T87 models include dipole tilt dependence.

(A more recent *Tsyganenko* [1989] model, the T89 model, incorporates the same ring current and polynomial magnetic fields as well as the magnetic field due to a cross-tail current sheet that consists of current flowing along Earth-centred circular arcs).

The survey of magnetic field models and modelling techniques that I have provided here is quite brief. An extensive review of the subject is given by *Tsyganenko* [1990]. I would like to conclude this section with a philosophical note. A great deal of effort has been expended to derive models of magnetic fields due to magnetospheric currents. In the end, however, the most widely used models either consist of, or incorporate, a vector field with polynomial components. The usefulness of a model is directly related to both ease of use and reasonableness of the magnetic field values. The almost universal usage of the three models discussed in the previous paragraph is partially due to ease of implementation and use. It is also due, however, to the lack of any alternative magnetic field models (i.e., that might better satisfy any number of physical criteria) that provide demonstrably *better* magnetic field values.

Testing Global Models of the Magnetospheric Magnetic Field

The complicated nature of the sources of extraterrestrial magnetic field dictates that the functions used in empirical magnetic field models are themselves quite complex. Accordingly, the testing of these models to determine their validity is a laborious task involving trial and error procedures. *Fairfield* [1991] evaluated the T87 model magnetic field using a large number of *in situ* measurements of the magnetic field. He concluded that while the model agrees well with the observations, the model field is not “stretched” or “taillike” enough in the near-Earth

nightside magnetosphere. While no such comparison is currently available for the T89 model, *Tsyganenko* [1989] presented a compilation of values of the magnetic field inclination angle at geosynchronous orbit measured by *Lin and Barfield* [1984] using the GOES 2 spacecraft. He compared these measured inclination angles with those inferred with the T87 and T89 models to show that the T89 model is an improvement over the T87 model in this regard.

An interesting test of empirical models that has been suggested by *Walker* [1976] and *Voigt* [1986] is to determine if the model magnetic field satisfies a stress balance condition. There has been work done along this line [e.g., *Walker and Southwood*, 1982; *Kivelson and Spence*, 1988]; however, we do not currently know if the magnetosphere is even in equilibrium [e.g., *Erickson and Wolf*, 1980; *Voigt and Wolf*, 1988]. Even if the magnetosphere is in equilibrium, we do not know what the actual stress balance relationship should be or if it is possible to write down a tractable stress balance relationship that is globally applicable. Furthermore, there is a problem in determining the “average” $\vec{J} \times \vec{B}$ force from the average magnetic field due to the nonlinear dependence of this force on the magnetic field and the fact that even though the relationship between \vec{J} and \vec{B} (in time independent situations) is linear in reality, if the data from which the model average values are derived are not uniformly distributed in both time and space, then $\langle \vec{J} \rangle$ is not given by $\mu_0 \vec{\nabla} \times \langle \vec{B} \rangle$.

In this section, I explore four aspects of the T87 and T89 model magnetic fields. In a sense, this can be considered an application of four tests to these models. The results of these tests point out shortcomings in the models. I conclude this chapter with a discussion of how these shortcomings are my motivation for developing a new type of magnetic field model. I have chosen the T87 and T89 magnetic field

models to examine because, at the present time, they (primarily the T87 model) are the most widely used magnetospheric magnetic field models. Like all models, they have shortcomings. Focussing on some of these shortcomings should not be considered as mere criticism of what are, arguably, the best magnetospheric models available today.

T87 Cross-Tail Current

The T87 magnetic field model contains a contribution due to a model cross-tail current system, as described above. It is reasonable to explore how well this model current system matches the actual cross-tail current system. The use of the taper function $f(Y_{\text{gsm}})$ as discussed above changes the magnetic field due to the infinite current sheets. Consequently, to study the model cross-tail current it is necessary to evaluate the curl of the modified (by the taper function) magnetic field. I do this analytically by determining the appropriate derivatives and, as a check, by using finite difference techniques. In the following paragraphs, “model cross-tail current” refers to $\mu_0 \vec{\nabla} \times \vec{B}_{\text{ct}}$, where \vec{B}_{ct} is the $Kp = 3$ T87 cross-tail current magnetic field.

Figures 6a and 6b are contour plots of the Y_{gsm} and Z_{gsm} components of the T87 model cross-tail current in the plane $X_{\text{gsm}} = -25 R_E$. I show model cross-tail current line traces, projected into the $X_{\text{gsm}} = -25 R_E$ plane, in Figure 7. The start points for each trace are at $X_{\text{gsm}} = -25 R_E$, $Y_{\text{gsm}} = 0$ and at Z_{gsm} values separated by $1 R_E$ intervals ranging from $-6 R_E$ to $6 R_E$. I have traced the current lines outwards in both directions from the start points. Perhaps the most striking feature of these figures is the diversion of cross-tail current out of the equatorial plane in the $\pm Z_{\text{gsm}}$ direction. All of the *actual* cross-tail current does divert and closes over the northern and southern lobes. At $25 R_E$ down the magnetotail, the

magnetosphere has a nearly circular cross-section of radius $\sim 23 R_E$. From the current line traces in Figure 7, it appears that at least some of the model cross-tail current is diverting *through* the region of space that, in reality, contains the magnetospheric lobes. This diversion of model cross-tail current is a consequence of the use of the flaring function $f(Y_{gsm})$. Below, I discuss three questions regarding the cross-tail current that are important for users of the T87 model.

First, what fraction of the model cross-tail current diverts and flows through the region of space corresponding to the magnetotail lobes? One way to quantitatively answer this question is to calculate model current fluxes through the surfaces of a rectangular box. The rectangular box I will use for this is of length L along the X_{gsm} direction. The two "end" surfaces are in the planes $X_{gsm} = -25 R_E \pm L/2$. The four corners of both of the two end surfaces are at $(Y_{gsm}, Z_{gsm}) = (0, 0)$, $(0, 10 R_E)$, $(21 R_E, 10 R_E)$ and $(21 R_E, 0)$. I place a corner of the end surfaces at $(Y_{gsm}, Z_{gsm}) = (21 R_E, 10 R_E)$ because a $23 R_E$ radius magnetopause would pass roughly through this point. The four "side" surfaces of the rectangular box are in the $Y_{gsm} = 0$, $Y_{gsm} = 25 R_E$, $Z_{gsm} = 0$ and $Z_{gsm} = 10 R_E$ planes. The model cross-tail current enters the box through the $Y_{gsm} = 0$ side. Provided that $L \leq 1 R_E$, the current flux across this surface is

$$I \simeq L \times \int_{Z_{gsm}=0}^{Z_{gsm}=10R_E} J_y(-25R_E, 0, Z_{gsm}) dZ_{gsm} \quad (28)$$

This current is roughly $L \times 17 \text{ mA/m}$. The flux through the Z_{gsm} side is identically zero ($J_z = 0$ in the equatorial plane). I estimate the flux through the $Z_{gsm} = 10 R_E$ and $Y_{gsm} = 21 R_E$ sides by evaluating integrals similar to that in equation 28. The net fluxes through these surfaces are out of the box and are $L \times 8 \text{ mA/m}$ for the

$Z_{gsm} = 10 R_E$ side and $L \times 9 \text{ mA/m}$ for the $Y_{gsm} = 21 R_E$ side. Thus, slightly less than half of the model cross-tail current diverts through the region corresponding to the lobe and slightly more than half flows out of the region of space that would, in reality, be the magnetosphere. A small fraction (~ 0.04) of the current entering the box through the $Y_{gsm} = 0$ side leaves the box through the two ends.

Second, is it reasonable to think of this diverted current as a good representation of the actual closure currents? The amount of cross-tail current that has diverted out of the equatorial region within the volume of space occupied by the actual magnetosphere is only half of the total cross-tail current. Furthermore, this diverted current does not flow around the lobes, but through them. This is clear from both Figure 7 and from the fact that the Z_{gsm} component of the model cross-tail current maximizes at $Y_{gsm} = \Delta y / \sqrt{3}$. This is roughly at $Y_{gsm} = 11.6 R_E$, well inside of where the actual magnetopause is. I must conclude that the answer to this question is that the diverted current is not a good representation of the added closure currents.

Third, what are the consequences of the differences between the model and actual cross-tail current system? In reality, the entire cross-tail flows across the equatorial region and closes around the magnetospheric lobes. It is clear that the model cross-tail current does not do this. Several consequences of this discrepancy can be found by looking at the model magnetic field, specifically the entire $Kp = 3$ T87 model magnetic field, including the field due to the terrestrial dipole. Figure 8 is a contour plot of the magnitude of the sum of the model magnetic field and an appropriate terrestrial dipole field on the surface $X_{gsm} = -25 R_E$. The contours are separated by 2 nT intervals, starting at 10 nT. The peak magnetic field strength in the region corresponding to the magnetospheric lobes is $\sim 23 \text{ nT}$. At $Z_{gsm} \sim 13 R_E$,

the magnetic field is largest in the centre of the tail and falls off with increasing Y_{gsm} . This variation of $|\vec{B}|$ within the magnetotail is due to the unrealistic closure model cross-tail current through the lobes; therefore, the variation is unrealistic.

In Figure 8, the lack of concentrated closure current on the magnetopause in the model is obvious: there is no boundary beyond which the model magnetic field is small. In reality, the closure currents contain the lobe field within the magnetotail. If the magnetosphere is closed, then the magnetic field just inside the magnetopause current layer will be parallel to that surface. In this case,

$$\frac{|YB_y + ZB_z|}{|B_x|\sqrt{Y^2 + Z^2}} = -\frac{aR}{dX_{\text{gsm}}} \quad (29)$$

where the magnetic field is that just inside the magnetopause and R is the radius of the magnetopause in an $X_{\text{gsm}} = \text{constant}$ plane. An estimate of the derivative on the right hand side of the above equation can be obtained from the empirical model of magnetopause radius of *Sibeck et al.* [1991]. Using their model for intermediate solar wind pressure ($1.47 \text{ nPa} < P < 2.60 \text{ nPa}$), at $X_{\text{gsm}} = -25 R_E$ this derivative is 0.23. For all of their models (5 pressure and 6 IMF ranges), this derivative falls between 0.16 and 0.28. As well, the tail flaring function of *Coroniti and Kennel* [1972] gives a value of 0.23 for this derivative. The quantity on the right hand side of equation 29 can also be determined from the T87 model, and the values calculated in the region where the actual magnetopause would be expected to be are plotted in Figure 9. These values were determined on a circular arc $24 R_E$ radius, from $Y_{\text{gsm}} = 0$ to $Y_{\text{gsm}} = 20 R_E$. It is clear that, while the values so obtained are reasonable around $Y_{\text{gsm}} = 0$, they are too large for larger Y_{gsm} values. Thus, the shape of the model field lines in this region is not realistic: they do not flare in

a way that corresponds to a realistic solar wind-magnetosphere interaction. The reason for this is the lack of realistic closure of the cross-tail current in the model.

In the previous paragraphs, I have focussed on the closure of the cross-tail current; however, the model cross-tail current differs from the actual one in other ways, as well. These differences are important for both mapping and stress balance considerations. For instance, the model cross-tail current strength decreases monotonically with increasing distance from the equatorial plane. There is, however, no reason to expect this to actually be the case. One reason why this might not be true is the existence of the diamagnetic current at the high-latitude edge of the CPS (as discussed in the introduction). In fact, *Olson and Pfitzer [1974]* found that in order to best represent the data with their model, the cross-tail current needed to be divided into two parts, one concentrated in the equatorial plane and the other several R_E above (and below) the equatorial plane.

T87 Field-Aligned Currents

Empirical models are data-based and there is some expectation that the magnetic effects of the field-aligned currents will be, at least partially, already included in these models; however, there are several reasons why the magnetic effects of the global field-aligned current system are probably not included in the T87 model. First, the averaged data set on which the model is based is unlikely to contain a realistic contribution due to the global system of field-aligned currents flowing in the magnetotail [*G. Rostoker*, private communication]. This is a consequence of the fact that the average magnetic field at a given location in geocentric solar-magnetospheric (gsm) coordinates determined from a data set, regardless of how the data is binned in terms of geomagnetic activity (i.e., Kp , AE etc.), will be

based on data from a variety of real activity levels. As well, thickening and thinning of the CPS and flapping of the magnetotail itself will lead to motion of the field-aligned current layers. Thus, for grid points near the high-latitude edge of the plasma sheet where the field-aligned currents are thought to flow, the actual field-aligned currents are as likely to flow above the observation point as below. Accordingly, over a large data set, some of the effects of the field-aligned currents will cancel out and the data points representing the averaged magnetic field values will not reflect the true size of the contributions of the field-aligned currents for any individual event. Second, the polynomial function used in the Tsyganenko models allows for a better fit to the data set used than would a model employing the model ring and tail currents alone. One way of looking at this is that the data-fitting technique will obtain values for the parameters associated with the polynomial functions in the model that are chosen in response to the difference between the sum of the best-fit model ring and tail currents and the actual average magnetospheric current system. Stating that the polynomial function models the effects of the field-aligned currents is to tacitly assume that this difference is almost entirely the average field-aligned current system. If this were demonstrably true, then the statement would be reasonable. As discussed above, however, there are a number of differences between the T87 model cross-tail current and the actual cross-tail current expected on the basis of magnetic field and particle measurements in the CPS and magnetotail lobes. Third, typical scale sizes of the current systems in the Tsyganenko magnetic field model range from several to tens of Earth radii. Therefore, it is not possible for the functions to adequately represent the magnetic effects of relatively thin ($\sim 1R_e$) current sheets, especially in the inner magnetosphere.

There is another, more subtle, reason why the global distribution of model field-aligned currents generally should be regarded as an artifact of the modelling procedure. Almost all existing magnetic field models have distributed magnetospheric current systems. In the development of all of these, there has been no attempt made to constrain the current systems so that the current is exactly transverse to the magnetic field [e.g., *Olson and Pfitzer, 1974*]. Indeed, this constraint would, in general, be unreasonable to impose. For example, the model magnetic field of *Mead and Fairfield [1975]* is a vector function, the components of which are second-order (at most) polynomials in the cartesian coordinates X_{gsm} , Y_{gsm} , and Z_{gsm} . The model is parameterized according to dipole tilt and geomagnetic activity. The coefficients are determined by least-squares fitting to a set of magnetic field measurements. If the terrestrial magnetic field is represented by a dipole and both the dipole tilt and the model field-aligned current are constrained to be zero (i.e. require $\vec{B} \cdot \vec{\nabla} \times \vec{B} = 0$), then it can be shown that the only possible non-trivial form for the polynomial functions gives

$$\vec{\nabla} \times \vec{B} = A(\rho)\hat{\phi} \quad (30)$$

where $A(\rho)$ is some scalar function of $\rho = \sqrt{X^2 + Y^2}$ and $\hat{\phi}$ is the unit vector in the azimuthal direction. This is a current distribution with current lines that are circles in planes of constant Z centered on the Z -axis. The only intramagnetospheric model currents would be azimuthally symmetric; therefore, only the magnetic effects of a ring type current could be modelled. If non-zero dipole tilt angles are allowed for and the model currents are constrained to be transverse to the model magnetic field, it can be shown that the only possible non-trivial form

of the polynomial functions gives

$$\vec{\nabla} \times \vec{B} = 0 \quad (31)$$

Constraining the field-aligned component of the model current to be zero everywhere for arbitrary dipole tilt angles forces the model current to be zero everywhere. Thus, if the magnetic effects of intramagnetospheric currents are modelled with the functions chosen by *Mead and Fairfield* [1975], there will be a field-aligned component of the model current. This is true for almost all empirical models. Exceptions are models like that of *Williams and Mead* [1965], where both symmetry and simplicity of the model (their model consists of a dipole with zero tilt and an infinitely thin current sheet on the equatorial plane) allow for a current distribution with zero field-aligned component everywhere. It is important to realize that such asymmetries in the magnetosphere do not demand the presence of real field-aligned currents. The key point here is that when simple functions are used to model the magnetic effects of distributed magnetospheric currents, the model currents will not, in general, be transverse to the model magnetic field. It is difficult to draw conclusions about the real field-aligned current distribution, based on such a model, because there will be model field-aligned currents regardless of whether or not the magnetic effects of field-aligned currents are actually present in the data.

In light of the argument presented above, it is interesting to look at the field-aligned component T87 model current system. According to Ampere's law, the field-aligned component of the current is

$$J_{\parallel} = \frac{1}{\mu_0} \frac{\vec{B} \cdot (\vec{\nabla} \times \vec{B})}{B} \quad (32)$$

In discussing the field-aligned currents in the magnetosphere it is customary to “normalize” the values of the field-aligned current obtained from equation 32 to what they would be if the current were to flow without diversion along a flux tube from where the current value is determined to the ionospheric footpoint of the field line passing through this point:

$$J'_{\parallel} = \frac{B_i}{B} J_{\parallel} \quad (33)$$

This quantity, J'_{\parallel} , is the amount of current, at the location where the field-aligned current is determined, that is contained in a flux tube having an ionospheric cross-sectional area of 1 m^2 . Figures 10 and 11 are contour plots of J'_{\parallel} on the $X_{\text{gsm}} = -6.73 R_E$ and $X_{\text{gsm}} = -25 R_E$ surfaces. The magnetic field I use here is the T87 $Kp = 3$ model. The contour plots in Figure 10 illustrate that in the model there is large scale Region II sense model current further from the equatorial plane than large scale Region I sense model current in the near-Earth region and large scale Region II sense model current distributed throughout the entire cross-section of the magnetotail $25 R_E$ from the Earth. The patterns present in these figures are not consistent with those expected, based on either an extension of accepted low-altitude field-aligned current patterns into the night-side magnetotail or observations of Region I sense current in the PSBL (see introduction).

It is also interesting to look at how J'_{\parallel} varies along a magnetic field line. The solid curve in Figure 12 is a plot of J'_{\parallel} determined by applying Ampere’s law to the $Kp = 3$ T87 model field, along a field line that starts in the equatorial plane at $(X_{\text{gsm}}, Y_{\text{gsm}}) = (-8 R_E, -11 R_E)$ and has its ionospheric footpoint in the northern hemisphere ($s = 0$ corresponds to the equatorial end of the field line).

For the purpose of comparison, I include the dashed curve which gives values of J'_{\parallel} determined with the use of the Vasyliunas equation (see introduction). While the values given by the dashed curve cannot be trusted (the T87 model does not satisfy $\vec{B} \times (\vec{\nabla} \times \vec{B}) = \vec{\nabla}G$, a criterion that must be met if the Vasyliunas equation is to be correctly used), the values do show the trend expected of actual field-aligned current along a flux tube: there is a region of field aligned current generation near the equatorial end of the flux tube and a region through which field-aligned current flows, without diversion, to the ionosphere. On the other hand, values of J'_{\parallel} obtained using Ampere's law (solid curve) are large only near the equatorial end of the flux tube. Regardless of the value of J'_{\parallel} obtained using Ampere's law, its variation along the flux tube is clearly unrealistic.

Based on the above arguments, I conclude that, globally, the magnetic effects of the large-scale field-aligned currents are not included in the T87 (or any existing) empirical magnetic field model. That there might be spatially-limited regions where these effects could be represented by the model is not inconsistent with this view [e.g., *Spence et al.*, 1988]; however, even if realistic field-aligned currents are present in a limited region of a model, it is the global distribution of these currents that must be realistic if their effects on mappings generated by the model are to be believed.

Flare of T87 and T89 CPS Field Lines

Mappings from the ionosphere to the magnetosphere, and vice-versa, depend on the properties of the magnetic field everywhere along the field lines between the ionospheric and magnetospheric regions in question. One property of the magnetic field that directly affects mappings is the "flare" of the magnetic field away from

the noon-midnight meridian. To help discuss this property of the magnetic field, I define the flare angle (θ_f) of the magnetic field as

$$\theta_f = \tan^{-1} \left(\frac{B_y}{(B_x^2 + B_z^2)^{\frac{1}{2}}} \right) \quad (34)$$

Figures 13a and 13b are contour plots of the flare angle of the T87 and T89 model fields, respectively, on the surface $X_{\text{gsm}} = -8 R_E$. Figure 13c is a contour plot of the ratio of the flare angle of the T87 model to that of the T89 model on the same surface. Figure 14 is the same as Figure 13, with the quantities all determined on the surface $X_{\text{gsm}} = -15 R_E$.

Figures 13 and 14 illustrate clearly that the T89 model magnetic field is significantly more flared than that of the T87 model in the region of space that corresponds to the CPS. The T87 and T89 model magnetic fields are differently flared because of the different representations of the cross-tail currents in the two models. The cross-tail current in the T89 model is more curved in the equatorial plane than that of the T87 model. This leads to the T89 model field being more radial in the CPS region than is the T87 model field.

In this section, I attempt to determine which of the two models is more realistic in terms of the flare of the model magnetic field with respect to the noon-midnight meridian. One way to try to determine which model is more realistically flared would be to look at the Y_{gsm} component of the model magnetic fields in comparison to Y_{gsm} in the data set from which the models were derived; however, both the variability and the smallness of Y_{gsm} in this region of space would make this comparison difficult. Below, I describe a test of the flare of the T87 and T89 model magnetic fields. My approach is to use the magnetic field models, in conjunction

with an accepted ionospheric electric potential distribution, to infer an observable quantity. This quantity is the convection electric field in the equatorial plane of the magnetosphere. I compare the qualitative features of the model inferred convection pattern with the same features of the actual convection pattern. Below, I show that the convection pattern inferred using the T87 model differs qualitatively from that inferred using the T89 model. Furthermore, the difference between the two inferred convection patterns is primarily due to the different flare of the two model magnetic fields. Finally, I argue that the T89 model magnetic field is more realistically flared because the T89 model inferred convection pattern is more realistic, when compared with the actual convection pattern.

Figure 15 is a contour plot of ionospheric electric potential values given by the Heppner-Maynard model appropriate for IMF B_y positive and K_p in the range from 3+ to 4-. This figure corresponds to Heppner-Maynard model A shown in Figure 2 and was prepared using a computer coded version of the model described in *Rich and Maynard* [1989]. Superposed on Figure 15 are the ionospheric footpoints of field lines, generated by both the T87 and T89 models, that cross the equatorial plane at intervals of $2 R_E$ along the line from $Y_{gsm} = -20 R_E$ to $Y_{gsm} = 20 R_E$ at $X_{gsm} = -31 R_E$.

I stress that the purpose of this work is not to determine CPS convection velocities. Rather, I am seeking to develop methods to test the validity of model magnetic fields. I compare the convection distributions derived from *in situ* measurements with convection patterns inferred from two magnetic field models and the Heppner-Maynard ionospheric convection model to help evaluate the magnetic field models. The results of this research can be used to direct research aimed at improving the magnetic field models.

In mapping the ionospheric potential pattern to the neutral sheet, I assume there are no parallel electric fields. Figures 16a and 16b show the neutral sheet convection potential pattern produced by mapping Heppner-Maynard model A to the neutral sheet using the T87 and T89 models, respectively. In each case, I use the Tsyganenko model appropriate for $Kp = 4$. For the terrestrial field I use an appropriate dipole and zero dipole tilt.

I assume that ideal MHD is valid in the neutral sheet region and use $\vec{V} = \vec{E} \times \vec{B}/B^2$ to infer the convection velocity from the mapped ionospheric potential pattern and the tail magnetic field. Figure 17 shows the variation of the inferred convection velocity with position in the neutral sheet.

Figures 17a and 17b illustrate that the T87 model, in conjunction with the Heppner-Maynard convection model A, yields a convection pattern with a narrow ($|Y_{\text{gsm}}| < 10 R_E$) stream of earthward moving CPS plasma. The convection velocity in the equatorial plane for large values of $|Y_{\text{gsm}}|$ is small. The T89 model mappings yield a convection pattern with earthward moving plasma over a much larger ($|Y_{\text{gsm}}| < 20 R_E$) stream. The dawn-dusk asymmetry in the inferred pattern is due to asymmetries in the Heppner-Maynard model since the Tsyganenko models are symmetric in Y_{gsm} .

The striking difference between the predicted earthward flow pattern in the CPS for the T87 and T89 models leads to the question of which pattern is better supported by observations. In the introduction, I reviewed experimental results as well as theoretical considerations and the results of MHD simulations that indicate the earthward convection velocity in the CPS should be uniformly distributed across the CPS or even weaker at the centre of the tail than the flanks. Thus the mapping of the Heppner-Maynard electric field pattern into the magnetotail

produces more realistic CPS convection results when the T89 model is used.

I qualify my results by noting that I only use the magnetic field and ionospheric potential models appropriate for relatively large Kp . Strictly speaking, the conclusion that the T89 model provides a better mapping of the electric potential distribution must be restricted to higher Kp versions of the models. As well, the Heppner-Maynard potential pattern is presented in a frame of reference that rotates with the Earth. I have not attempted to account for this for the following two reasons. First, I am primarily interested in Earthward component of the convection velocity (V_x) in the CPS. Corotation effects on V_x near the noon-midnight meridian are negligibly small. Second, it is not clear how corotation effects project into the magnetosphere at high latitudes.

The differences between the inferred convection patterns are easily accounted for. In the CPS the T89 model field is much more flared than that of the T87 model. The dawn-dusk electric field is therefore concentrated in a much narrower region of the equatorial plane for the T87 model. Since field-aligned currents increase the flaring of CPS field lines (at least in the "solonoidal" region in the inner magnetosphere), it would be interesting to see how adding field-aligned currents to the T89 model would change the electric field mapping. This should lead to the expected region of low electric field in the centre of the tail.

In this section, I have described an important test of the mapping capabilities of the T87 and T89 model magnetic fields. The results presented here should suggest caution to those using the T87 model field in magnetospheric mapping studies.

T89 Equatorial B_z in the noon-midnight Meridian

Here, I simply point out a disturbing feature of the T89 model magnetic field,

namely the occurrence of negative model B_z at some locations in the model neutral sheet. On the basis of observations of B_z in the neutral sheet I conclude that this is an artifact of the model and not a real effect. The model is and will be used in studies where B_z inferred mapping from the ionosphere to the neutral sheet region is of crucial importance. As well, the model is used to provide a “realistic” magnetic field in theoretical studies. This property of the model should be a consideration in the interpretation of the results of such studies.

I use the T89 model field in conjunction with the magnetic field of a geocentric dipole with magnitude of $30,438 \text{ nT } R_E^3$. The dipole tilt angle is the number of degrees between the Sun-Earth line and the dipole equatorial plane, positive dipole tilts corresponding to the Sun-Earth line being in the northern hemisphere. The model output is presented in gsm coordinates. The model neutral sheet is defined as the surface where the model magnetic field B_x component changes from negative (away from the Earth) to positive (toward the Earth).

Figure 18 is a plot of the value of B_z as a function of position in the noon-midnight meridian for points in the model neutral sheet for the $Kp=0$ version of the model with a dipole tilt of 16° . In Figure 19 I show, for various dipole tilt angles, the position of the model neutral sheet in the midnight meridian plane as well as where in the model neutral sheet the Z component of the model magnetic field is negative. Figures 19a and 19b are for the T89 $Kp=0$ and $Kp=3$ models respectively. Similar figures prepared using the $Kp=1,2,4$ and $Kp > 4$ versions of the model are all virtually the same as that for the $Kp=3$ version. Figures 20a and 20b display field line traces generated with the $Kp=0$ version of the model with 16° and 32° tilts respectively.

In chapter 1, I reviewed observational evidence that indicates that, on average,

B_z in the neutral sheet is positive Earthward of $X_{\text{gsm}} = -50 R_E$. I conclude that the regions of negative B_z in the T89 model neutral sheet are an artifact of the model and not representative of the actual B_z distribution in the neutral sheet. As can be seen in Figure 18, the values of B_z in the neutral sheet given by the model are smaller than would be expected, even when they are positive.

From Figures 19a and 19b, it is clear that large regions of the model neutral sheet are in “magnetic islands” or are threaded by field lines that are essentially open at both ends or close at great distances from the Earth. While in reality these regions should be threaded by closed field lines rooted in the ionosphere, according to the T89 model they are not connected to the ionosphere along magnetic field lines. A corollary to this is that the mapping of field lines from critical ionospheric regions (for instance the most poleward region of closed field lines) to the equatorial plane inferred by the T89 model should not be trusted. For comparison purposes I point out that the regions of negative B_z in the model neutral sheet are not a feature of the T87 model, at least as far as $60 R_E$ down the magnetotail.

The unrealistic distribution of B_z in the model neutral sheet is not surprising for two reasons (Tsyganenko, 1991, private communication). First, *Tsyganenko* [1989] uses a series of axially symmetric current disks centered on the Earth to represent the cross-tail current system in the T89 model. The magnetic field due to these disks is then adjusted to account for the redistribution of the current flowing around the dayside of the magnetosphere. On the nightside the current flow lines in the model cross-tail current region are roughly circles centered on the Earth. The contribution to the Z_{gsm} component of the model field near the noon-midnight meridian due to the cross-tail current at the flanks is therefore negative. If this current flow pattern near the flanks is not realistic, then it is possible that

the small or negative model B_z values in the neutral sheet could be due, in part, to how the cross-tail current is represented. Second, the rms deviation of the Z_{gsm} component of the magnetic field is large in comparison to its average value in the region tailward of $X_{\text{gsm}} = -20 R_E$ (see Figure 1 of *Fairfield* [1986]). This makes the problem of accurate representation of the average neutral sheet B_z with a model that is obtained via least squares fitting to a large data set of *in situ* measurements a difficult one.

I suggest that an additional constraint be imposed in the development of future magnetic field models of this type. An empirical model of the distribution of B_z in the neutral sheet can be determined from *in situ* measurements. Only verifiable neutral sheet vicinity measurements should contribute to this empirical model. The global empirical model being developed would then be constrained to have a neutral sheet B_z distribution that agrees closely with the experimentally determined one.

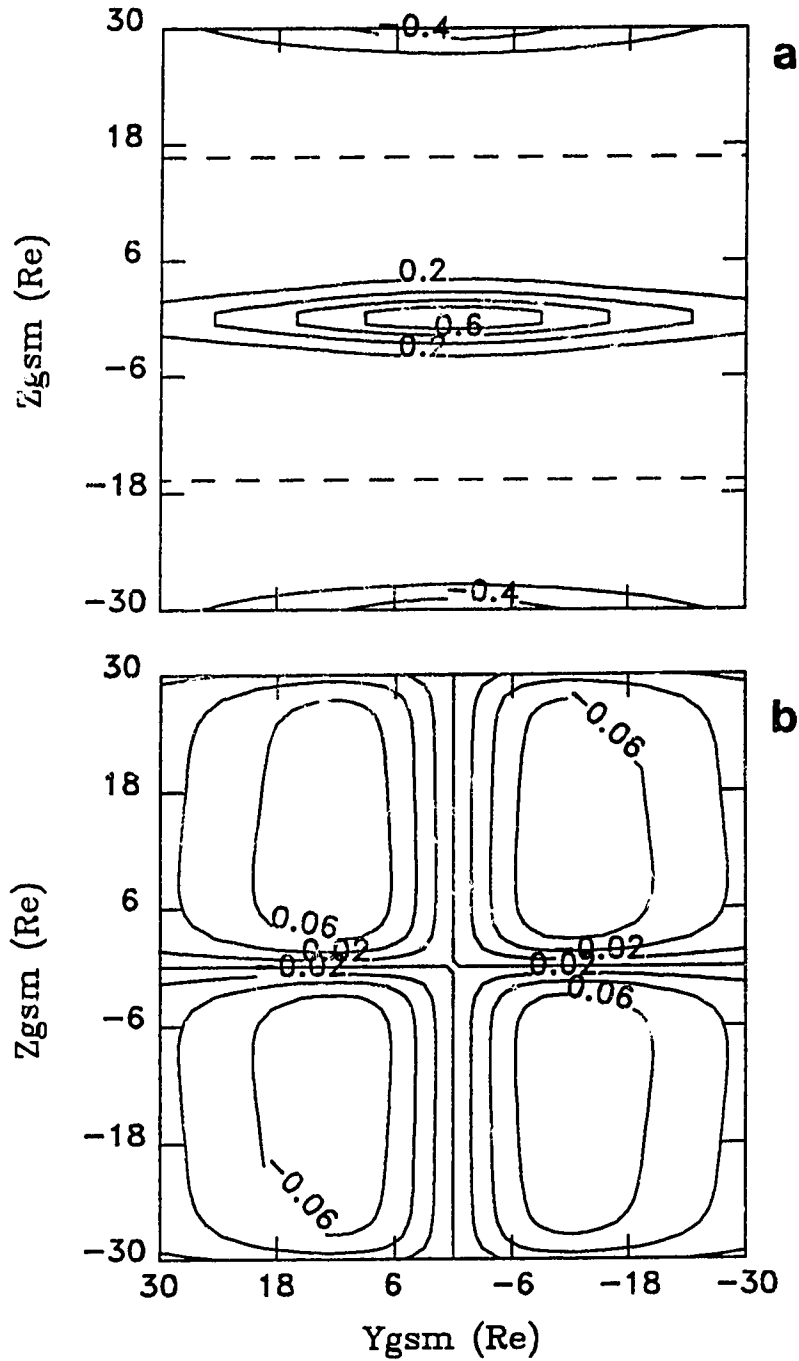


Figure 6. Contours of constant (a) J_y and (b) J_x evaluated on the plane $X_{gsm} = -25 R_E$. The current is determined by using Ampere's law with the T87 $Kp = 3$ cross-tail current magnetic field model. The values are expressed in nA/m^2 . The dashed curves on Figure 6a are $J_y = 0$ contours.

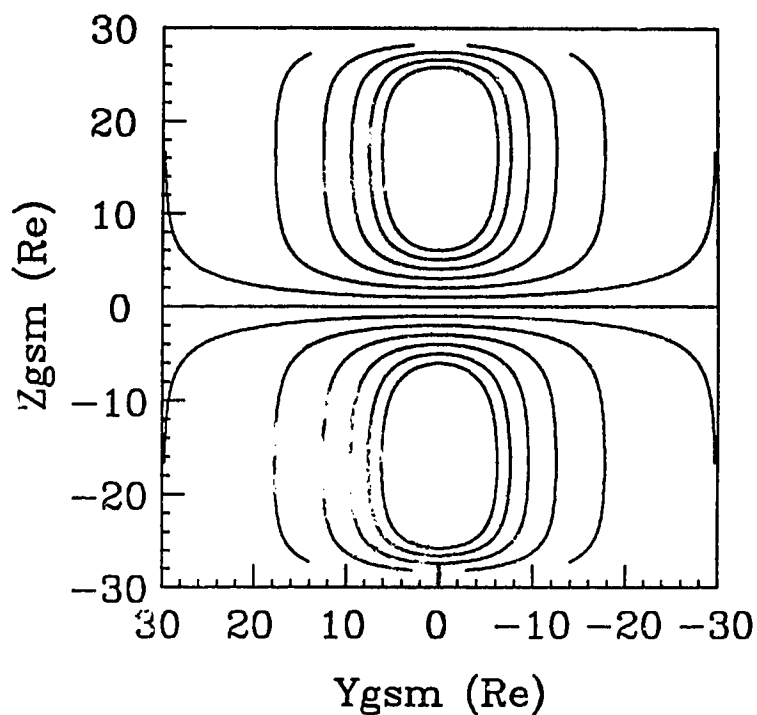


Figure 7. Cross-tail current line traces for the T87 $K_p = 3$ model projected in the $X_{gsm} = -25 R_E$ plane. To produce this figure, thirteen current line traces were started on the noon-midnight meridian at $X_{gsm} = -25 R_E$. The current lines were traced in both directions away from the start points (i.e., parallel to the current towards dusk and antiparallel to the current towards dawn). The start points for the traces were at Z_{gsm} values ranging from $-6 R_E$ to $6 R_E$, evenly spaced at $1 R_E$ intervals in Z_{gsm} . The values were determined by applying Ampere's law to the T87 model cross-tail current magnetic field.

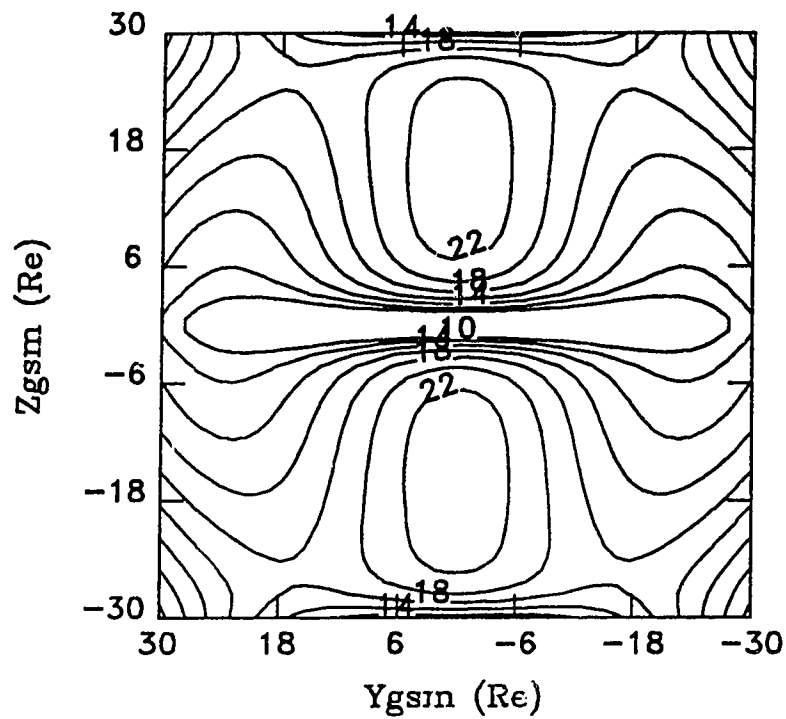


Figure 8. Contours of constant magnetic field strength (in nT) on the $X_{gsm} = -25 R_E$ plane for the T87 $Kp = 3$ model including a terrestrial dipole field. The smallest contour value is $|\vec{B}| = 10$ nT and the contours are separated by 2 nT.

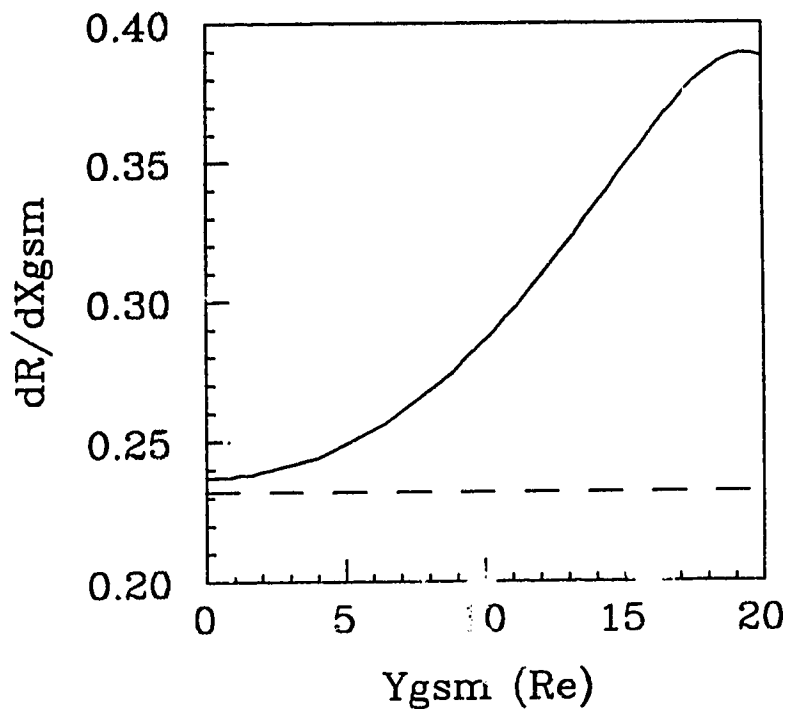


Figure 9. Flare of field lines for the T87 $Kp = 3$ model in the vicinity of the solar wind-magnetosphere interface (solid curve). The dashed curve is what this flare would be in a closed magnetosphere of circular cross-section with radius given by *Sibeck* [1991] (intermediate pressure model-see text). Flare is expressed in terms of dR/dX_{gsm} , where R is the cross-sectional radius of the magnetotail.

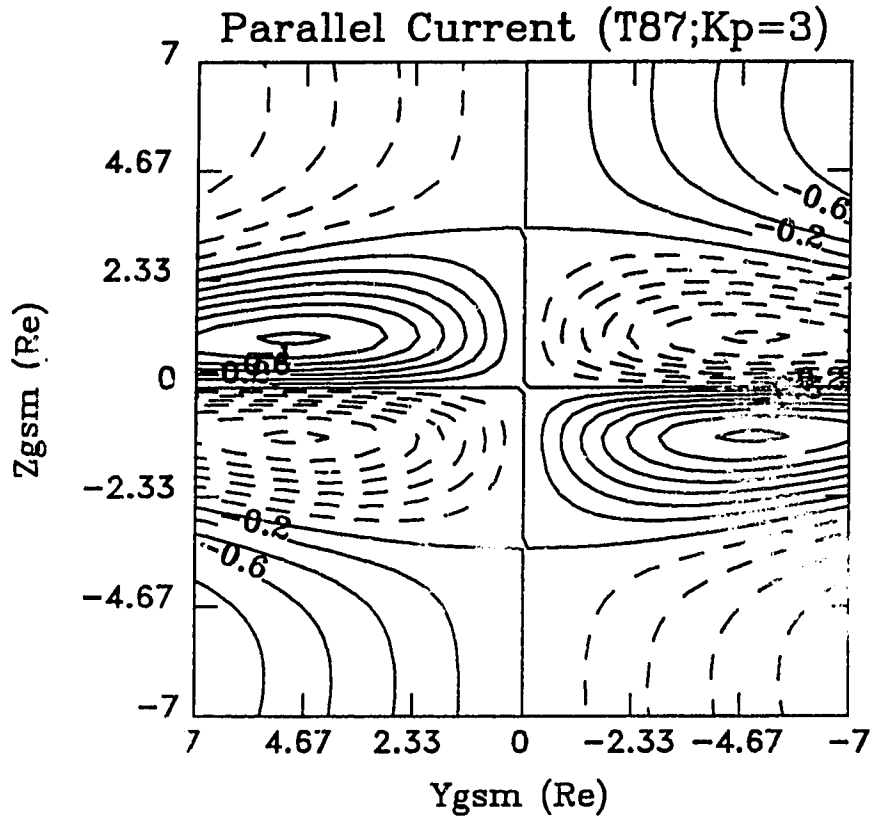


Figure 10. Field-aligned component of the T87 $Kp = 3$ model current on the plane $X_{gsm} = -6.73 R_E$. The values were determined by applying Ampere's law and are normalized to what the field aligned current would be if it was mapped, without diversion, to the ionosphere (see text). The contours are separated by $0.2 \mu A/m^2$. Contours indicating positive values are dashed while the zero and negative contours are solid. In the northern ($Z_{gsm} > 0$) and southern ($Z_{gsm} < 0$) hemispheres, current flowing towards the Earth is indicated by positive and negative values respectively.

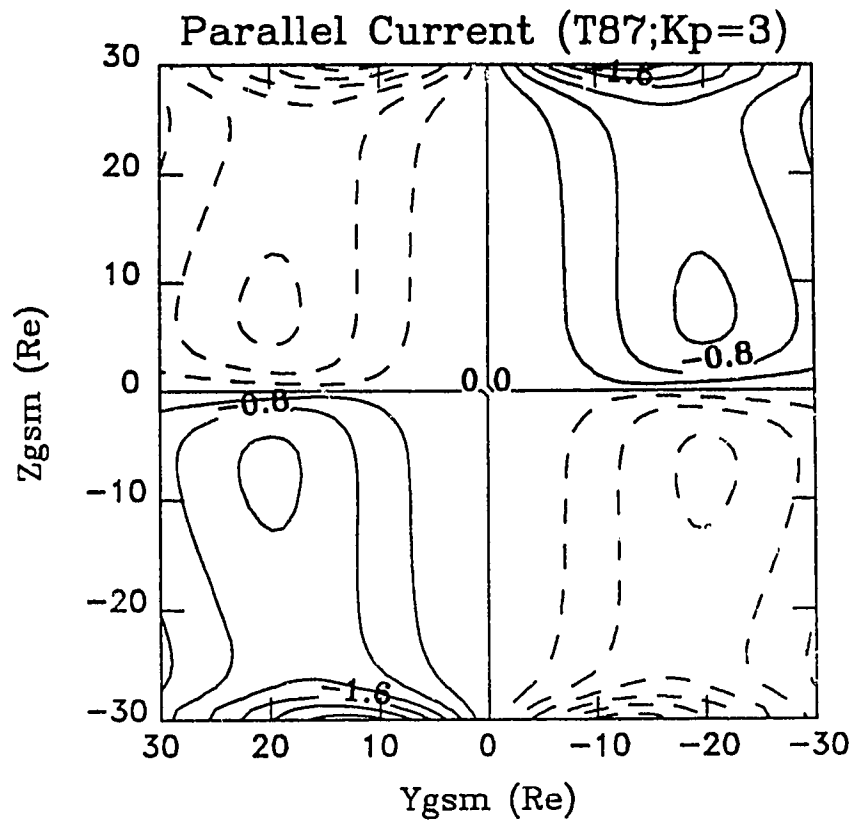


Figure 11. The same as Figure 10, but showing values of field-aligned current on the plane $X_{gsm} = -25 R_E$ with a contour separation of $0.4 \mu A/m^2$.

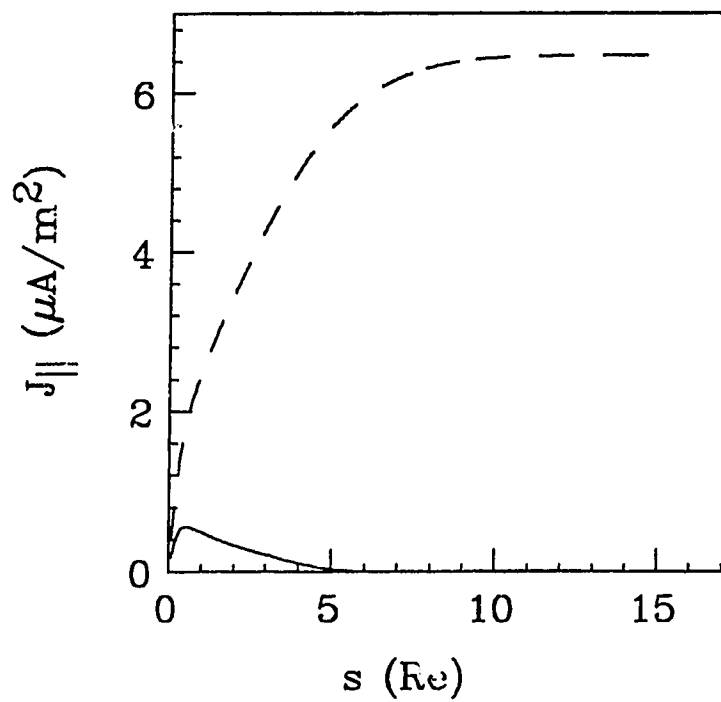


Figure 12. Normalized field-aligned T87 $Kp = 3$ model current along a model field line. The current is obtained by using the Vasyliunas equation (dashed) and Ampere's law (solid) with the model magnetic field. $s = 0$ corresponds to the equatorial end of the field line.

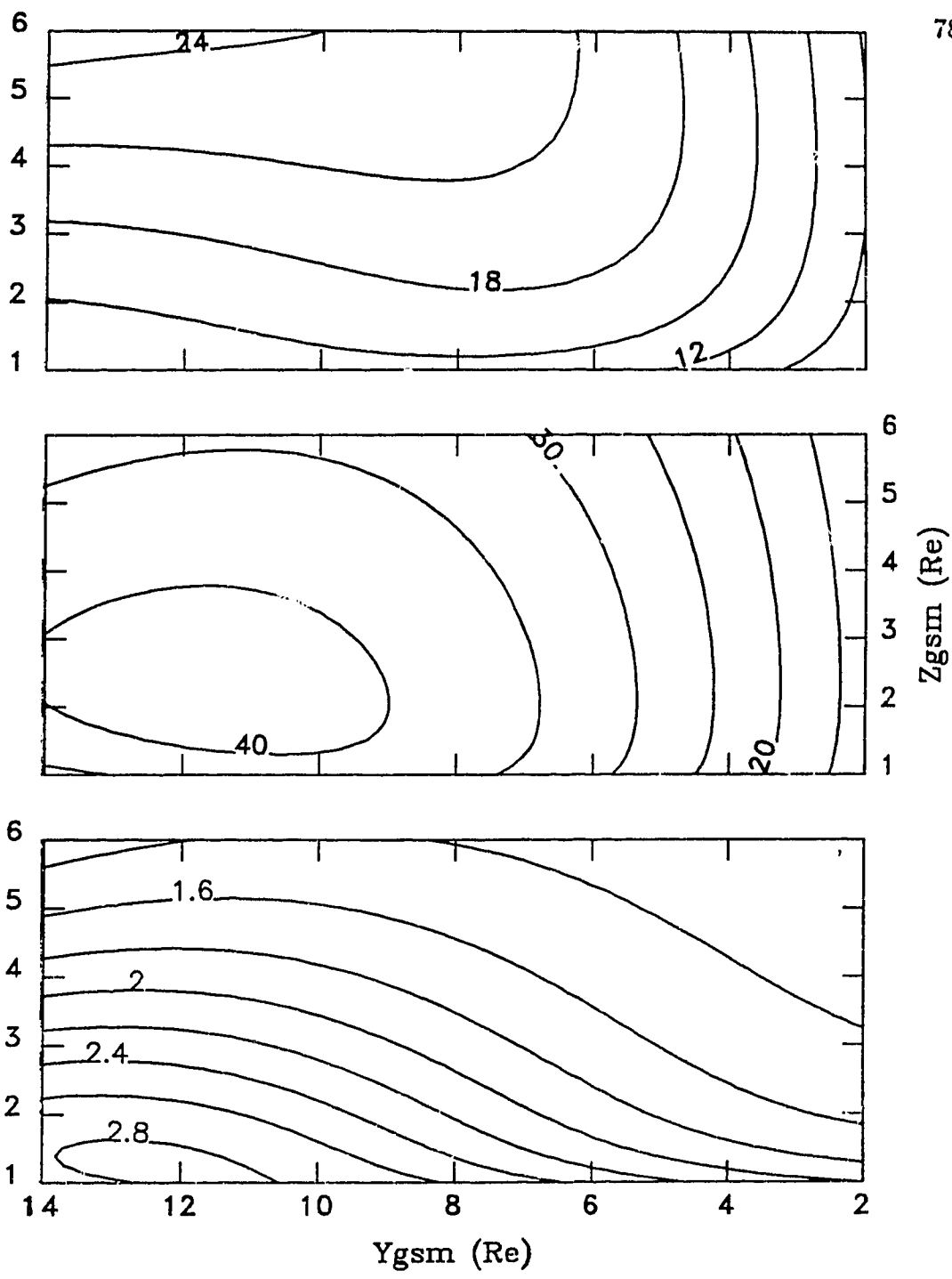


Figure 13. Flare angle (in degrees) of the (a) T87 and (b) T89 $Kp = 4$ model magnetic fields at $X_{gsm} = -8 R_E$. (c) Contours of constant value of the ratio of the flare angle of the T89 model field to that of the T87 model field on the same surface.

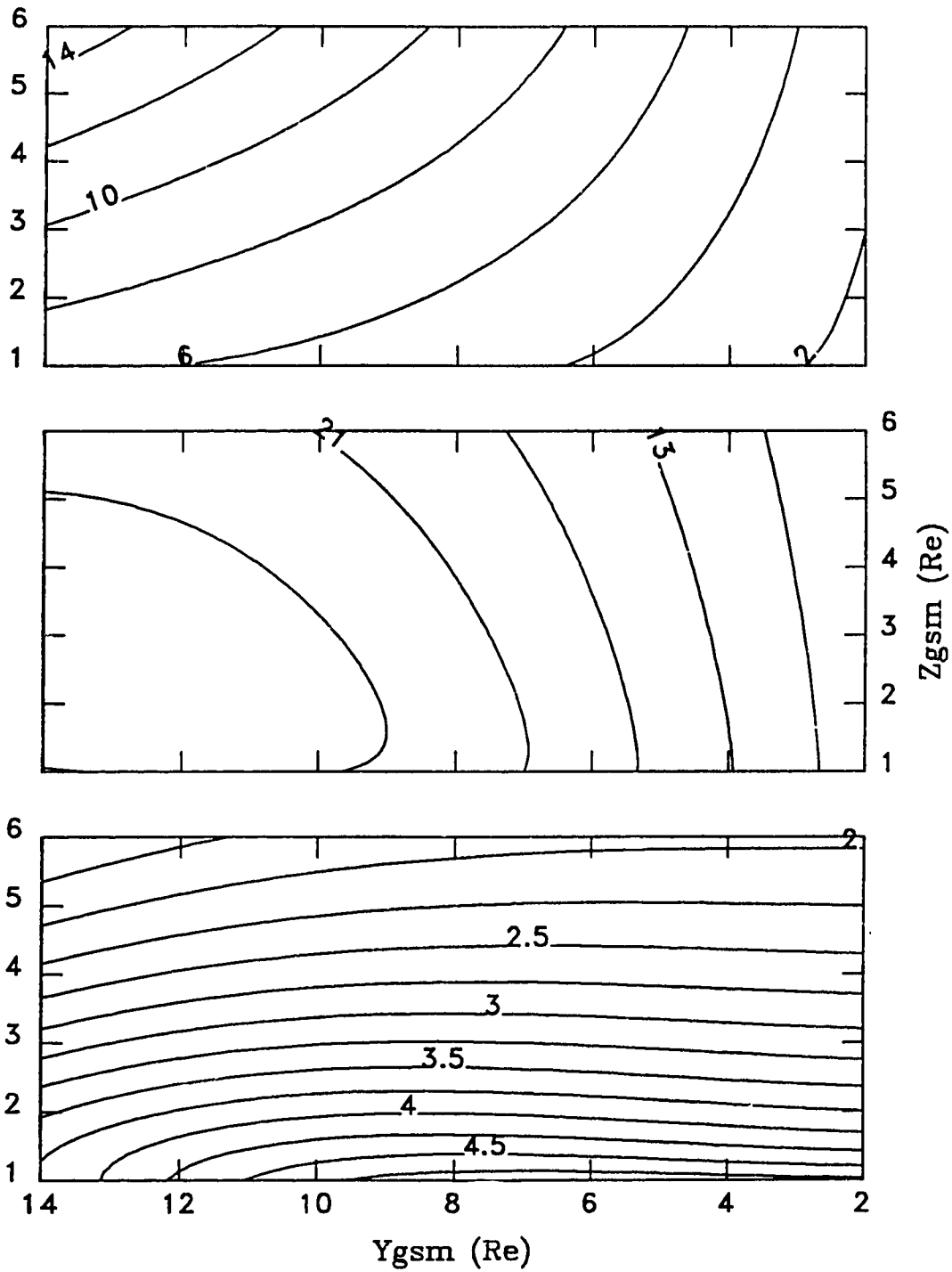


Figure 14. Same as Figure 13, but on a surface at $X_{gsm} = -15 R_E$.

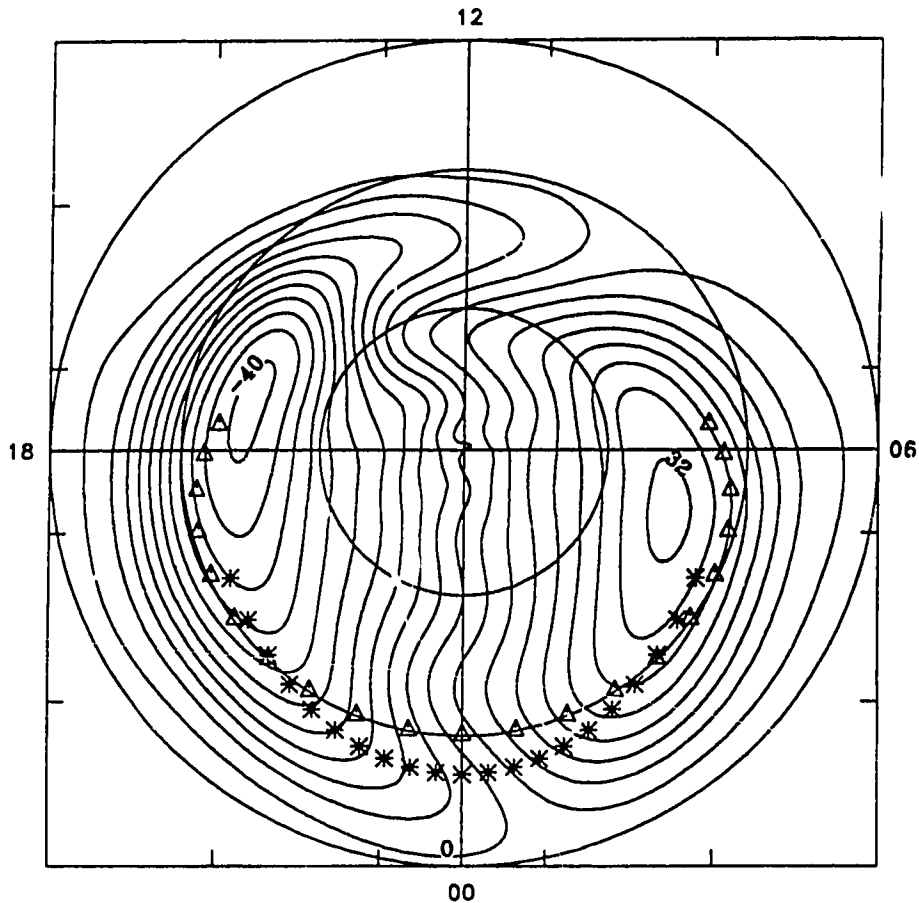


Figure 15. *Heppner and Maynard [1987]* ionospheric electric potential pattern A prepared using code described in *Rich and Maynard [1989]*. The contour intervals are 4 kV. The potential at the centre of the dawn side convection cell is roughly 75 kV greater than at the center of the dusk side convection cell. The circles are at latitudes of 60°, 70° and 80°. Superimposed on the pattern are ionospheric footpoints of model field lines that start at the equatorial plane at $X_{gsm} = -31 R_E$. The triangles and asterisks mark footpoints of T87 and T89 model field lines, respectively. The startpoints for the field lines had Y_{gsm} values ranging from $-20 R_E$ to $20 R_E$ at $2 R_E$ intervals.

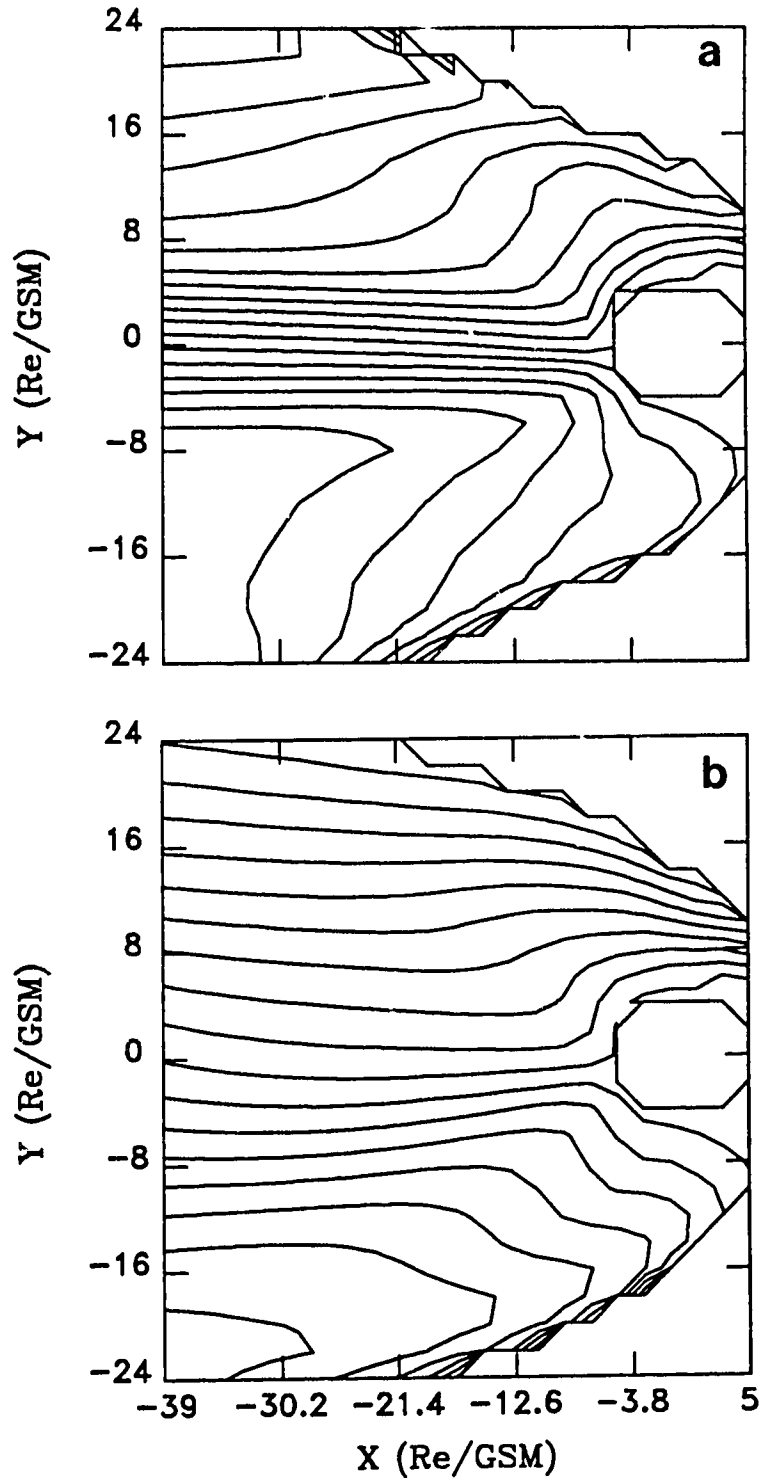


Figure 16. Contours of constant inferred potential in the equatorial plane for the (a) T87 and (b) 1989 $K_p = 4$ models and *Heppner and Maynard* [1987] ionospheric convection pattern A. The contour intervals are 4 kV.

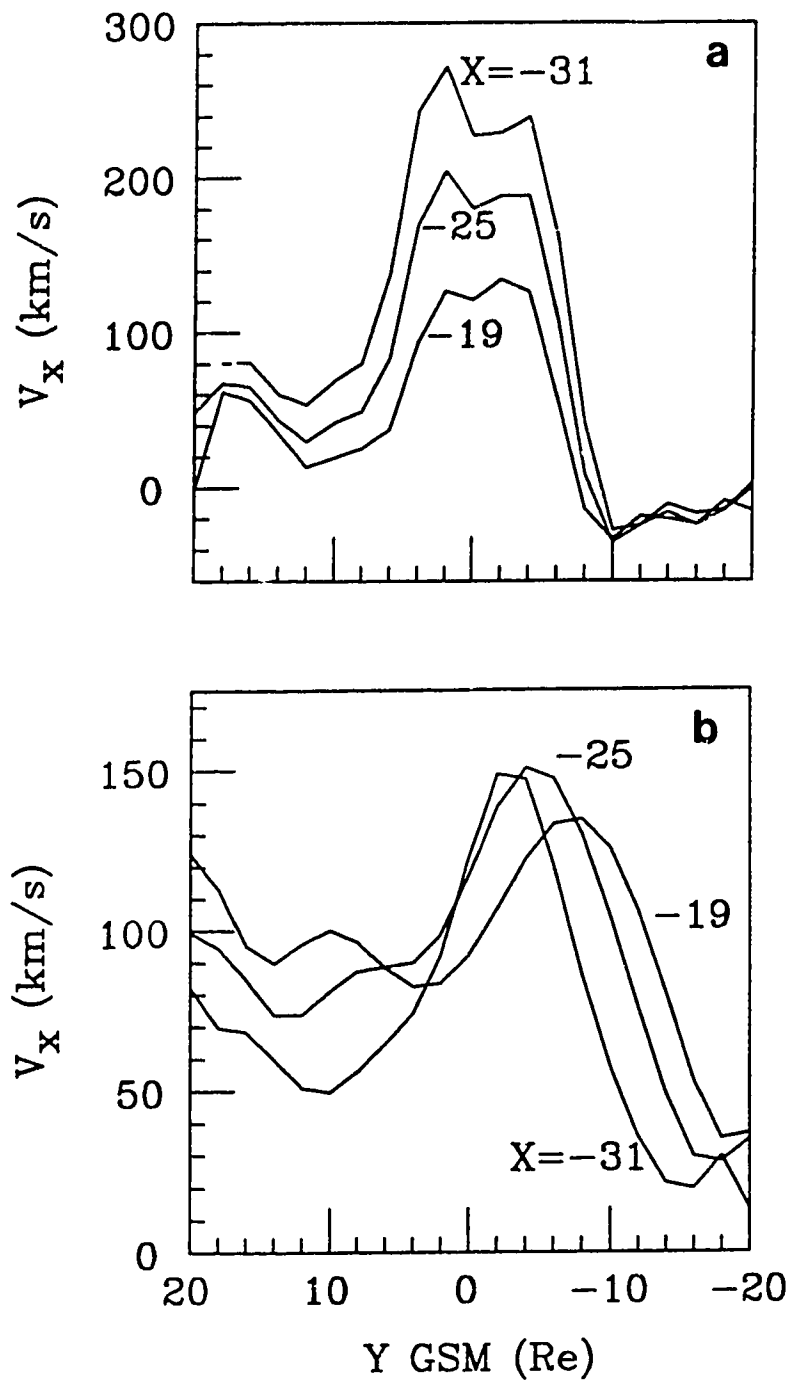


Figure 17. X_{gsm} component of the inferred convection velocity in the equatorial plane for the (a) T87 and (b) T89 $Kp = 4$ models.

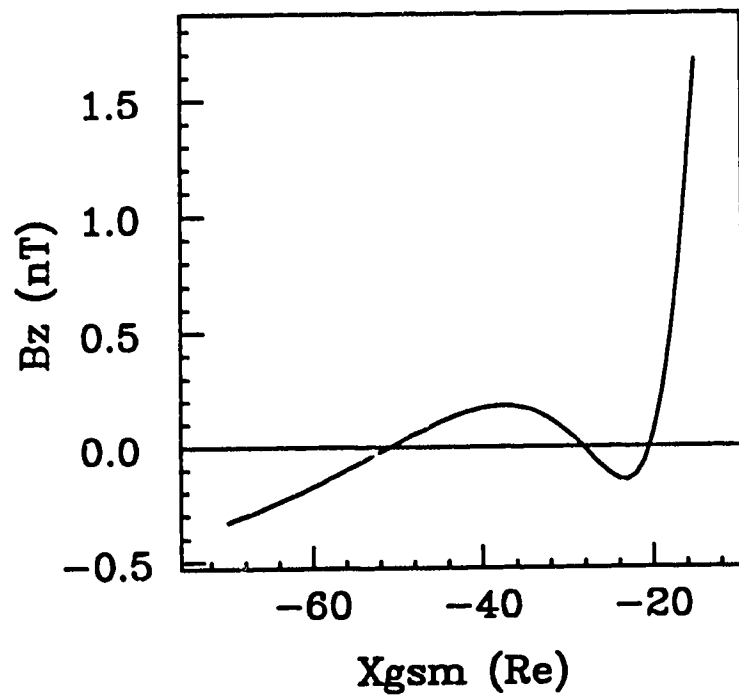


Figure 18. Equatorial B_z for the T89 $Kp = 0$ model with a 16° dipole tilt.

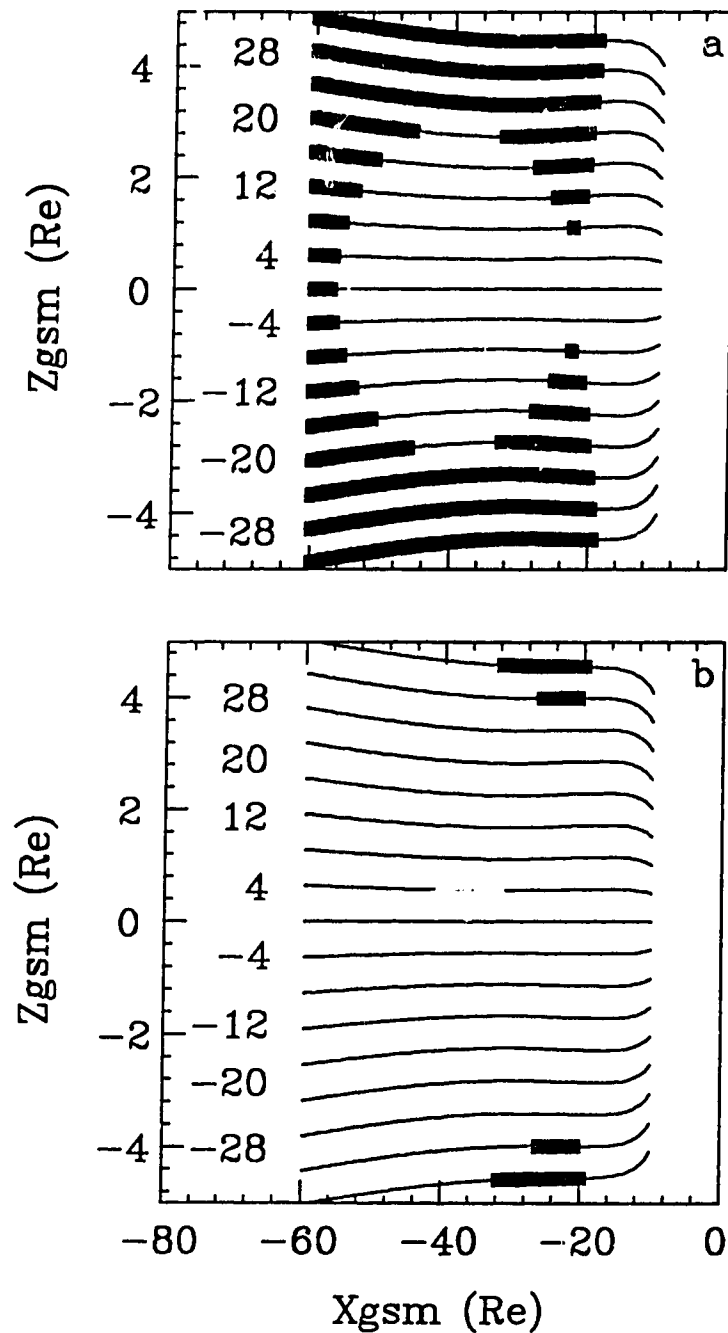


Figure 19. Regions of negative B_z in the the T89 model neutral sheet for various dipole tilt angles and (a) $Kp = 0$ and (b) $Kp = 3$. The lines show the position in the gsm XZ plane of the model neutral sheet. The numbers at the left end of the curves indicate the dipole tilt angles used. There are 17 curves corresponding to neutral sheets for the model with 17 different evenly spaced dipole tilt angles between -32° and 32° . The thick sections of the curves correspond to where in the model neutral sheet B_z is negative.

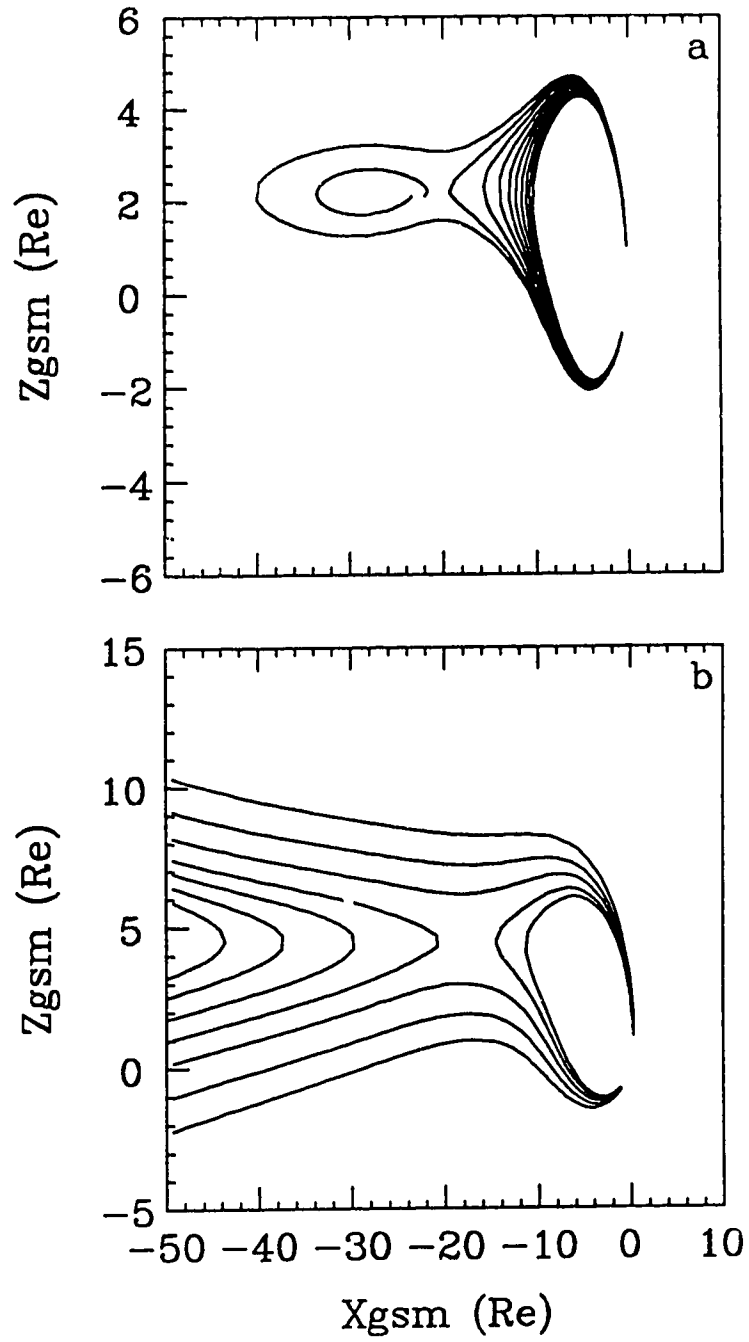


Figure 20. Field lines traced with the T89 $K_p = 0$ model with a dipole tilt of (a) 16° and (b) 32° . Note the different X and Z scales.

Rationale for the Development of New Modelling Techniques

Since the development of early empirical models [e.g., *Olson and Pfitzer, 1974; Mead and Fairfield, 1975*], models of the Earth's magnetic field have gradually become more realistic. These improvements resulted from the use of better functions to represent the magnetic field, as well as an ever-increasing data base of *in situ* magnetic field measurements. Since the beginning of the 1980s, the space physics community has adopted the magnetic field models developed by *Tsyganenko and Usmanov [1982]* and *Tsyganenko [1987;1989]* and most efforts made to relate ionospheric observations to prospective source regions in the magnetosphere use one or another of Tsyganenko's models. The level of sophistication of present models gives one hope that the ability to map from the magnetosphere to the ionosphere, and vice versa, will soon be part of the repertoire of space physicists. It is true, however, that even the magnetic field models presently available have deficiencies that might affect the validity of mappings. As discussed in this chapter, these deficiencies result from differences between the actual magnetospheric current system and those currents consistent with, via Ampere's law, the model magnetic fields.

The remainder of this thesis deals with my own work towards the development of a magnetospheric magnetic field model. I split this task into two parts. These are the development of a model simulating the magnetic effects of (1) the field-aligned currents and (2) the transverse currents. A method similar to that of the *Olson [1974]* (a wire model) is used in each case. My reason for using this approach is that, in light of the material presented in this chapter, I feel it is important to have a magnetic field model with a very realistic current distribution. In particular, the model currents should flow along paths that are as close as possible to those the actual currents follow. To circumvent the problems associated with the use of

infinitesimally thin wire elements, I have developed a model that is built up using current elements that are of finite cross-section as well as length. The resulting current and magnetic field are finite everywhere.

The model of the magnetic effects of field-aligned currents I describe in the next chapter was first developed to be added to a pre-existing magnetic field model. My feeling was that this background field should be either the T87 or T89 model, since these two models are far and above the most widely used. I chose the T87 model over the T89 model for reasons based on the work presented in this chapter and summarized in the following paragraph.

In the night-side magnetotail, the T89 model magnetic field is more flared away from the noon-midnight meridian than is the T87 model field. This additional flare provided a more realistic description of the earthward flow of plasma in the central plasma sheet than could be obtained from the T87 model, in light of the consequences of mapping an ionospheric equipotential pattern into the nightside magnetosphere. Furthermore, examination of the expected variation of the B_z component of the tail field along the noon-midnight meridian [see *Rostoker and Skone, 1993*] reveals that the T87 model provides a better representation of the observations than does the T89 model. In particular, the T89 model B_z is too small, or even negative. In comparison to the T87 model, the greater flare of the T89 model magnetic field appears to be an improvement, but the T89 model equatorial B_z distribution near midnight is inferior. Both the greater flare and the small B_z values are a consequence of differences between the two models in the choice of functions used to represent the magnetic effects of the cross-tail current. There is, however, another current system that can have an appreciable effect on both the flare of the magnetic field and the distribution of B_z near midnight: the

large scale field-aligned currents. One effect that these currents are expected to have in the magnetotail is to make the CPS magnetic field more flared. I conclude that it would be most reasonable to add these effects to the T87 model field.

3. Modelling the Magnetic Effects of Magnetospheric Currents: A New Approach

My objective here is to develop a useful representation of the magnetic effects of large-scale magnetospheric current systems. I therefore restrict my attention to current distributions that do not vary in time. The current continuity equation

$$\vec{\nabla} \cdot \vec{J} + \frac{\partial \rho}{\partial t} = 0 \quad (35)$$

follows directly from Maxwell's equations. For time-independent situations the current distribution must be divergence free:

$$\vec{\nabla} \cdot \vec{J} = 0 \quad (36)$$

The relationship between the magnetic field and the current distribution can be determined from Maxwell's equations. For time-independent situations, Ampere's law follows:

$$\vec{\nabla} \times \vec{B} = \mu_0 \vec{J} \quad (37)$$

Using Helmholtz's Theorem [cf. *Arfken*, 1985], the time-independent Maxwell equations yield the Biot-Savart law:

$$\vec{B}(\vec{r}) = \frac{\mu_0}{4\pi} \int dV' \frac{\vec{J}(\vec{r}') \times (\vec{r} - \vec{r}')}{|\vec{r} - \vec{r}'|^3} \quad (38)$$

In the development of models of the magnetic effects of distributed currents within the magnetosphere, it is customary to stipulate a current distribution and then to use the Biot-Savart law to determine the corresponding magnetic field. A simple example of this approach is the use of model wire loops to represent currents in the magnetosphere. The magnetic field of any closed circuit made of infinitesimally thin wire can be determined to arbitrary accuracy using the Biot-Savart law. The standard approach is to construct the loops out of finite-length segments of infinitesimally thin straight wire. The contribution to the integral in equation 38 from current flowing in the segment of wire is in the azimuthal direction about the wire segment:

$$B_\phi(\rho, z) = g_0(\rho, z)f_0(\rho, z) \quad (39)$$

$$g_0(\rho, z) = \frac{\mu_0 I}{4\pi} \frac{1}{\rho} \quad (40)$$

$$f_0(\rho, z) = \frac{z_1 - z}{\sqrt{\rho^2 + (z_1 - z)^2}} - \frac{z_0 - z}{\sqrt{\rho^2 + (z_0 - z)^2}} \quad (41)$$

Here, the z -axis is parallel to the wire segment, the wire segment has endpoints at $z = z_0$ and $z = z_1$ with $z_1 > z_0$ and a current I is flowing along the segment from z_0 to z_1 . The current distribution that is consistent with this magnetic field can be determined from Ampere's law:

$$J_\rho = -\frac{1}{\mu_0} \frac{\partial B_\phi}{\partial z} \quad (42)$$

$$J_z = \frac{1}{\rho\mu_0} \frac{\partial(\rho B_\phi)}{\partial\rho} \quad (43)$$

For the magnetic field given in equation 39, these give

$$J_\rho = \frac{I\rho}{4\pi} \left(\frac{1}{(\rho^2 + (z_1 - z)^2)^{\frac{3}{2}}} - \frac{1}{(\rho^2 + (z_0 - z)^2)^{\frac{3}{2}}} \right) \quad (44)$$

$$J_z = \frac{I}{4\pi} \left(\frac{z_0 - z}{(\rho^2 + (z_0 - z)^2)^{\frac{3}{2}}} - \frac{z_1 - z}{(\rho^2 + (z_1 - z)^2)^{\frac{3}{2}}} + \frac{2(\text{H}(z - z_1) - \text{H}(z - z_0))\delta(\rho)}{\rho} \right) \quad (45)$$

where δ and H are the Dirac delta and Heaviside functions, respectively. The third term in the brackets in equation 45 is the (infinite) current density of the finite wire element. The presence both of the other two terms in equation 45 and the radial component is, at first glance, surprising. Applying Ampere's law to the magnetic field given in equation 39 yields a current that is distributed throughout space and yet this magnetic field, according to our naive application of the Biot-Savart law, is that of a straight current carrying wire of finite length. The problem lies in the current distribution used in the original Biot-Savart law integration. This current has a source (at $z = z_0$) and a sink (at $z = z_1$) and therefore the current is not divergence-free and thus is not consistent with any time-independent solution of Maxwell's equations. The Biot-Savart law integral, however, gives the magnetic field that corresponds to a given current distribution for time independent conditions only. The integral in equation 38 is over all space and, consequently, over complete circuits. When a complete model current circuit is constructed using finite lengths of infinitesimally thin straight wire segments, provided the current on

every element is the same, the current density will be zero everywhere except on the wire elements. As I discussed in chapter 2, finite-length wire segments were used to construct models of magnetospheric current systems by *Olson* [1974], who used this technique to model the effects of the ring current and the cross-tail current with closure around the magnetospheric boundary.

It is possible to specify a current distribution and use the Biot-Savart law integral to calculate the contribution to the total magnetic field. It is, however, exceedingly difficult to evaluate this integral for all but the simplest of geometries. Current elements with geometries simple enough to allow for straightforward evaluation of the Biot-Savart law integral typically have magnetic fields with singular points. An example is the infinite magnetic field strength near the infinitesimally thin wire elements discussed above. Another possibility is to specify a magnetic field with the desired properties. The corresponding current distribution can be determined with Ampere's law. As I pointed out above, the Biot-Savart law is a solution to Ampere's law and the two approaches are completely equivalent. My goal here is to use a cylindrical current element with an azimuthal magnetic field. The current density is to be finite everywhere, aligned with the axis of the cylinder inside of the cylinder, and small, or zero, outside of the cylinder. For illustrative purposes, I let the symmetry axis of the cylindrical element be the z -axis, where z_0 and z_1 are the locations of the two ends of the element; the plane perpendicular to the z direction and located midway between z_0 and z_1 is the "midplane" of the element. The element is of radius a . The magnetic field is in the azimuthal (ϕ) direction and is azimuthally symmetric:

$$B_\phi = F(\rho, z) \tag{46}$$

Any function of this form is divergence-free. The magnetic field due to the current element is of the same form as that due to a finite length of current-carrying wire:

$$B_\phi = g(\rho, z)f(\rho, z) \quad (47)$$

For our current elements, the function $g(\rho, z)$ will be the magnetic field of a current-carrying cylinder of radius a and infinite length centred on the z -axis. The function $f(\rho, z)$ is an envelope function, limiting the extent of the effects of the current element in the z direction. Below, two different types of current elements that can be used to build up a model of the magnetospheric currents are discussed.

The magnetic field of the first type of current element (herein referred to as a type I element) is

$$B_\phi = g_1(\rho, z)f_1(\rho, z) \quad (48)$$

where

$$g_1(\rho, z) = \alpha \begin{cases} 1/\rho & \rho > a \\ \rho/a^2 & \rho < a \end{cases} \quad (49)$$

and

$$f_1(\rho, z) = \frac{1}{2} \left(\frac{(z - z_0)}{\sqrt{\rho^2 + (z - z_0)^2}} - \frac{(z - z_1)}{\sqrt{\rho^2 + (z - z_1)^2}} \right) \quad (50)$$

This magnetic field is the same as that of the finite length of current-carrying wire except for the radial dependence of the function g . For values of $\rho > a$, the function

is the same as the magnetic field in equation 39, and hence the current associated with this element for $\rho > a$ is the same as the current given in equation 44 and 45 with I replaced by $2\pi\alpha/\mu_0$. According to Ampere's law, the current density associated with this current element for $\rho < a$ is

$$J_\rho = \frac{\alpha\rho^3}{2a^2\mu_0} \left(\frac{1}{(\rho^2 + (z_1 - z)^2)^{\frac{3}{2}}} - \frac{1}{(\rho^2 + (z_0 - z)^2)^{\frac{3}{2}}} \right) \quad (51)$$

$$J_z = \frac{\alpha}{2a^2\mu_0} \left(\frac{2(z_1 - z)}{\sqrt{\rho^2 + (z_1 - z)^2}} - \frac{2(z_0 - z)}{\sqrt{\rho^2 + (z_0 - z)^2}} \right. \\ \left. + \frac{\rho^2(z_0 - z)}{(\rho^2 + (z_0 - z)^2)^{\frac{3}{2}}} - \frac{\rho^2(z_1 - z)}{(\rho^2 + (z_1 - z)^2)^{\frac{3}{2}}} \right) \quad (52)$$

This is the same as the current density in equations 44 and 45, except that the term describing the line current on the z -axis in the expression for J_z has been replaced by the third and fourth terms given in equation 52. The magnetic field associated with this element is finite everywhere, as is the current density. Figure 21 is a plot of $f_1(\rho, z)$. Figure 22 is a three dimensional plot of current and magnetic field line tracings for a type I current element.

The magnetic field of the second type of current element (herein referred to as a type II element) is

$$B_\phi = g_2(\rho, z)f_2(\rho, z) \quad (53)$$

where

$$g_2(\rho, z) = \alpha \begin{cases} a^{(\gamma-1)}/\rho^\gamma & \rho > a \\ \rho/a^2 & \rho < a \end{cases} \quad (54)$$

and

$$f_2(\rho, z) = \frac{1}{2} \{ \tanh[D_0(z - z_0)] - \tanh[D_1(z - z_1)] \} \quad (55)$$

Here, γ is a parameter normally set to 1. With Ampere's law, the current density that corresponds to this magnetic field can be determined. Setting $a = \text{constant}$ and $D = D_0 = D_1$, this gives

$$J_\rho = -\frac{D\alpha}{2\mu_0} \{ \text{sech}^2[D(z - z_0)] - \text{sech}^2[D(z - z_1)] \} \begin{cases} 1/\rho & \rho > a \\ \rho/a^2 & \rho < a \end{cases} \quad (56)$$

$$J_z = \frac{\alpha}{2\mu_0 a^2} \{ \tanh[D(z - z_0)] - \tanh[D(z - z_1)] \} \begin{cases} (1 - \gamma)(a/\rho)^{\gamma+1} & \rho > a \\ 1 & \rho < a \end{cases} \quad (57)$$

Figure 23 is a plot of $g_2(\rho, z)$ for several different values of γ and Figure 24 is a plot of $f_2(\rho, z)$. In Figure 25, I show current line tracings of \vec{J} for a number of different values of γ .

The current line traces I have shown in Figure 22 illustrate that the current flowing along the axis of a type I current element diverts radially away from the axis beyond the "end" of the element and returns, outside of the element ($\rho > a$), to flow back into the other end of the element. The magnetic field lines are circles centred on the element's axis. The magnetic field-current pattern here is like that of a solenoid, but with the current and magnetic field transposed. For a type II element, the magnetic field lines will again be axisymmetric circles; however, the pattern of the current flow, after it diverts away from the end of the cylinder, depends on the selection of the parameter γ . Figure 25 shows that, depending on

the value of γ , the current will either flow towards larger z , radially away from the cylinder's axis, or return to the other end of the element.

Example Uses

The following three examples help to illustrate the rationale behind the choice of functions describing the current elements. For the first example, I consider N of these elements, with $N \gg 1$ and the axis of each element parallel to that of all others. The superscript i denotes quantities associated with the i th element. The elements are stacked end to end along the z -axis:

$$z_i^i = z_0^{i+1} \quad (i = 1, 2, \dots, N - 1)$$

The point where the magnetic field is to be determined (ρ, z) is selected to be somewhere between the endpoints of the first (z_0^1) and N th (z_1^N) elements, which are in turn selected so that

$$(z - z_0^1) \gg \rho \quad \text{and} \quad (z_1^N - z) \gg \rho$$

This gives

$$\frac{1}{2} \{ \tanh[D(z - z_0^1)] - \tanh[D(z - z_1^N)] \} \simeq 1$$

and

$$\frac{1}{2} \left(\frac{z - z_0^1}{\sqrt{\rho^2 + (z - z_0^1)^2}} - \frac{z - z_1^N}{\sqrt{\rho^2 + (z - z_1^N)^2}} \right) \simeq 1$$

Using type II elements and setting

$$\gamma^i = \gamma = 1 \quad a^i = a \quad D_0^i = D_1^i = D \quad (\text{all } i)$$

The magnetic field due to these current elements is given by

$$B_\phi = g_2(\rho, z) \sum_{i=1}^N f_2^i(\rho, z) \quad (58)$$

which is just

$$B_\phi = \frac{g_2(\rho, z)}{2} \{ \tanh[D(z - z_0^1)] - \tanh[D(z - z_1^N)] \} \quad (59)$$

or, using the restrictions placed on z , z_0^1 and, z_1^N above,

$$B_\phi \simeq \alpha \begin{cases} 1/\rho & \rho > a \\ \rho/a^2 & \rho < a \end{cases} \quad (60)$$

If type I elements are used (with $a^i = a$ (all i)), then the same total magnetic field is obtained. This is the magnetic field due to an infinitely long current-carrying wire of finite radius a , with a distributed current density along the axis of

$$J_z = \frac{2\alpha}{\mu_0 a^2} \quad (61)$$

Thus, stacking identical elements of either type end to end along a straight line gives the magnetic effect of a long cylinder of finite radius carrying current. The current that flows out of the end of one element flows smoothly into the end of the next

element and so on. The idea behind this approach is to create the magnetic effects of current-carrying flux tubes by stacking these elements, one after another, along model magnetic field lines. The ends of elements stacked along curved diverging field lines will not match up exactly and current will “leak” out at the junctions. If type I current elements are used and care is taken to close the circuit, the current will be identically zero away from the elements. This will not be true for type II elements.

For the second example, I consider three type I current elements, oriented so that the endpoints of each element are on the vertices of an equilateral triangle. The axis of each of the three elements is one of the sides of the triangle. As well, each axis lies in the plane $X = 0$ (arbitrary units). The endpoint of one element is the startpoint of the next. The elements are of radius 1.3 and length 10. Figure 26 consists of two vector plots of electric current in the $X = 0$ plane. The current vectors shown are the sum of the current due to all three elements. Points indicate vectors of length (identically) zero. The vector plots show current flowing along an element and then diverting to flow parallel to the axis of the next and so on. There are large regions of space with no current. As well, there are regions well away from the triangle where the current is small, but finite. This configuration of current elements is a model of distributed current flowing in a triangular circuit. The non-zero current away from the triangular circuit is “extraneous” and, ideally, should be as small as possible.

In Figure 26, points where the current is identically zero are located so that, for each of the three elements, the perpendicular distance from the axis of that element is greater than the radius of that element. The magnetic field at such a point is, according to equation 48, the magnetic field due to a closed circuit consisting of

3 straight lengths of infinitesimally thin wire and hence is curl-free. On the other hand, if the perpendicular distance from a point to the axis of any one of the three elements is less than the radius of that element, the magnetic field is not curl-free. There is finite current everywhere in a cylinder centred on the axis of any one of the elements.

Figure 27a is a vector plot showing electric current on the $X = 0$ plane within such a cylinder and beyond the end of the current element: in particular, it is beyond the end of the element that is the base of the triangle in Figure 26. From Figure 27a, it is clear that there is current flowing both away from (in the centre of the cylinder) and towards the current element. The currents associated with each element are divergence free. As such, the flux of current through a cross section of the cylinder, away from the current element, should be exactly zero. Figure 27b shows values of this flux across $y = \text{const}$ surfaces (i.e., surfaces perpendicular to the axis of the cylinder). This flux is exactly zero through surfaces at Y values beyond the region of intersection of the two current elements. In Figure 27b, I also include a curve giving values of $\int |J_y| dx dz$ over the same surfaces. These results illustrate that the magnitude of the extraneous current becomes small, in comparison to that within the element, at even small distances from the end of the element.

For the third example, I use a large number of type II elements to model the magnetic field in the region of space around two current sheets. The model current sheets are of finite width, thickness and length. Each sheet is built up by adding together a number of type II current elements, the axis of each being parallel to the X direction. One sheet carries current flowing in the negative X direction, the other in the positive X direction. Figures 28a and 28b are two vector plots

showing the magnetic field due to this current configuration. The plots are for a plane perpendicular to the X direction and halfway between the ends of the two model current sheets. The current sheets in Figure 28a are twice as wide as those in Figure 28b. *Fung and Hoffman* [1992] used a similar current configuration to model the magnetic effects of field-aligned current sheets as seen by satellites in low-Earth orbit. They argued that by using model current sheets of finite thickness and width, they could better determine the orientation of actual field-aligned current sheets relative to the trajectory of a satellite passing through them.

I have outlined these three example uses of the current elements for the following reason. In order to build up a realistic magnetospheric magnetic field model, it is necessary to represent the magnetic effects of distributed magnetospheric currents. Short of numerically solving the equations that describe physics of the magnetospheric system, the best approach to this problem is to prescribe a realistic current system and evaluate the magnetic field that is consistent with that system. I feel that the current elements that I have developed are a valuable tool that can be used for this purpose. The first example illustrated how these elements, stacked end to end, can be used to represent the magnetic effects of an infinitely long current carrying cylinder of finite radius. With the second example, I showed that these current elements, connected end to end, can be used to model the magnetic effects of a volume filling current flowing in a closed loop. The third example was my attempt to illustrate how, by stacking these currents side by side, the magnetic effects of a thick current sheet can be modelled.

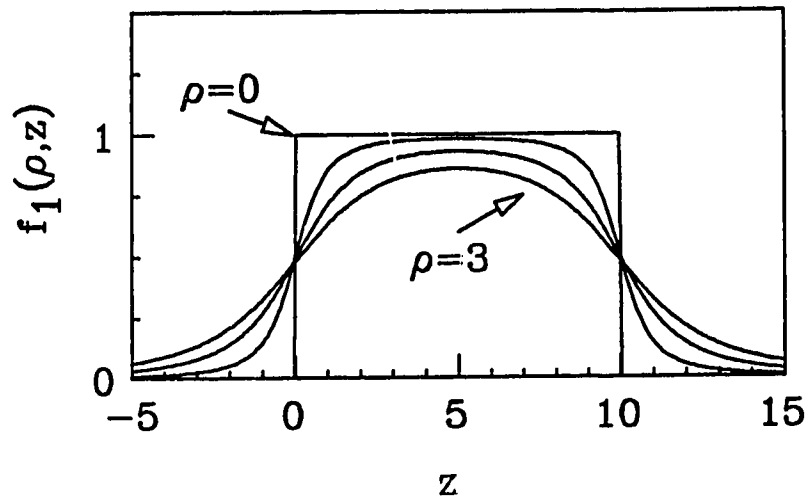


Figure 21. The function $f_1(\rho, z)$ for $\rho=0, 1, 2$, and 3. Here, $z_0 = 0$ and $z_1 = 10$. The curves for $\rho=0$ and $\rho=3$ are labelled. The two intermediate curves are for $\rho=1$ and $\rho=2$.

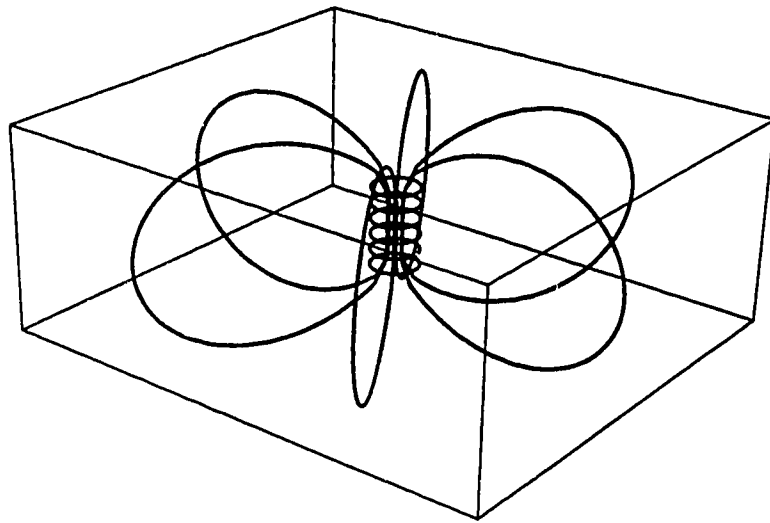


Figure 22. Current and magnetic field line traces for a type I current element. The small stacked circles near the centre of the figure are magnetic field line traces: the radius of each of these circles is slightly larger than that of the current element. The bottom magnetic field line trace and the top magnetic field line trace are in the $z = z_0$ and $z = z_1$ planes. These traces, therefore, roughly mark the outline of the cylindrical current element. The six roughly 'D' shaped curves are electric current line traces.

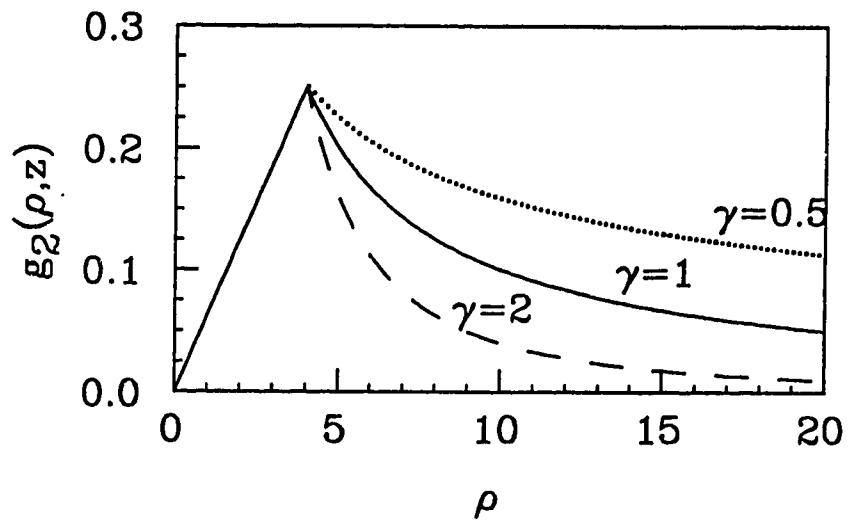


Figure 23. The function $g_2(\rho, z)$ for $z = 0$, $a = 4$ and three different values of γ . Note that the curve for $\gamma = 1$ is also the curve for $g_1(\rho, z)$.

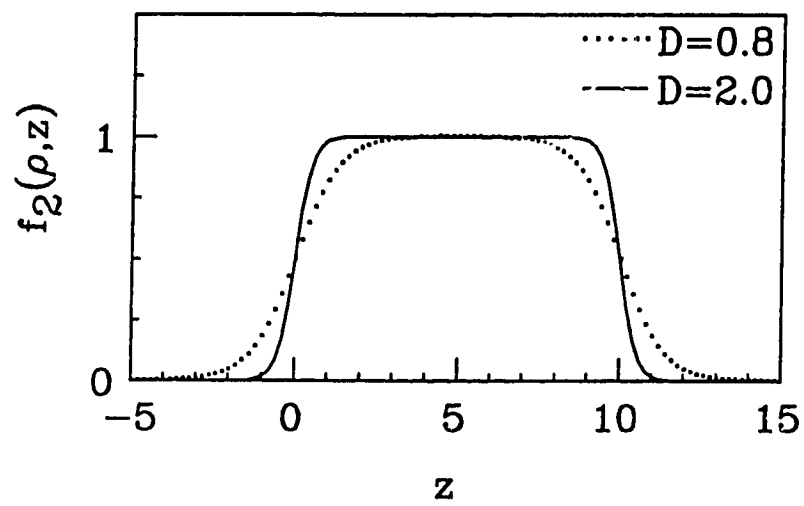


Figure 24. The function $f_2(\rho, z)$ for two different values of D , where $D = D_0 = D_1$. Here, $z_0 = 0$ and $z_1 = 10$. Note that this envelope function is independent of ρ .

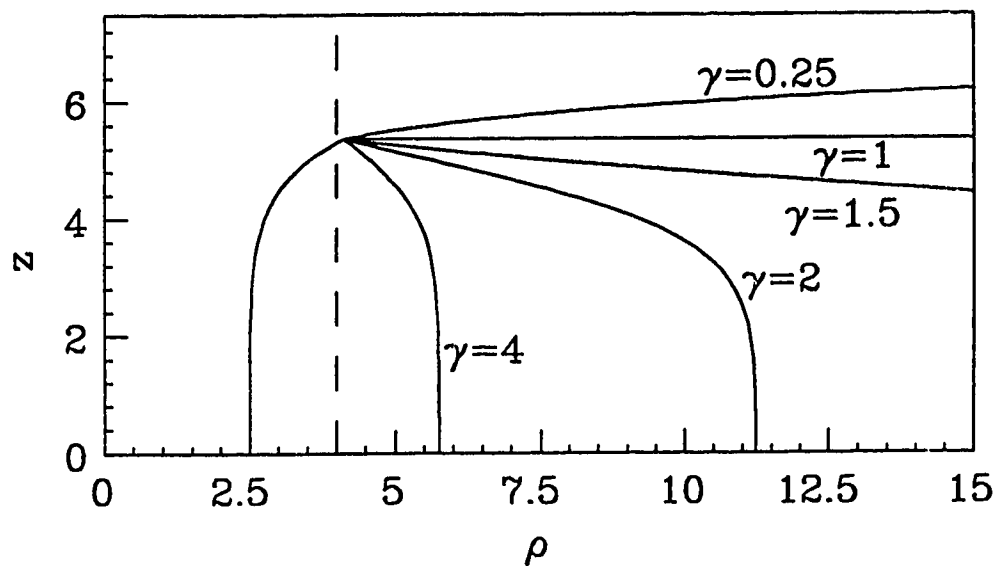


Figure 25. Current line traces projected in the ρz plane for a type II current element. Here $a = 4$, $z_0 = -5$, $z_1 = 5$, $D_1 = D_2 = 0.75$ and $0.25 \leq \gamma \leq 4$.

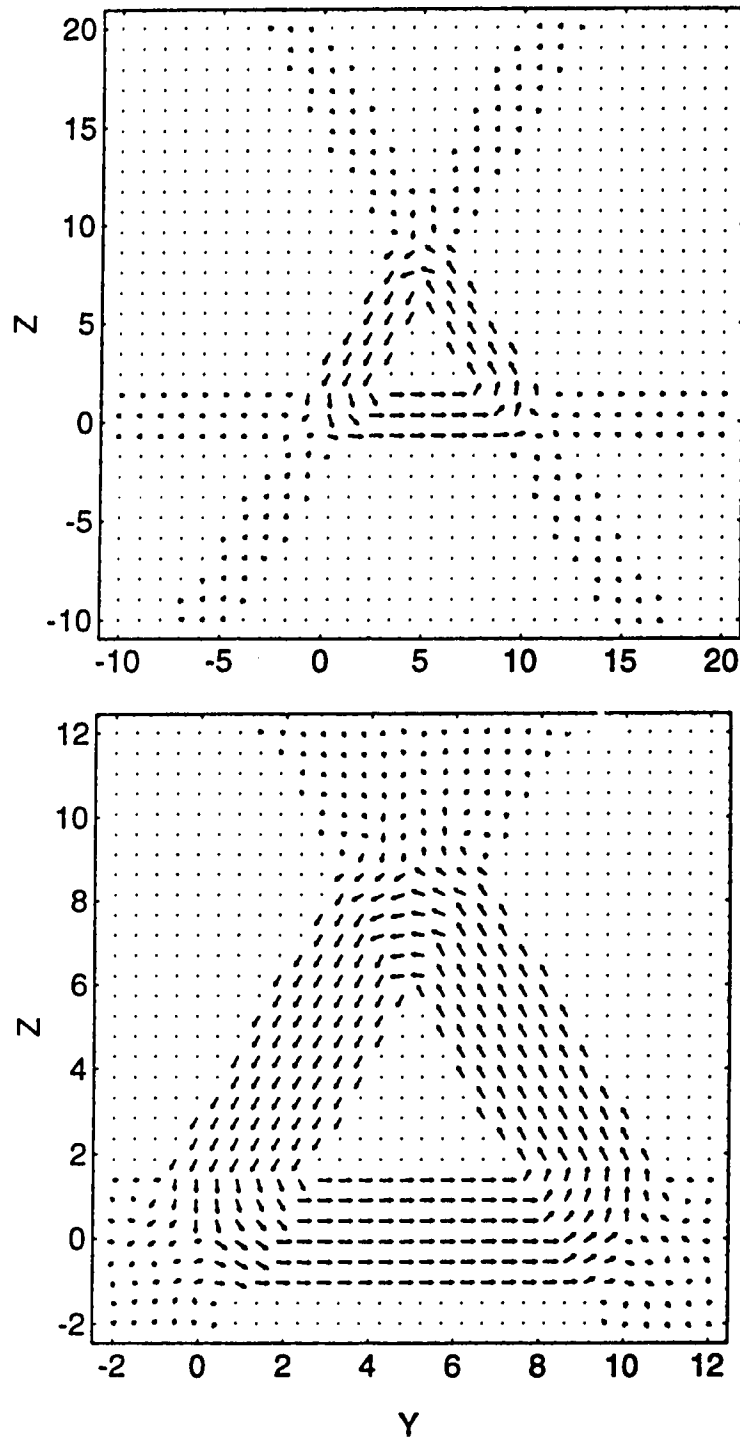


Figure 26. Electric current vectors in the YZ plane for a circuit constructed with three type I current elements. Vectors shown as points are of length (identically) zero. The bottom panel is an enlargement of the central portion of the top panel.

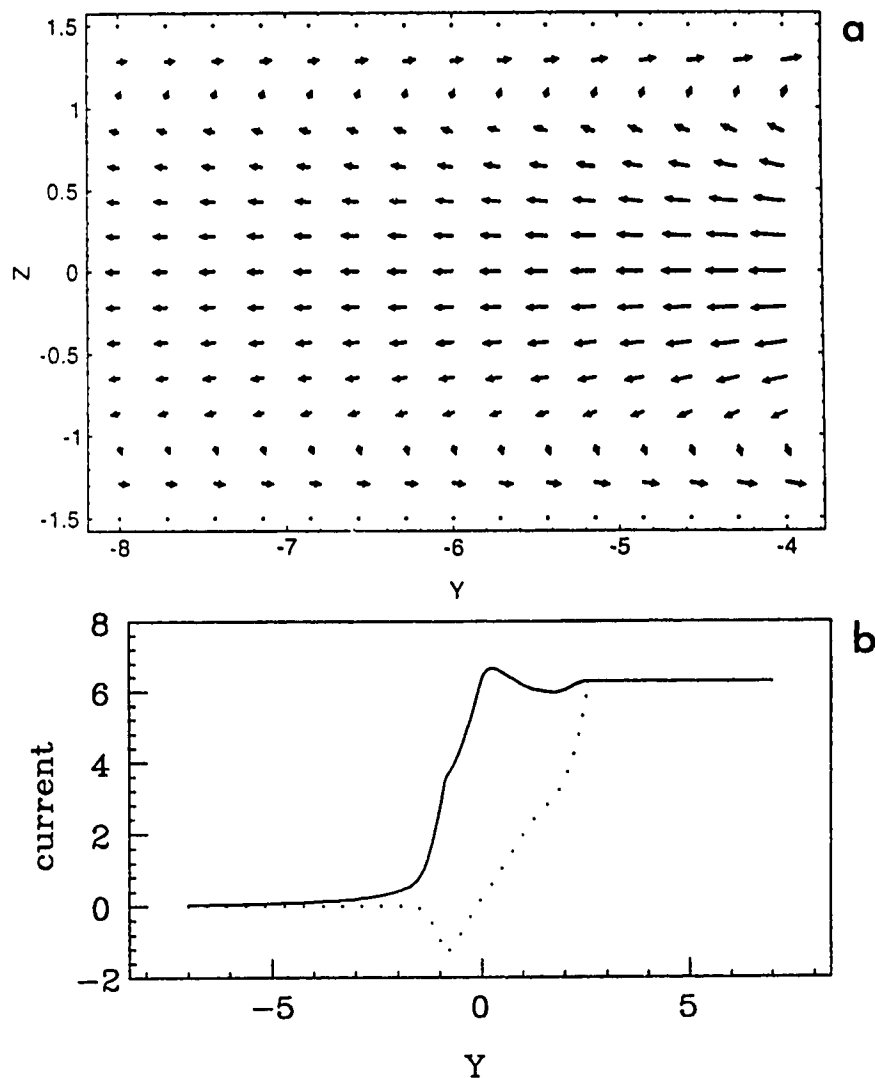


Figure 27. Extraneous current in the example circuit shown in Figure 26. (a) Electric current vectors in the YZ plane for the same circuit shown in Figure 26. The current vectors are shown in a region along the axis of one of the three current elements, but beyond the end of the current element. (b) Total current, obtained by summing the current from all three elements, in the cylinder centred on the axis of one of the three current elements in the circuit. The cylinder has the same radius as the current element. Values of total current crossing a plane of constant Y , along the Y axis, from outside the end of the current element, to inside the current element. The solid and dotted curve show values of $\int |J_y| dx dz$ and $\int J_y dx dz$, respectively. In both cases, the integral is carried out over the cross section of the cylinder.

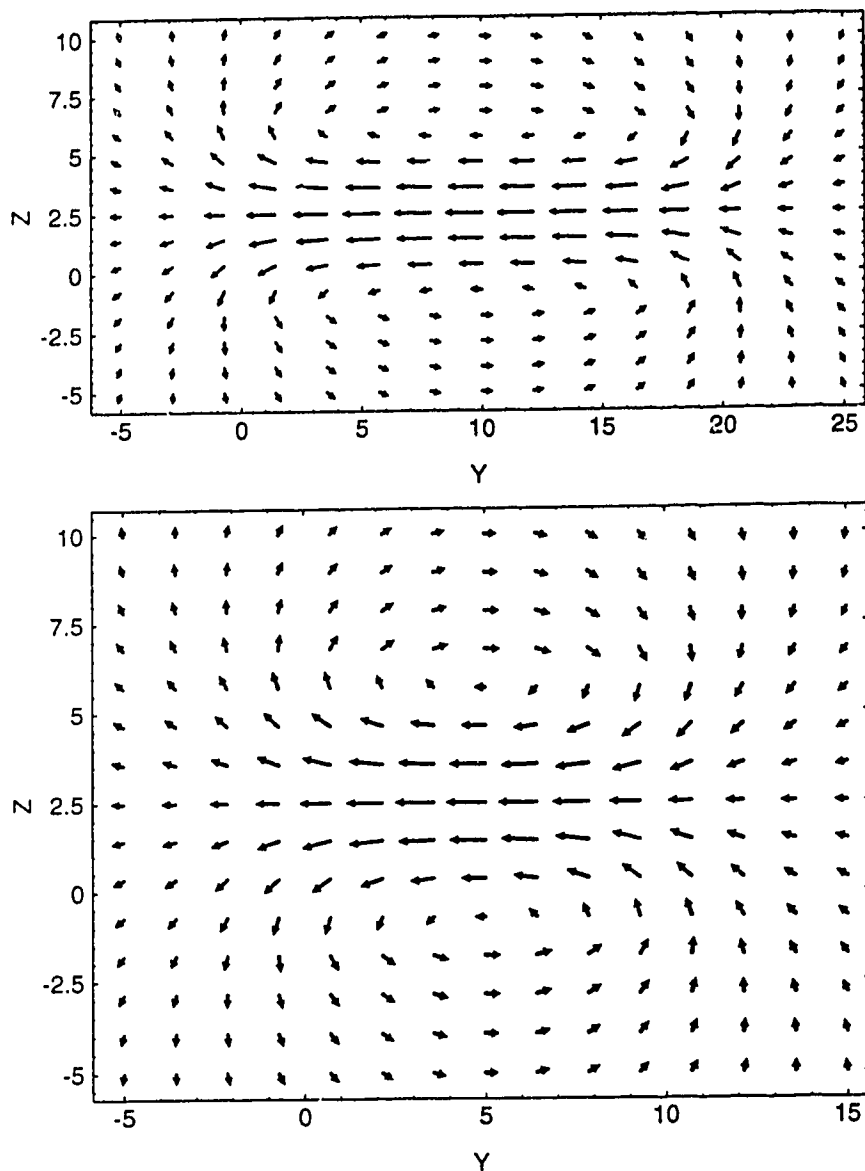


Figure 28. Magnetic field due to two current sheets. Each current sheet consists of 200 type II current elements with axis parallel to the X axis. The current elements are of radius 2. One current sheet is in the $Z = 0$ plane and the other is in the $Z = 5$ plane. The current sheets extend (a) 20 and (b) 10 units in the Y direction.

Elements of a Global Model: Transverse Currents

The remainder of this chapter contains a description of a model of the magnetic effects of the cross-tail, ring and field-aligned current systems that were described in the introduction. I divide this description into two sections, the first and second describing the models of the magnetic effects of the transverse and field-aligned currents, respectively. In chapter 2, I reviewed previously developed models of the ring and cross-tail current systems.

Model Ring Current

Using type I current elements, I build up an azimuthally symmetric model ring current. The axis of each element used to build up the model ring current is the sm equatorial plane; however, since I only treat zero dipole tilt situations in this thesis, the sm and gsm coordinate systems are the same.

To start with, I build up the magnetic effects of a single ring of current by stacking the current elements, end to end, along a circle in the equatorial plane centred on the Earth. The start- and end-points of each element are on this circle. My model ring current consists of a number of these loops, each one following a circle of slightly different radius than that of every other one. I choose the radii of these loops so that the concentric rings are evenly distributed between roughly 4 and 8 R_E from the centre of the Earth. I show curves made up of straight lines between the start- and end-points of each element on each model current ring in Figure 29.

For the work presented in this thesis, I build up each current ring out of forty elements. The current in the model rings flows from east to west. The radii of each

current element is larger than the distance between adjacent current rings. This overlap allows for a relatively smooth magnetic field distribution. I provide values of the magnetic field, in the equatorial plane, due to this model ring current in Figure 30. The three curves all show equatorial magnetic field values for a model ring current carrying a total current of 1.2 MA. The solid and dotted curves show B_z due to a current constructed of the 19 rings illustrated in Figure 29. In one case (solid curve), each contributing current element is of radius $2 R_E$ while in the other case (dotted curve) each element is of radius $1 R_E$. The dashed curve gives values of B_z due to one ring of radius $6 R_E$ where each contributing current element is of radius $0.5 R_E$.

The graph in Figure 31 shows the relationship between the natural logarithms of the equatorial magnetic field strength and the radial distance from the centre of the Earth. In this case, the magnetic field is the total magnetic field due to the model ring current built up as shown in Figure 29 and a terrestrial dipole. The straight line of slope -1 is for the case of zero added ring current. The other two curves are for the cases of a ring current carrying a current of 5 and 10 MA. In the region beyond the model ring current, the field due to the dipole and ring current behaves like that of a dipole of larger strength than that of the Earth. Each 1 MA of current in this ring current configuration has the effect of increasing the earth's dipole field, in the equatorial region outside of the ring current region, by $\sim 2340 \text{ nTR}_E^3$ or by a factor of roughly 0.08.

Model Cross-Tail Current With Closure

The model cross-tail current system is, as well, built up with a large number of type I current elements. Figure 32 shows the theta shaped circuits used to construct

the model cross-tail current system. The curves shown in the figure are made up of straight line segments joining the endpoints of the current elements used to construct the circuits. The theta shaped circuit consists of a neutral sheet current built up of current elements with axes all lying in the equatorial (gsm) plane. The direction of model current flow along the equatorial portion of the circuit is east to west (or dawn to dusk). In the vicinity of the dusk magnetopause, the current divides into two closure currents, one around each of the two magnetospheric lobes.

The equatorial segment of each circuit is a segment of a circle. The centre of the circle is on the X_{gsm} axis, either sunward (for curvature around the Earth) or tailward (for curvature away from the Earth). The radius of the circle determines how curved the current path is in the equatorial plane. The closure of the current over the magnetopause is, in this model, in a plane that passes through the two ends of the equatorial segment of the circuit. This plane can be parallel to the Z_{gsm} direction or tilted earthward or tailward with respect to that direction.

A complete specification of the model current system involves the specification of the following: (1) the Earthward and tailward extent of the cross-tail current system; (2) the number of theta current circuits; (3) the radius of each current element; (4) the centre of the circle that the equatorial segment of the circle follows; (5) the shape of the magnetopause; (6) the tilt, with respect to the Z_{gsm} direction, of the plane containing the magnetopause segment of the theta current; (7) the amount of current carried by each theta shaped circuit. In chapter 4, I describe the use of this model for quantitative mapping, along magnetic field lines, between the ionosphere and the magnetosphere. In that section, I discuss the basis for my specification of each of the above.

Figures 33 and 34 are contour plots showing model magnetic field magnitudes

on the $X_{gsm} = -25 R_E$ surface. The magnetic field here is due to a terrestrial dipole, a model ring current carrying 1.2 MA of current and the model tail current system described here. In Figure 33, the sharpness of the boundary between the model magnetosphere and the interplanetary medium is evident in the sharpness of the change in magnetic field strength at the model magnetopause. The contour plot in Figure 34 shows the model magnetic field strength in the region outside of the model magnetosphere. In comparison to the magnetic field strength within the model magnetosphere, the values are small, but not zero. That the field is not zero is a consequence of the fact that the magnetopause currents are not truly shielding, in the sense that shielding the interplanetary medium from the magnetospheric magnetic field has not been a consideration in the choice of where to locate the currents and how much current to use.

It is interesting to compare the contour plots in Figures 33 and 34 with the one showing magnetic field strengths on the same plane, but given by the T87 model (Figure 8). I point out, also, that the magnetic field in the lobe regions given by my model is curl-free: any point outside of the current elements that make up the theta shaped circuits, and inside the model magnetosphere, is not within any one of the infinitely long cylindrical regions that have extraneous finite current within them (see Figures 26 and 27 and the accompanying text).

In chapter 2, I showed that the shape of T87 model field lines, in the region where the actual magnetopause typically is located, is unrealistic. For field lines just inside the magnetopause, I argued, this flare should be equal to the rate of change of magnetopause radius with X_{gsm} (see equation 29). In Figure 35, I show values of the flare of the magnetic field from my model, as determined using the left-hand side of equation 29. The three curves give values of this flare, at $X_{gsm} = -25 R_E$, on three

lines passing through the model magnetopause. The three lines are each parallel to the Z_{gsm} direction and are at $Y_{\text{gsm}} = 0$, $Y_{\text{gsm}} = 10 R_E$ and $Y_{\text{gsm}} = 20 R_E$. For the results shown here, the model magnetopause is fit to the empirical relationship of *Sibeck et al.* [1991] between magnetosphere radius and X_{gsm} appropriate for solar wind dynamic pressures in the range from 2.6 to 4.9 nPa. The current elements used to build up the magnetopause part of the cross-tail current system are all of radius $1 R_E$. At $X_{\text{gsm}} = -25 R_E$, the centres of these elements are on a circle of radius $23 R_E$. For a magnetopause shaped exactly the same as the surface given by Sibeck's empirical relationship, the derivative dR/dX_{gsm} should be -0.21 at $X_{\text{gsm}} = -25 R_E$. The value of this derivative, as given by the flare of magnetic field lines in my model, is roughly -0.2 just inside the model magnetopause current layer, over a large range of Y_{gsm} values. Figure 36 shows values of the model magnetic field strength along the same three $Y_{\text{gsm}} = \text{const}$ lines on which the values of magnetic field flare shown in Figure 35 were determined.

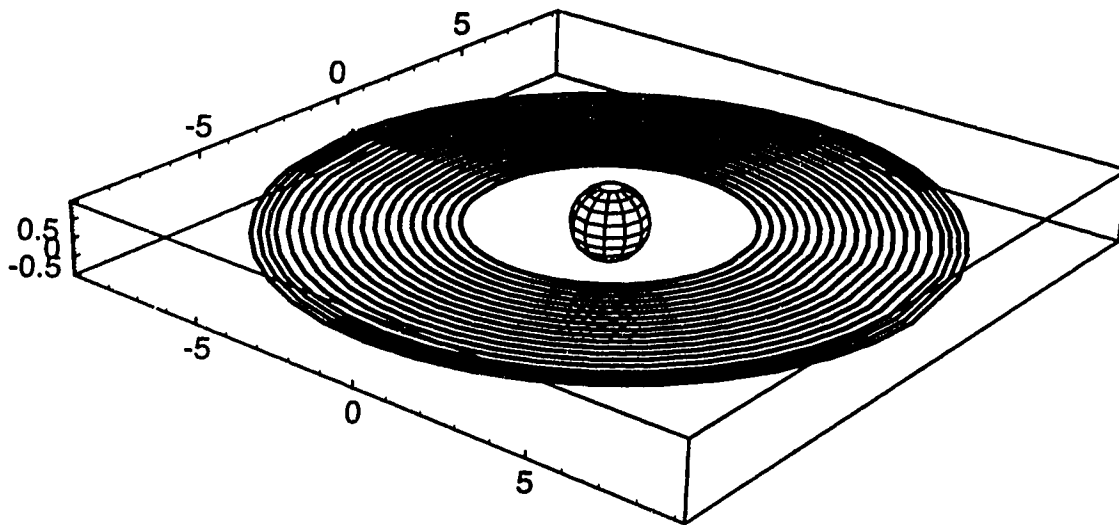


Figure 29. Location of current elements used to build up a model ring current. The 19 curves shown here are approximations of Earth-centred circles. Each curve is constructed with 40 straight line segments. These segments are the axis of current elements used to build up the model ring current.

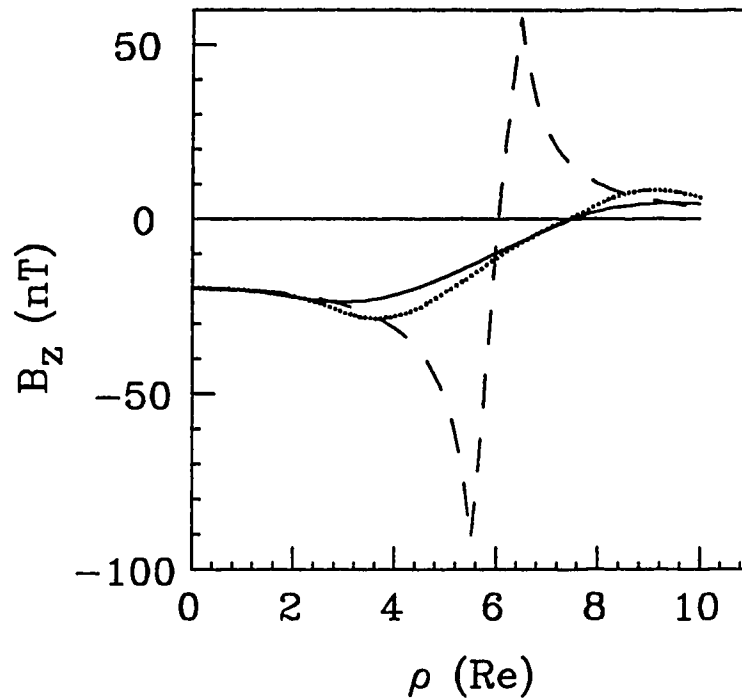


Figure 30. Northward (Z_{gsm}) component of magnetic field in the equatorial plane due to three model ring currents. Here, ρ is $\sqrt{X_{gsm}^2 + Y_{gsm}^2}$. The dotted and solid curves show values of the magnetic field due to the ring current configuration in Figure 29, where the radii of the current elements are 1 and 2 R_E , respectively. The dashed curve shows values of magnetic field due to a model ring current constructed out of one current loop. In the latter case, the radii of the current elements are 0.5 R_E and the centre of each element is at $\rho = 6 R_E$. In each case, the total ring current is 1.2 MA and is flowing from east to west.

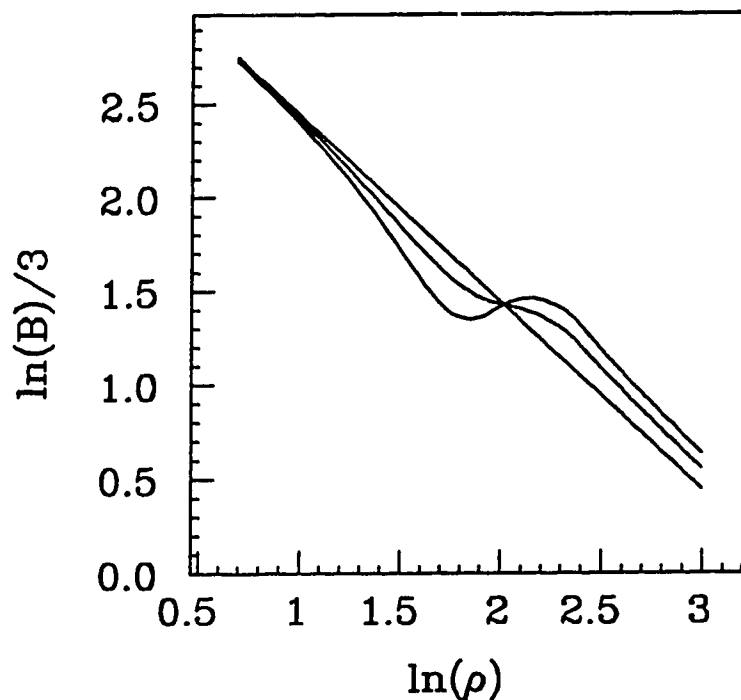


Figure 31. Magnetic field intensity in the equatorial plane due to a terrestrial dipole and a model ring current. The magnetic field due to the dipole alone is the straight line of slope -1. The other two curves correspond to the magnetic field due to the dipole and a model ring current. In each of these two cases, the model ring current corresponds to that shown in Figure 29. The radii of the current elements are $2 R_E$. The curve closest to the straight line (dipole only curve) is for a ring current with a total current of 5 MA. The third curve is for a 10 MA ring current.

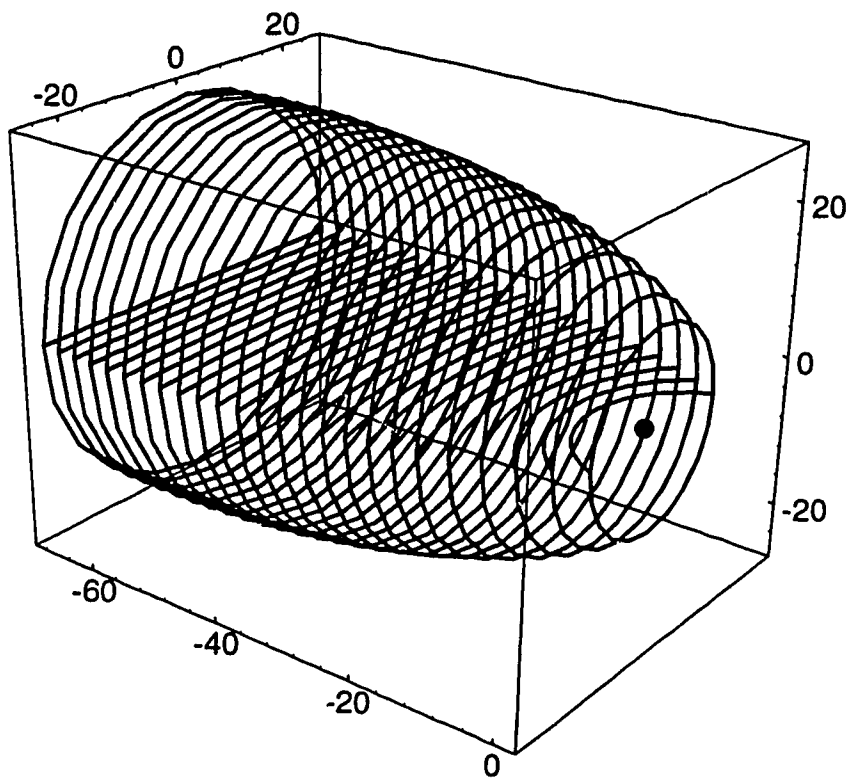


Figure 32. Current flow paths for the model cross-tail current system. The curves shown here are drawn by connecting, with straight line segments, the start- and end-points of the current elements used to build up "theta" shaped circuits.

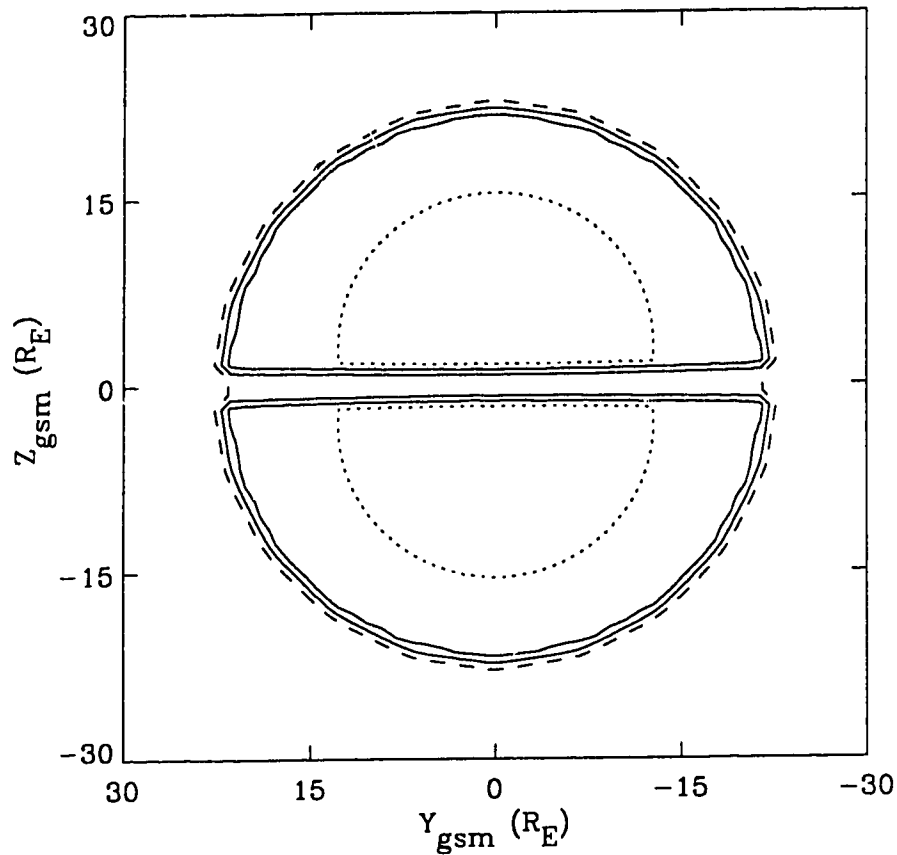


Figure 33. Model magnetic field magnitude on the $X_{\text{gsm}} = -25 R_E$ surface. The magnetic field is the sum of those due to a terrestrial dipole, a model ring current carrying a total current of $1.2 MA$ and a model cross-tail current system constructed as shown in Figure 32. The peak value is 23.5 nT . Contours for $|\vec{B}|=10, 14, 18$ and 22 nT are plotted. The dashed (outermost) contour indicates values of $|\vec{B}|=10 \text{ nT}$ and the two dotted contours indicate values of $|\vec{B}|=22 \text{ nT}$.

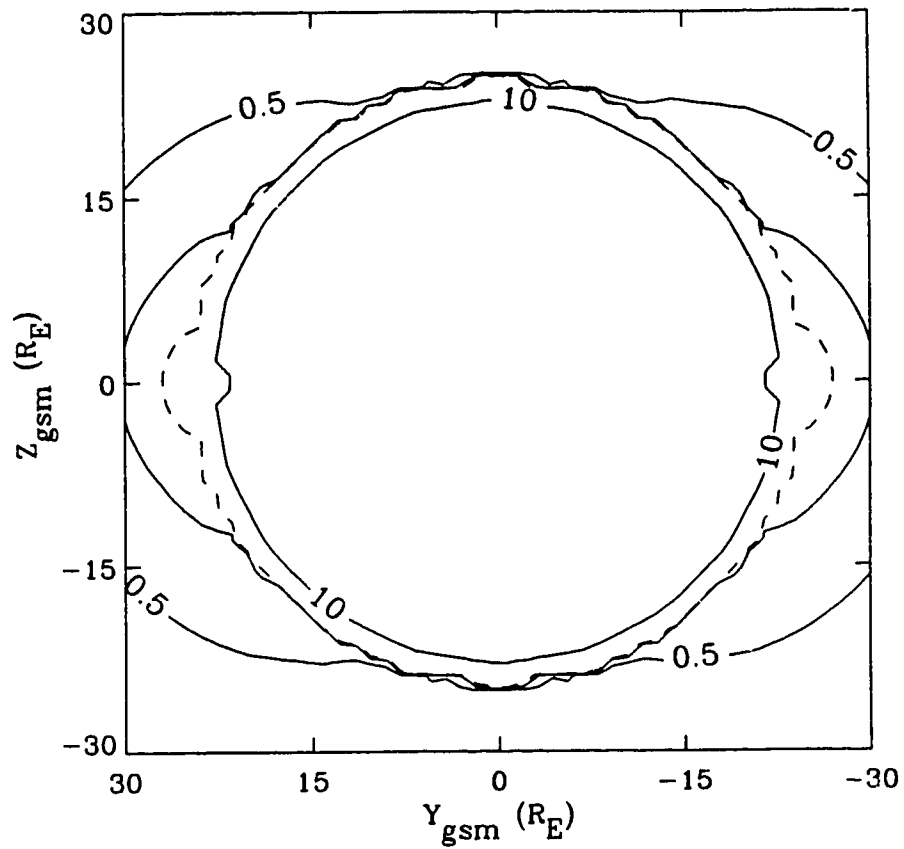


Figure 34. Model magnetic field magnitude on the surface $X_{gsm} = -25 R_E$. The magnetic field is from the same model as described in the caption for Figure 33. Here, values outside of the model magnetosphere are shown. The nearly circular $|\vec{B}|=10$ nT contour is in (roughly) the centre of the model magnetopause current carrying region. The dashed contour is for $|\vec{B}|=0.9$ nT and the other two solid contours are for $|\vec{B}|=0.7$ nT and $|\vec{B}|=0.5$ nT.

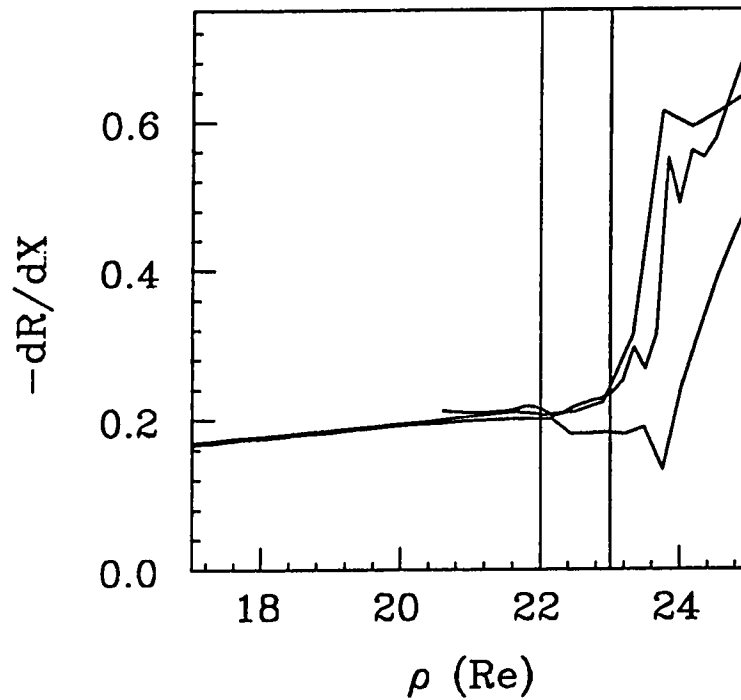


Figure 35. Flare of model magnetic field lines as calculated using the left-hand side of equation 29. The values are plotted as a function of radial distance from the X_{gsm} axis (i.e., $\rho = \sqrt{Y_{\text{gsm}}^2 + Z_{\text{gsm}}^2}$). The values shown are calculated along three $Y_{\text{gsm}} = \text{const}$ lines in the $X_{\text{gsm}} = -25 R_E$ plane (in particular, $Y_{\text{gsm}} = 0$, $Y_{\text{gsm}} = 10 R_E$ and $Y_{\text{gsm}} = 20 R_E$). The two vertical lines indicate, roughly, the location (in terms of ρ) of the centre and inner edge of the model magnetopause current layer.

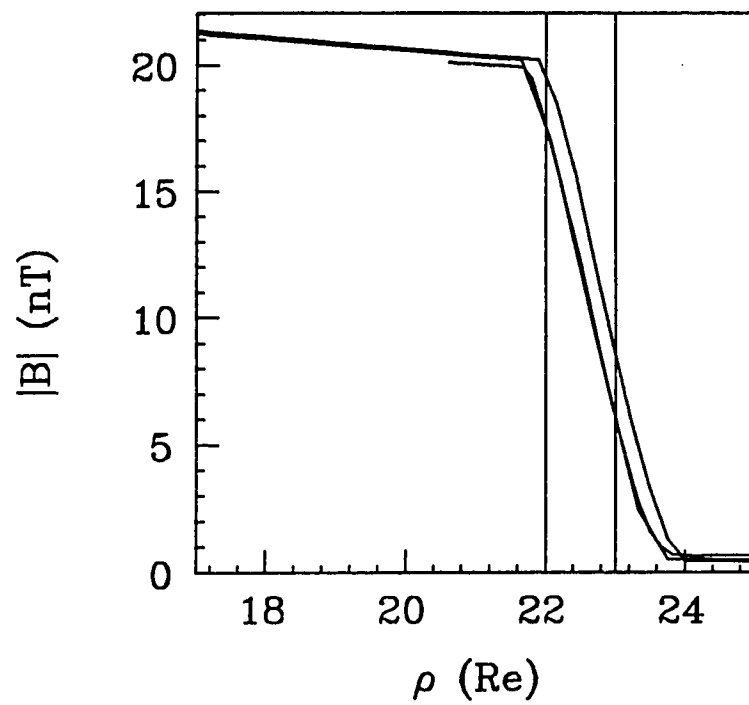


Figure 36. Model magnetic field strength on the same three $Y_{gsm} = \text{const}$ lines on which the values shown in Figure 35 were determined.

Elements of a Global Model: Field-Aligned Currents

There have been a number of efforts to model the effects of field-aligned currents in the magnetosphere. Early work involved the addition of the magnetic field due to currents flowing along dipolar magnetic field lines to that of the dipole. For example, *Kisabeth* [1979] used the Biot-Savart law to evaluate the magnetic field due to field-aligned current configurations. Developing such a model required both a reasonable model of the field-aligned current distribution and an efficient numerical method of determining the magnetic field. *Kisabeth* [1979] used a model current system proposed by *Boström* [1971] as a building block to construct a large-scale model current system. He used the following three techniques to evaluate the magnetic field due to the model current system: (1) direct integration of the Biot-savart law integral; (2) determination of a magnetization distribution equivalent to the current distribution and using that magnetization distribution to calculate the appropriate magnetic scalar potential; (3) determination of a magnetic charge distribution from which a magnetic scalar potential can be determined [*Kisabeth*, 1979]. The second and third methods were developed by *Kisabeth* [1979] in order to decrease the amount of computer time necessary to calculate the model magnetic field.

In more recent years, the object of most studies of the magnetic effects of the field-aligned currents has been to include their effects in a realistic magnetospheric magnetic field model. *Kaufmann and Larson* [1989] developed a model of field-aligned currents in order to study how the magnetic field due to these currents might affect the mapping of electric potential distributions from the ionosphere to the magnetosphere. They used *Olson and Pfitzer's* [1974] technique to model the magnetic effects of the field-aligned current system. Their model of the field-

aligned current system consisted of a number of current loops, each of which was constructed from a number of finite length wire elements. The current loops were placed on a background magnetic field. It was necessary to perform several iterations, tracing new field lines upon which to put current loops, using the background magnetic field and the magnetic field of all of the loops. They found that it was generally possible, using their technique, to construct "self-consistent" configurations of these field-aligned currents. Here, self-consistent is taken to mean that the added current is indeed field-aligned. *Stern* [1993] and *Tsyganenko* [1991] have been working towards a more general representation of the magnetic field caused by the large-scale field-aligned currents. Both Stern and Tsyganenko are developing analytical functions to represent the magnetic field due to large sheet-like current structures, with the currents flowing in a pattern expected from observations of the ionospheric end of the current system [e.g., *Iijima and Potemra*, 1976]. Their approach is computationally more efficient than that of *Kaufmann and Larson* [1989]. As well, it is possible to use this technique to attempt to extract information about the distribution of field-aligned currents from a large data base of in situ magnetic field measurements. The approach of *Kaufmann and Larson* [1989] has the disadvantage that, because the current elements are segments of wire, the current density associated with the field-aligned current model is either zero or infinite. As well, there are singularities in the magnetic field: near the wire elements, the magnetic field becomes infinite. Their approach, however, leads to a current system that is actually field-aligned. Furthermore, it is flexible enough that the model field-aligned currents can be closed in the magnetosphere along any specified path and can be used to explore the consequences of different possible current closure paths. This is an important advantage, considering the lack of knowledge about

how these currents close in reality.

The approach I use in the development of the model presented here is similar to that of *Kaufmann and Larson* [1989]. I use a large number of current elements to construct a large scale field-aligned current system. The current elements, however, are not infinitesimally thin wire segments with an infinite current density. Instead, I use elements with current densities that are volume-filling.

I will add the effects of the field-aligned currents to a background model field that, presumably, does not already include these effects. Initially, I construct a model current-carrying flux tube using current elements by positioning the end-points of each element (i.e., the points at z_0 and z_1 along the z -axis of each element) on the magnetic field line. To create the magnetic effect of a field-aligned current sheet, I carry out this procedure along a large number of closely spaced field lines. I model the magnetic effects of the morning sector Region I and Region II current sheets by placing the ionospheric ends of these model sheets as indicated in Figure 37. By applying symmetry relationships, extended this pattern to model Region I and II currents in the evening and morning sectors in the southern and northern hemispheres. Each Region I flux tube has a corresponding Region II flux tube with an ionospheric footprint in the same magnetic meridian. The two flux tubes are connected in the ionosphere by a meridional current element. The closure of these currents in the magnetosphere is through one of two possible paths, illustrated in Figures 38 and 39. The first closure path (Figure 38) connects the Region I and Region II flux tubes through a radial current element in the equatorial plane while the second circuit connects the dawn and dusk sector Region II currents azimuthally in the equatorial plane and takes the Region I currents out to the distant magnetosphere.

In a process similar to one outlined by *Kaufmann and Larson* [1989], I retrace the field lines on which the current elements are centred a number of times using the modified magnetic field, in an attempt to iterate towards a field-aligned configuration. How field-aligned the final configuration will be is dependent on how much current is added and how far out in the magnetotail the currents are taken. It is essential that the current configuration be as close to field-aligned as possible if mapping studies can be carried out on field lines that are in the vicinity of the current sheets. A typical consequence of this condition not being met well enough is that the field lines of interest will cross a current sheet. If this happens, the integrated effects of the field-aligned currents along such a field line will be far from reasonable.

There are several criteria that I could use in the selection of the constant α (which is same for each element making along any given closed current loop). For a flux tube constructed with these elements, I could select α so that the current density in the ionosphere is some desired value. If this value is $J_{\parallel i}$ (in $\mu\text{A}/\text{m}^2$), and the expressions for the magnetic field due to either type I or type II elements are to give values in nT with the input parameters in units of Earth radii, then for any element along this model flux tube

$$\alpha = \mu_0 a_i^2 J_{\parallel i} 10^3 R_E / 2 \quad (62)$$

where a_i is the radius of the ionospheric end of the flux tube in Earth radii, $\mu_0 = 4\pi 10^{-7}$ and R_E is the radius of the Earth in meters. A second possibility is to select values of α so that the total amount of current flowing in the field-aligned circuit is some desired value. A third possibility is to parameterize the

amount of current in the model field-aligned current distribution so that a desired maximum perturbation of the eastward component of the magnetic field in the top-side ionosphere (i.e. at TRIAD altitude) is produced.

For this study, I choose values of the radius a of the elements so that, at the ionospheric end of the flux tubes, the current sheets have an ionospheric footprint with a north-south extent of roughly 1.5° . The radius a of the elements increases with increasing distance from the Earth, corresponding to the increasing cross-sectional area of the flux tube. The coefficient α , and therefore the amount of current carried by an element, is the same for each element of a model current loop.

A complication arises because of the use of cylindrical current elements and the fact that, in reality, circles in the ionosphere do not map to circles in the magnetosphere. A model flux tube, constructed out of cylindrical elements, will have an increasingly unrealistic cross-section with increasing distance from the Earth. A current sheet constructed from these flux tubes will remain a current sheet; however, the rate at which the current sheet thickens will not be "correct", in the sense that the magnetic flux contained in the current sheet will vary with distance from the Earth. Figure 40 shows a comparison of the thickness of a typical model current sheet with that of a current sheet that has the same ionospheric footprint but is also threaded constant magnetic flux. The model current sheets are always thinner than they would be if the magnetic flux threading them did not vary with distance from the Earth.

It would be possible to adjust the flux tube radii so that the magnetic flux threading a model current sheet does not vary with distance from the Earth. In the present work, however, I have not done this for the following two reasons,

one of which applies to the Region I current sheets and the other to Region II current sheets. First, in the inner magnetosphere, the difference between the model current sheet thickness and the correct current sheet thickness is small except near the equatorial plane, where the current is being diverted into transverse closure current. Therefore, this effect is not important for the model Region II currents. Second, although the effect is more important for the Region I currents (away from the equatorial plane the ratio of the correct to the modelled layer thicknesses can be 1.5 or more), several processes will broaden a current sheet causing it to have a larger ionospheric footprint than magnetic flux conservation alone would indicate. For example, the dawn-dusk electric field will cause charged particles in the PSBL to $\vec{E} \times \vec{B}$ drift towards the equatorial plane [e.g., *Onsager et al.*, 1991].

The model I have presented here provides magnetic field values due to night-side Region I and II currents on the dawn and dusk sides of the northern and southern hemisphere magnetosphere. The model currents close through two different paths, as I illustrate in Figures 38 and 39. In the near-Earth region, currents closed either way produce similar magnetic field perturbations. Here, “near-Earth” means Earthward of where field lines, on which model Region II currents are placed, intersect the equatorial plane. On the other hand, further out in the magnetotail, currents closed through the two possible paths will produce magnetic perturbations that differ significantly. To produce the results presented below, model Region II currents are placed on field lines that cross the equatorial plane roughly $8 R_E$ from the Earth. Here, the regions Earthward and tailward of $8 R_E$ are the inner and outer magnetosphere, respectively. For both regions, I discuss effects of added currents on the magnetic field and on mappings between the ionosphere and the region in question in the following chapter.

I use model currents constructed with type I elements and closed as shown in Figure 38 to produce the inner magnetosphere results. Figure 41 shows magnetic field vectors, due to the model current system, determined on a surface $6 R_E$ from the Z_{gsn} axis. In Figure 42, a latitude profile of the difference between the eastward components of the modified and background magnetic fields at TRIAD altitude (800 km) is shown. I present meridional profiles of the Z_{gsn} and azimuthal (ϕ) components of the magnetic field due to the current sheets on a surface $6.63 R_E$ from the Earth's centre on the 0300 hours MLT and 0125 hours MLT meridians in Figures 43 and 44, respectively. Away from the edges of the current sheets and in the near-Earth region, where the azimuthal component of the background magnetic field is small, the peak azimuthal component of the magnetic perturbation due to the field-aligned currents should vary as $1/R_{xy}$, where R_{xy} is the distance from the Z_{gsn} axis. Figure 45 shows a comparison of the model peak perturbations in the 0300 hours MLT meridian with those expected on the basis of a $1/R_{xy}$ dependence.

Figures 46 through 49 show effects of field-aligned currents on the magnetotail magnetic field. Currents closed radially in the equatorial plane (i.e. as in Figure 38) decrease B_z near midnight in the equatorial plane and increase the flare of the CPS magnetic field away from midnight. On the other hand, a current system with Region II currents closed azimuthally through a "partial ring current" and Region I currents taken out to the distant magnetotail (i.e. as in Figure 39) will increase B_z near midnight in the equatorial plane, but will have little effect on the flare of the CPS magnetic field relative to the noon-midnight meridian. It is often assumed that the field-aligned currents will cause an increase in equatorial B_z near midnight [e.g., *Rostoker and Boström, 1976; Donovan et al., 1992*]. That field-aligned currents could also cause a decrease in equatorial B_z near midnight is

an interesting and unexpected result that could help to explain *Fairfield's* [1986] observation that in the equatorial magnetotail, B_z is observed to be larger at the flanks than near midnight.

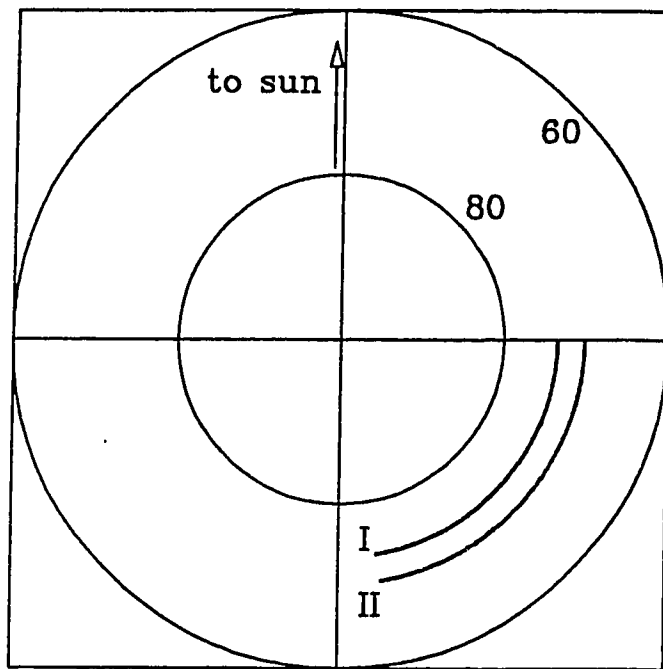


Figure 37. View from above the north pole of the northern polar region showing a locus of points used as footprints of the model night-side Region I (marked 'I') and II (marked 'II') currents.

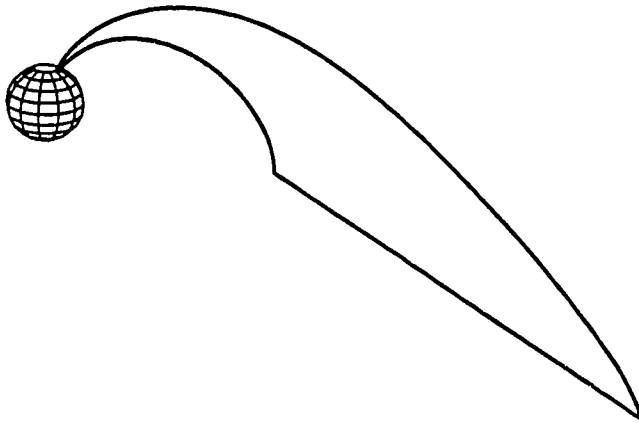


Figure 38. One closure path of field-aligned currents used in this study. Here, the Region I and Region II current elements are closed with north-south current elements in the ionosphere and radial current elements in the equatorial plane of the magnetosphere.



Figure 39. One closure path of field-aligned currents used in this study. Here, Region I and Region II current elements are joined in the ionosphere with north-south current elements. The dawn-side Region II current is connected to the dusk-side region II current azimuthally in the equatorial plane. The region I currents are taken out to the outer magnetosphere.

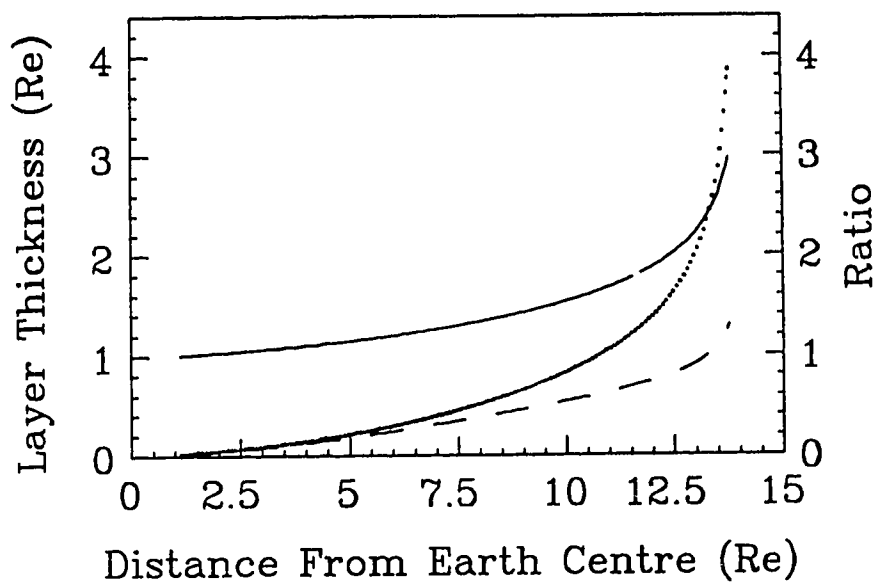


Figure 40. Current sheet thickness as a function of distance from the Earth. These values are determined along a field line traced using the T87 $K_p = 2$ magnetic field model. The field line footprint is in the ionosphere at 69° latitude and 0200 hours MLT. The expected thickness, based only on magnetic flux conservation, of a current sheet that is $0.030 R_E$ thick in the ionosphere and is centred (latitudinally) on this field line is shown by the dotted curve. The dashed curve shows the thickness of a model current sheet. The solid curve shows the ratio of the expected current sheet thickness to the model current sheet thickness.

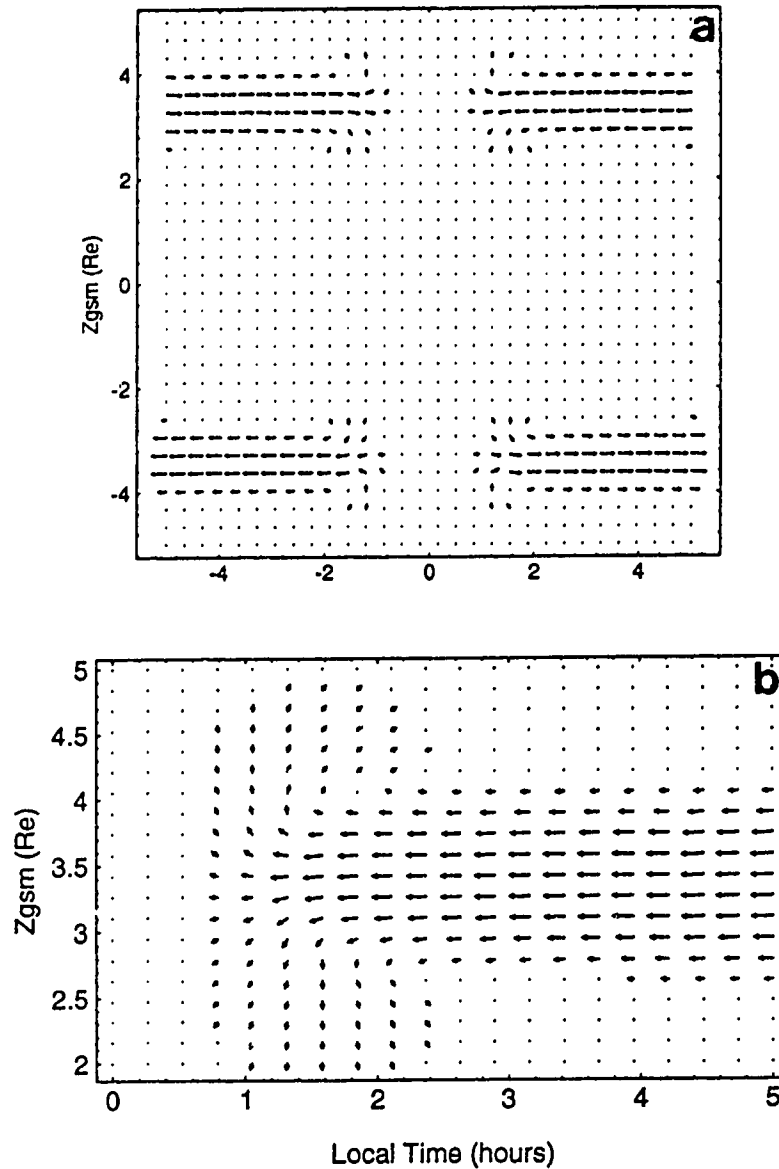


Figure 41 . Vector plots showing (a) the perturbation magnetic field due to the four lobed field-aligned current pattern and (b) a more detailed view of the magnetic perturbation due to the morning sector northern hemisphere currents. Both plots show values determined on a surface $6 R_E$ from the Z_{gsm} axis. Panels a and b show only vectors with magnitudes larger than 15 and 10 per cent of the maximum value on the plot, respectively.

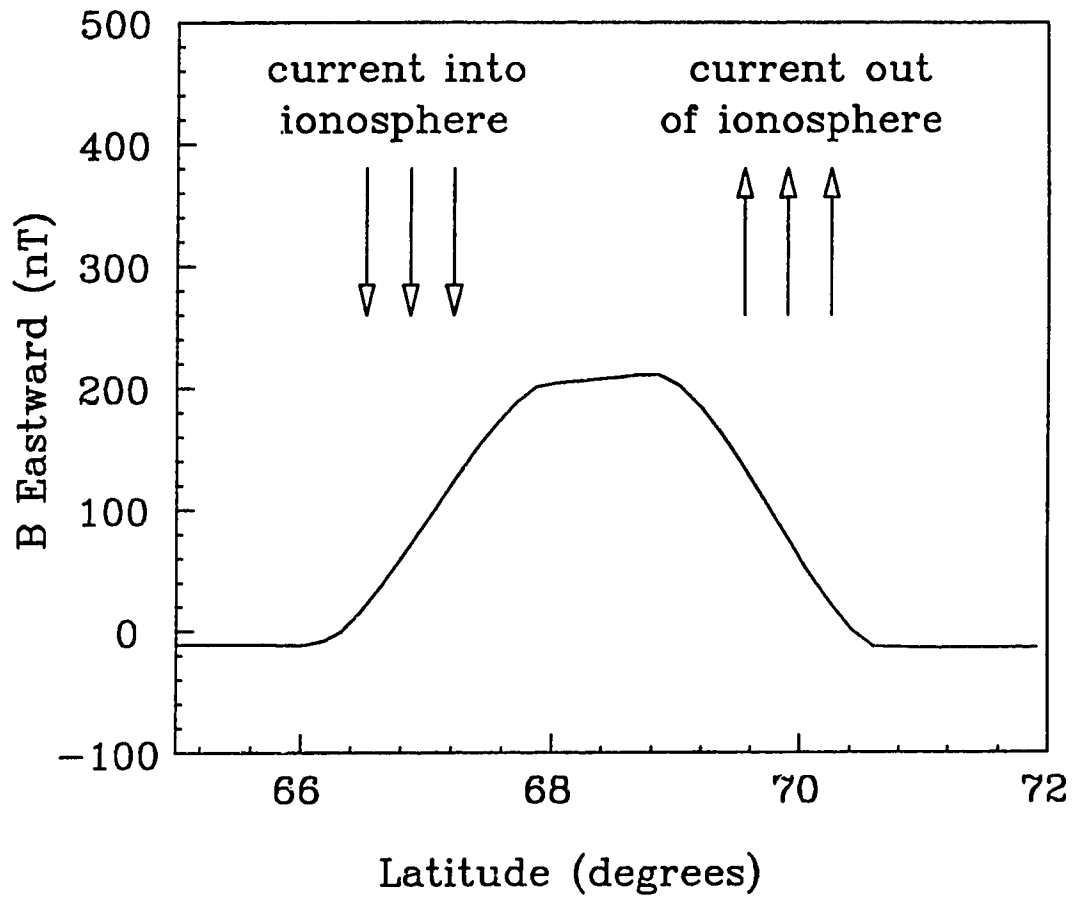


Figure 42 . The eastward perturbation magnetic field at TRIAD altitude (800 km) and 2100 hours MLT due to the model field-aligned current system. The current system used here is a mirror image (in the noon-midnight meridian) of a current system with ionospheric footprints as shown in Figure 37. Note the similarity to Figure 1.

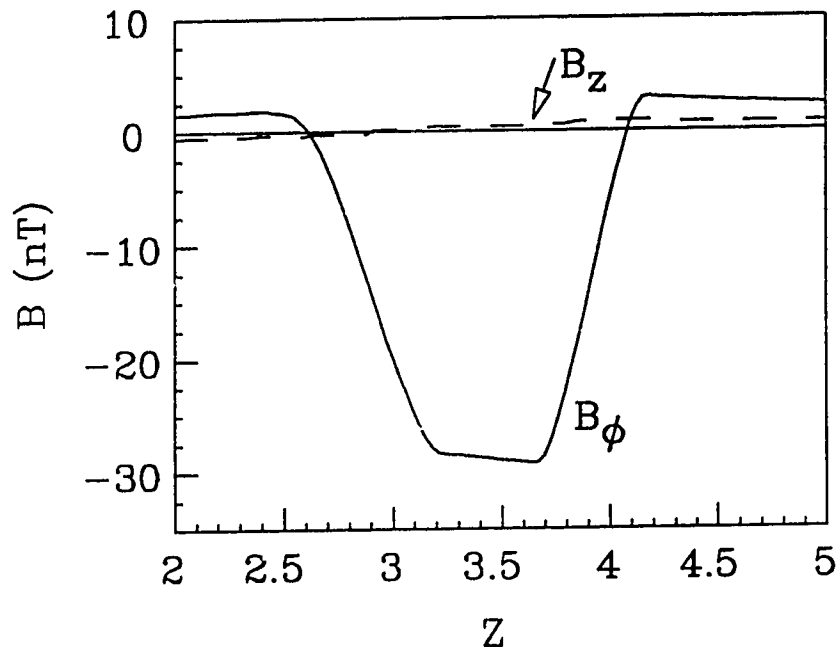


Figure 43. Magnetic field due to the model field-aligned current system on a surface $6.63 R_E$ from the Earth's centre (geosynchronous orbit distance). For points on the curve at 0300 MLT from $Z_{\text{geom}} = 2 R_E$ to $Z_{\text{geom}} = 5 R_E$, the azimuthal (solid curve) and Z (dashed curve) components of the magnetic field due to the model field-aligned currents are shown. The field-aligned current consists of Region I and Region II currents with ionospheric footprints as shown in Figure 37. Type I current elements are used. The amount of current in the field-aligned current system gives a 450 nT eastward magnetic field perturbation at TRIAD altitude.

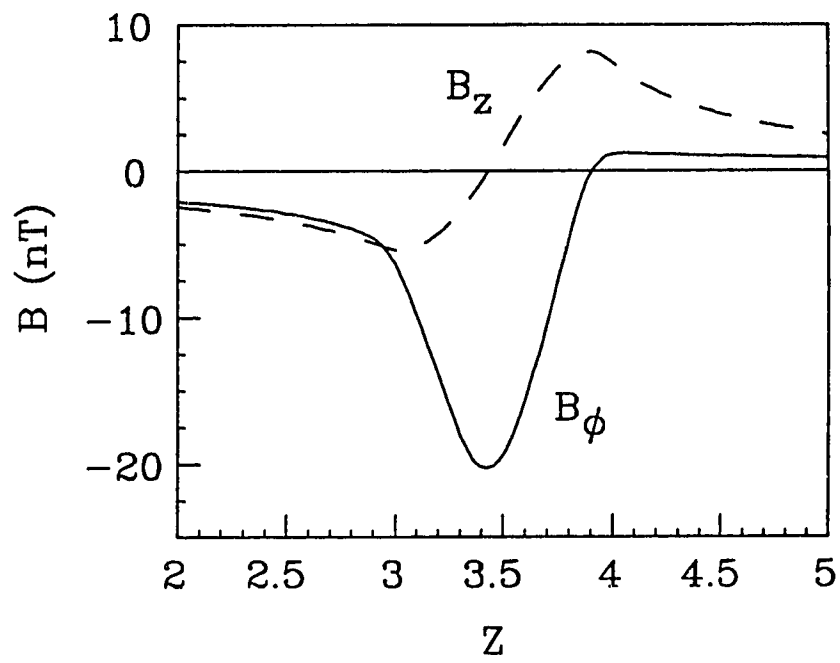


Figure 44. Same as Figure 43, but values determined on a curve at 0125 MLT.

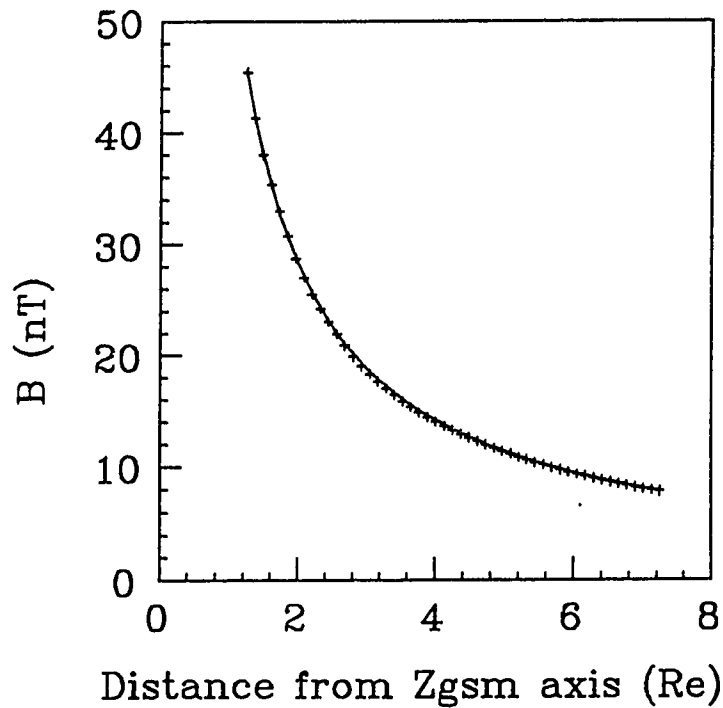


Figure 45. The expected (solid curve) and model (crosses) maximum values of the azimuthal magnetic field due to a model field-aligned current system as a function of distance from the Z_{gsm} axis. The model current system consists of Region I and Region II currents with ionospheric footprints as shown in Figure 37. Type I current elements are used. The current system spans 5.5 hours of local time from 0030 hours MLT to 0600 hours MLT. The values shown here are from 0300 hours MLT.

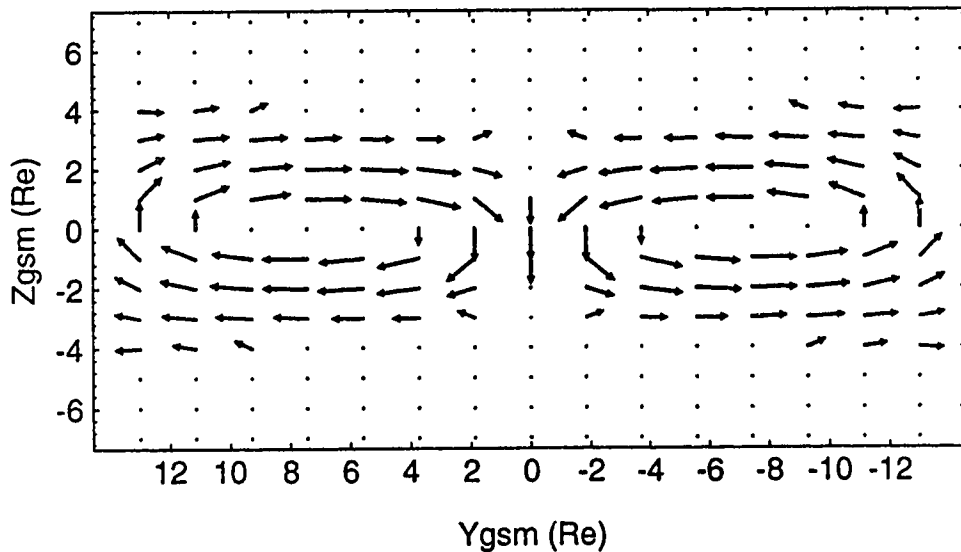


Figure 46. Magnetic field due to added field-aligned and closure currents on the surface $X_{gsm} = -15 R_E$. The amount of current added gives an eastward perturbation of 125 nT at TRIAD altitude. The Region I and II currents are closed in the magnetosphere as shown in Figure 38. The peak magnitude of vectors on this plot is 5.7 nT and all vectors with magnitudes less than 2 nT are set to zero length for clarity.

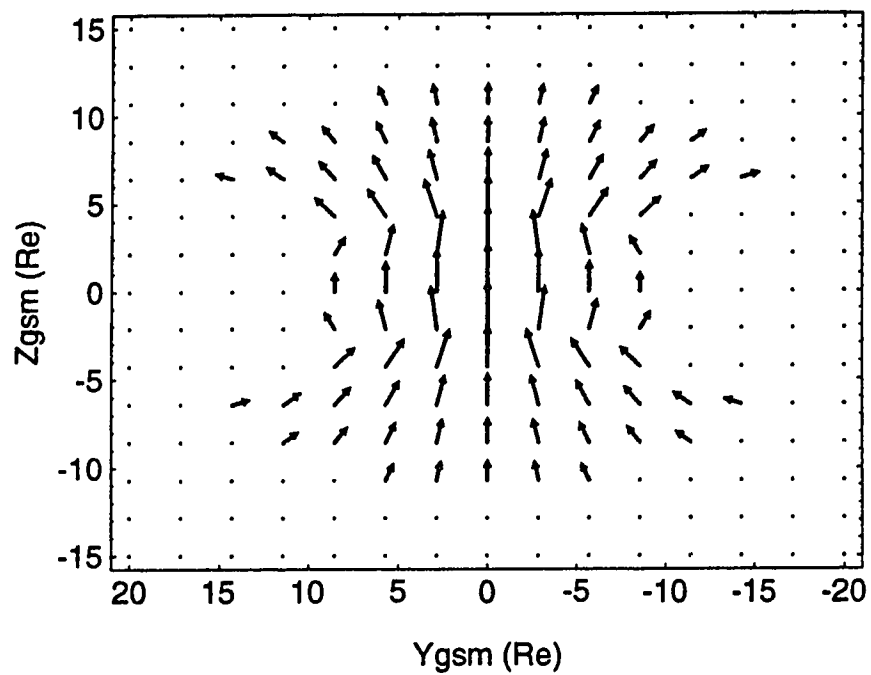


Figure 47. Magnetic field due to added field-aligned and closure currents on the surface $X_{gsm} = -15 R_E$. The amount of current added gives an eastward perturbation of 65 nT at TRIAD altitude. The Region I and II currents are closed in the magnetosphere as shown in figure 39. The peak magnitude of vectors on this plot is 3.9 nT and all vectors with magnitudes less than 1 nT are set to zero length for clarity.

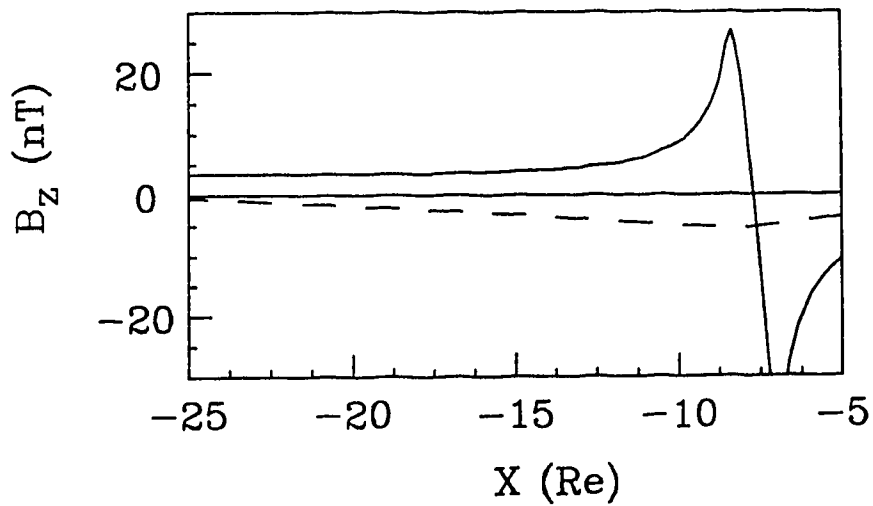


Figure 48. Equatorial B_z in noon-midnight meridian due to added field-aligned and closure currents. The current system producing the values shown by the dashed curve gives an eastward magnetic field perturbation of 125 nT at TRIAD altitude and is closed as shown in figure 38. The solid curve shows values produced by a field-aligned current system that gives an eastward magnetic field perturbation of 62.5 nT at TRIAD altitude and is closed as in figure 39.

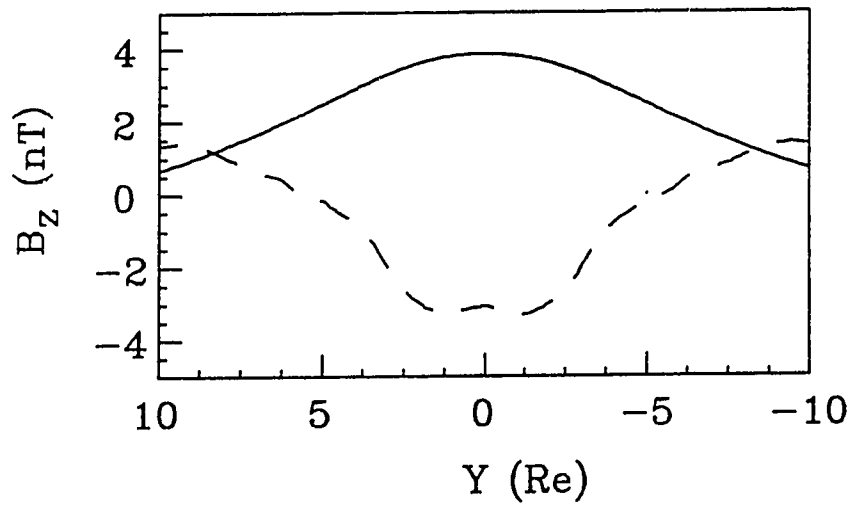


Figure 49. Equatorial B_z at $X_{\text{gsm}} = -15 R_E$ due to added field-aligned and closure currents. The current systems producing results shown by the solid and dashed curves are described in the caption for figure 48.

4. Applications

In this chapter I present results obtained from applications of the modelling technique I outlined in chapter 3. I begin with an exploration of how field-aligned currents affect mappings between the ionosphere and the magnetosphere. Following this, I describe my efforts to construct a global model of the magnetospheric magnetic field that includes contributions due to the ring, Chapman-Ferraro and cross-tail currents. I then discuss how mappings obtained using this new model are influenced by field-aligned current effects. Finally, using this model, I map auroral features observed by the Viking Satellite UV imager into the magnetotail.

Effects of Field-Aligned Currents on Mappings

The results presented in this section were produced using an *ad hoc* model of the magnetic effects of field-aligned currents superposed on the T87 model field. In chapter 2, I argued that the global effects of the field-aligned currents are not included in empirical models and the rationale behind the decision to add the effects of field-aligned currents to the T87 magnetic field model.

I have used this model to investigate the effects of field-aligned currents on mapping between the ionosphere and geosynchronous orbit. Field lines are traced from a point that is $6.63 R_E$ from the Earth's centre. Two ionospheric footprints of this point are determined by tracing field lines towards the ionosphere using both the T87 model and a modification of it that includes field-aligned current effects. The footprint determined from a T87 model tracing will differ, in both longitude and latitude, from the footprint obtained from a tracing produced by the modified T87 model. These differences are determined for points on two curves, one at 0300

hours MLT and the other at 0125 hours MLT. Each curve covers the range from 2 to 5 R_E above the equatorial plane ($2 < Z_{gsm} < 5$) on a surface 6.63 R_E from the Earth's centre. I show the results for 0300 and 0125 hours MLT in Figures 50 and 51, respectively. These results were produced using an amount of field-aligned current that gives an eastward magnetic perturbation of 420 nT at TRIAD altitude.

Figure 50, together with Figure 51, illustrates that the longitude shift of the ionospheric footprint of points at geosynchronous orbit is largest for points that are between the Region I and II currents. The maximum longitude shift is a function of the amount of current flowing in the added current system (Figure 52).

In the outer magnetosphere ("outer" here means beyond Region II currents), the manner of current closure has a significant effect on the magnetic perturbations produced. This was clearly illustrated in chapter 3 where I showed the magnetic perturbations due to current systems closed as shown in Figures 38 and 39 (see Figures 46 through 49). To illustrate the possible effects of field-aligned currents on mapping between the ionosphere and the outer magnetosphere, field line traces were produced using the T87 $Kp = 2$ model with various amounts of added field-aligned current. Figures 53 and 54 show that a field line (defined here by its ionospheric footprint) is swept towards the flanks of the magnetosphere, due to the magnetic effects of field-aligned currents that are closed as shown in Figure 38. The field line traces shown in both figures are terminated where the field line crosses the equatorial plane.

Figures 53 and 54 show that field-aligned currents, closed radially in the equatorial plane, cause CPS field lines equatorward of the Region I currents to flare away from midnight. The equatorial crossing point of a field line traced from a specified point in the ionosphere moves away from midnight (to larger $|Y_{gsm}|$) if the mag-

netic effects of field-aligned currents are added to the background magnetic field model. The shift increases with both the amount of added field-aligned current and the ionospheric footprint latitude. This result has been discussed qualitatively by *Lui and Krimigis* [1984], who suggested that the magnetic shear between field-aligned current sheets is an important factor in determining where field lines in the high-latitude plasma sheet will cross the equatorial plane. The field lines are traced using a model with field-aligned currents closed as shown in Figure 38; the same has not been done using currents closed as shown in Figure 39. The vector plots in Figures 46 and 47 clearly show, however, that the effect of field-aligned currents closed as shown in Figure 38 on B_y , in the CPS, is much larger than that of currents closed as in Figure 39. Thus, the latter field-aligned currents will have much less effect on the flare of CPS field lines.

The mapping results presented here indicate that, due to the magnetic effects of field-aligned currents, field lines threading the CPS might cross the equatorial plane much further from midnight than mappings based on empirical models that do not include these effects would indicate. This is an important result because, for instance, it could shed light on whether or not high-latitude regions of the evening sector auroral oval are connected to the LLBL along magnetic field lines [cf. *Rostoker*, 1991]. To answer this question convincingly, one way or another, it will be necessary to develop an empirical model that incorporates the global effects of field-aligned currents; however, unless the path of closure of these currents is correct in the model, it is unlikely that the mappings so produced will be any more trustworthy than those available with present models.

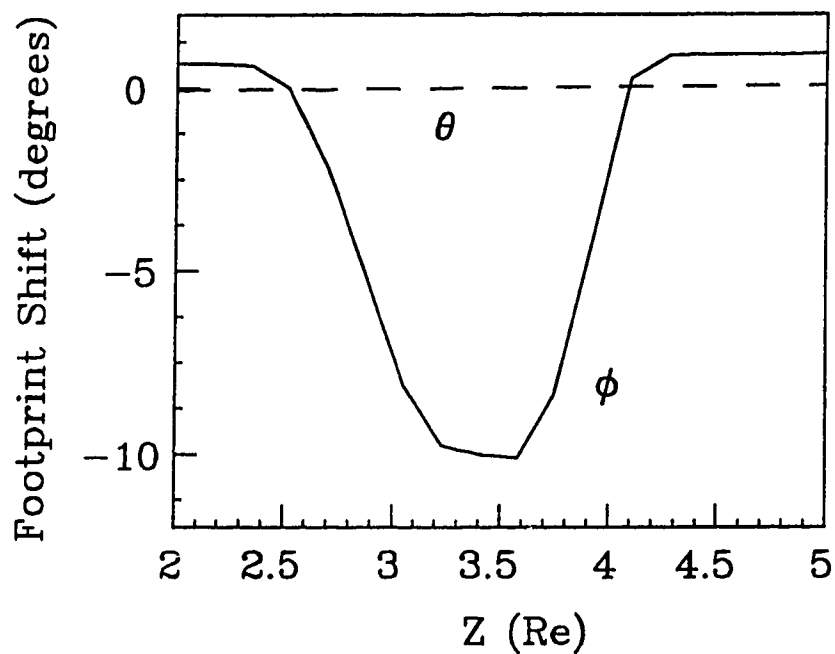


Figure 50. Shift in longitude (solid curve marked ϕ) and latitude (dashed curve marked θ) of the footprints of field lines traced towards the Earth from points on a curve at geosynchronous distance and 0300 hours MLT. The values on the plots are obtained by tracing field lines towards the Earth first using the T87 model and then using the T87 model with field-aligned currents added. The model field-aligned current system used here is the same as that used to produce the results shown in figure 43.

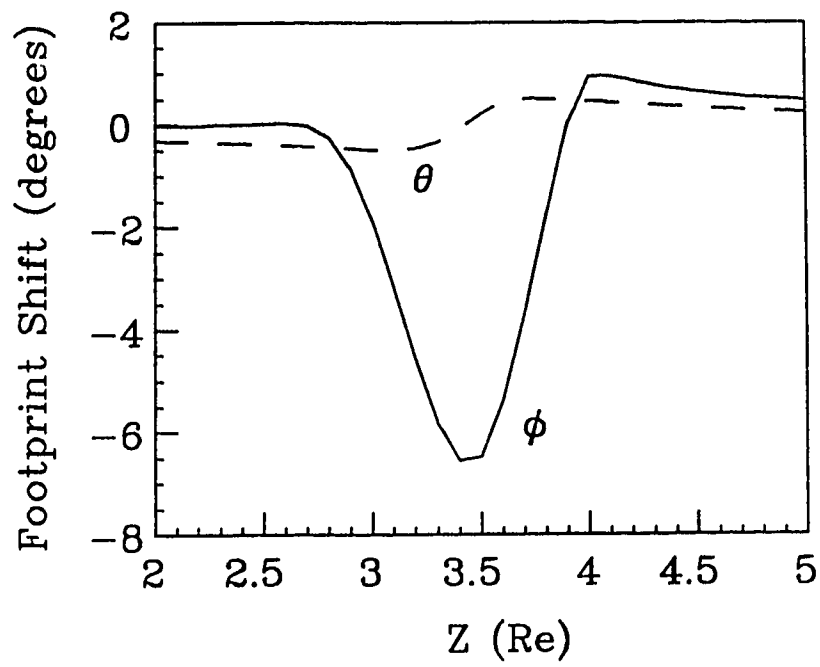


Figure 51. Same as figure 50, but values determined on a curve at 0125 hours MLT.

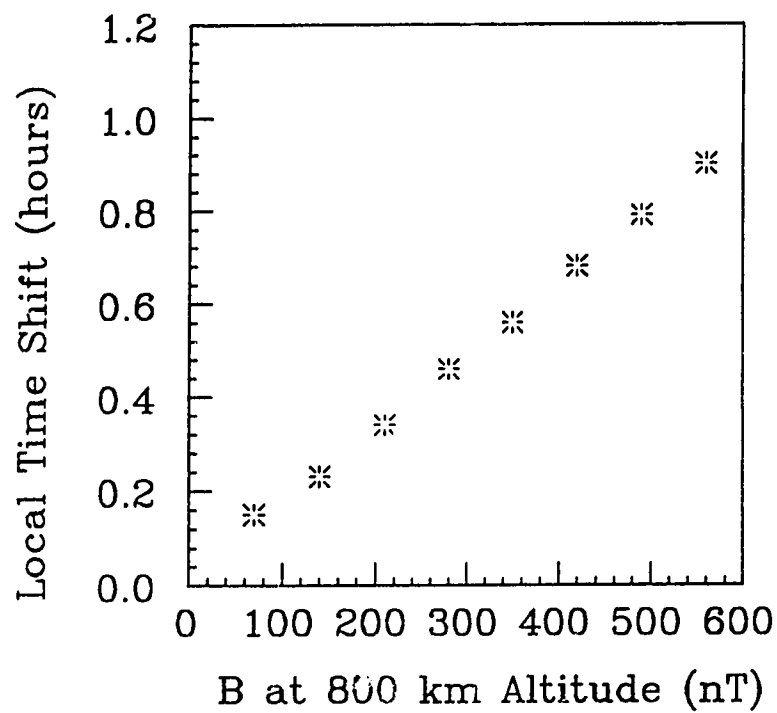


Figure 52. Maximum westward local time shift of the ionospheric footprint of field lines traced from points at 0300 hours MLT and on a surface $6.63 R_E$ from the Earth's centre. The local time shift is plotted as a function of the maximum perturbation of the eastward component of the magnetic field at TRIAD altitude (800 km).

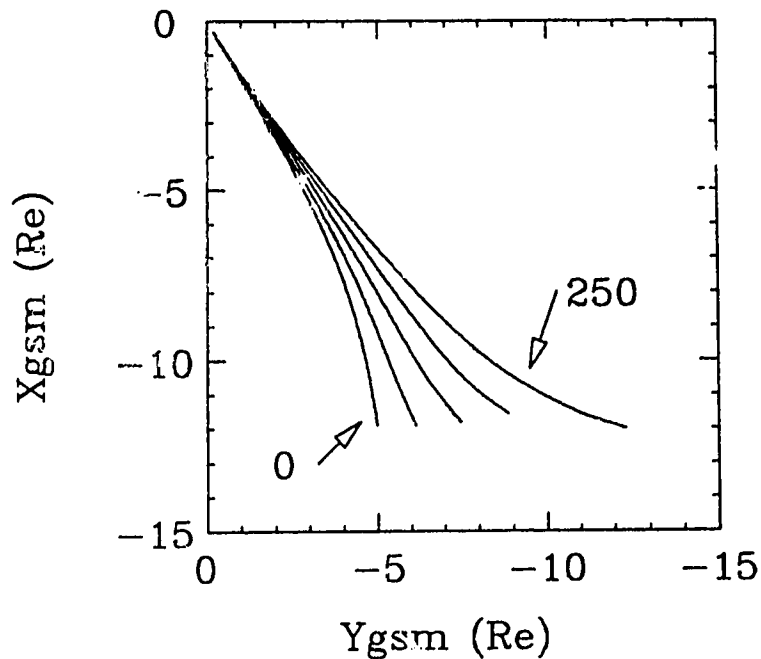


Figure 53. Projections in the XY_{gsm} plane of field lines traced using the T87 $Kp = 2$ model modified to include the magnetic effects of field-aligned and closure currents. The five field lines shown here were traced with amounts of field-aligned current added that would produce eastward perturbations of the magnetic field at TRIAD altitude of 0 nT, 62.5 nT, 125 nT, 187.5 nT and 250 nT. Only the field lines corresponding to 0 nT and 250 nT are labelled. 0 nT corresponds to no field-aligned current added. The field lines all have an ionospheric footprint at 68.6° latitude and 0200 hours MLT and terminate in the equatorial plane (i.e. at $Z_{gsm} = 0$).

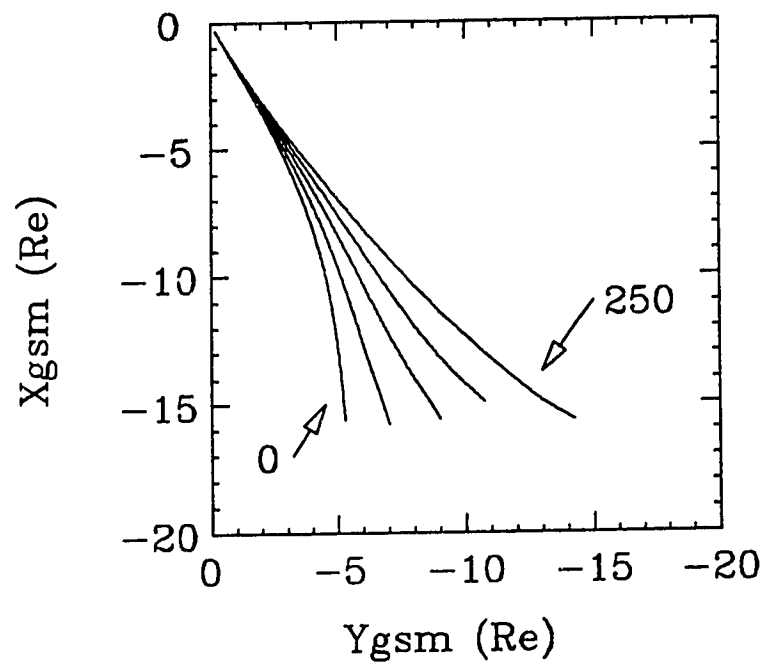


Figure 54. The same as figure 53, but for field lines with an ionospheric footprint at 69.45° latitude.

A New Global Model

In this section, I outline my efforts to develop a new global magnetic field model for the nightside magnetosphere. This model does not include the magnetic effects of field-aligned currents; however, it does include contributions from the Chapman-Ferraro, ring and cross-tail currents. I use the magnetic field due to the model ring and cross-tail current systems discussed in chapter 3 (see Figures 29 and 32). In the following paragraphs I shall briefly outline the model of the magnetic effects of the Chapman-Ferraro currents. As well, I shall explain how I parameterized the cross-tail current model and then chose those parameters. I conclude by presenting a model of the magnetospheric magnetic field (excluding field-aligned current effects) appropriate for an unspecified magnetospheric activity level and times when the dipole tilt angle is close to 0° .

The model for the magnetic effects of the Chapman-Ferraro currents is the same as that used by *Olson and Pfitzer*, [1974]. As I described in chapter 2, they used the technique of *Olson* [1969] to calculate magnetic field values due to the surface currents at various points in the magnetosphere. C. Pfitzer has made this array of values of the magnetic field available to me. I linearly interpolate between the values to obtain an estimate of the magnetic field. The magnetopause surface they used in their original calculation had a standoff distance of $10 R_E$ [C. Pfitzer, *personal communication*, 1993]. *Olson and Pfitzer* [1982] have developed a method of scaling these values with magnetospheric activity; however, I have avoided adjusting these magnetic field values for the following reason. The scaling process they developed involves the assumption that, for all magnetospheric activity levels, the magnetopause shapes are self-similar. That is, one magnetopause can be obtained by simply expanding or contracting another and not changing its shape.

On the other hand, the average magnetopause shape is expected to be different for different activity levels. In particular, increases in reconnection will lead to decreases in the standoff distance and an increase in the flare of the magnetotail [e.g., *Sibeck et al*, 1991].

The standard approach in magnetospheric modelling is to construct a model that depends on a relatively large number of parameters. For example, the T87 model field is specified by twenty linear and ten nonlinear parameters [*Tsyganenko*, 1987]. The large number of parameters, coupled with the inclusion of the power series function, allows the model to fit the data relatively well even though, as discussed in chapter two, the basic current systems in the model differ markedly from the real currents. This lack of correspondence between the model and actual current systems will always limit how usable and how trustworthy such a model is. As well, the T87 model is fit to the average of the data. The large number of parameters will allow this fit to be reasonably good; however, we have no guarantee that the *average* magnetic field configuration is a valid *instantaneous* magnetic field configuration. Also, the fitting process may introduce significant discrepancies between the real and model fields in regions not well represented in the data set. An example of this is the occurrence of regions of negative B_z in the T89 model neutral sheet that I discussed in chapter 2.

In what follows, I describe how I select the parameters that provide values for all properties that must be specified in the model. From the outset, I point out that in developing this model I have decided to keep the number of parameters as small as possible. The parameters describing the ring current and the thickness and inner edge location of the current sheet are specified *a priori*. The cross-tail current strength and curvature are then selected so that the model field fits the empirical

function of *Rostoker and Skone* [1993] for B_z in the neutral sheet and that of *Slavin et al.* [1985] describing the lobe field strength. There are differences between the model field in the regions of validity of those functions and the functions. This is not surprising: as I shall discuss in the concluding chapter, the model still lacks several key elements of reality.

For simplicity, I use the model ring current discussed in chapter 3 whose properties are illustrated in Figures 30 through 32. The current carried in the model ring current is westward and the radii of the elements used are each $2 R_E$. This reflects, roughly, the maximum distance above the equatorial plane of field lines that cross the equator in the ring current region. The total current carried is 3 MA. In the equatorial plane outside of the ring current region, the magnetic field produced by this current is very nearly dipolar. The strength of magnetic dipole that would produce this magnetic field is $\sim 25\%$ that of the terrestrial dipole (see chapter 3). This is an appropriate value for the dipole moment of the ring current system [*Schild, 1969*].

To specify the dimensions of the magnetotail, I use one of the empirical relationships of *Sibeck et al* [1991]. In particular, I choose the empirical model for the radius, as measured from the sun-Earth line, of the magnetotail, appropriate for solar wind pressures between 2.6 nPa and 4.9 nPa. My reason for using one of the empirical models of *Sibeck et al.* [1991] is that these models are based on the most comprehensive study of magnetopause location to date. As well, the particular model used gives a magnetopause standoff distance of $10 R_E$. Also, it was obtained by fitting to the locations of magnetopause crossings during times when the solar wind pressure fell within the stated range. the IMF direction was not a selection criterion. The surface that *Olson and Pfitzer* [1974] used as a magnetopause for

their Chapman-Ferraro current calculations also had a standoff distance of $10 R_E$. As well, the surface was obtained by balancing magnetospheric magnetic pressure with solar wind pressure (see Chapter 1) and the IMF was assumed zero in their calculations.

The thickness of the cross-tail current sheet is set to a constant value of $3 R_E$. While this cross-tail current model is a representation of the neutral sheet current, it is significantly thicker than the neutral sheet current is expected to be [Eastwood, 1974]. Using smaller radii current elements, however, leads to a coarse magnetic field in the vicinity of the neutral sheet when reasonable numbers of current loops (i.e., ~ 100) are used. In order to allow for a relatively smooth transition from tail-current to ring current, I place the inner edge of the tail current at $X_{gsm} = -7 R_E$ (at midnight), which is a reasonable location for the inner edge based on observational evidence [e.g., Frank, 1971]. The downtail extent of the model cross-tail current system is $70 R_E$. The curvature of the cross-tail current is specified in three locations. These are at the inner edge, at $X_{gsm} = -20 R_E$ and at $X_{gsm} = -70 R_E$. The measure of curvature that I use is the separation in X_{gsm} between the point where a given current line passes through midnight and where it intercepts the magnetospheric boundary (The current is forced to flow on a circular arc between those two points.). The cross-tail current strength is specified at the inner edge and at $X_{gsm} = -20 R_E$. Both the curvature and strength of the model cross-tail current vary linearly between the locations where they are specified. Beyond $X_{gsm} = -20 R_E$, the cross-tail current falls off as $|X^{-0.53}|$. This is the X_{gsm} dependence that Slavin *et al.* [1985] obtained by fitting a function to average lobe magnetic field strengths.

In order to allow for a relatively smooth transition between the ring current and

tail current, the latter must be curved in the equatorial plane. This curvature is supported by observation (see *Tsyganenko* [1989] and references therein). I assume that the current at the inner edge follows a nearly circular path and, as well, that in the distant tail it follows a nearly straight line across the tail. The actual values of curvature that I use are adjusted to improve the fit of the model to the average values of the magnetic field in the lobe and neutral sheet according to the empirical functions of *Slavin et al.* [1985] and *Rostoker and Skone* [1993], respectively.

In order to assess how well the model fits the two profiles I use the following three merit functions

$$(\Lambda_1)^2 = \frac{1}{25R_E} \int_{X_{gsm}=-45R_E}^{X_{gsm}=-20R_E} \left[\frac{B'_x(X, 0, 12) - B_x(X, 0, 12)}{B_x(X, 0, 12)} \right]^2 dX \quad (63)$$

$$(\Lambda_2)^2 = \frac{1}{30R_E} \int_{X_{gsm}=-40R_E}^{X_{gsm}=-10R_E} \left[\frac{B'_z(X, 0, 0) - B_z(X, 0, 0)}{B_z(X, 0, 0)} \right]^2 dX \quad (64)$$

$$(\Lambda_3)^2 = \frac{1}{30R_E} \int_{X_{gsm}=-40R_E}^{X_{gsm}=-15R_E} \left[\frac{B'_z(X, 10, 0) - B_z(X, 10, 0)}{B_z(X, 10, 0)} \right]^2 dX \quad (65)$$

and primed and unprimed quantities refer to the model and empirical quantities, respectively. For B_x at $Z_{gsm} = 12 R_E$ (Λ_1) I use the empirical function of *Slavin et al.* [1985], which is relevant for the tail lobe. For B_z in the neutral sheet along the sun-Earth line (Λ_2) and at $Y_{gsm} = 10 R_E$ (Λ_3) I use the empirical function of *Rostoker and Skone* [1993], which is relevant for the neutral sheet. The functions Λ_1 , Λ_2 and Λ_3 are rms fractional deviations. Setting the denominators in each of the three merit functions equal to unity changes the values given into actual

rms deviations. To obtain a first estimate of the cross-tail current strength at $X_{\text{gsm}} = -20 R_E$, I minimize (numerically) Λ_1 with respect to that strength. Then, with that parameter fixed, I minimize the sum of (Λ_2) and (Λ_3) with respect to the current strength at the inner edge. Successive iterations of this process do not change the values of these parameters significantly.

In the version of the model presented here, the cross-tail linear current density is 40 mA/m at $X_{\text{gsm}} = -20 R_E$ and 90 mA/m at the inner edge. The rms fractional deviations of the model lobe field from the final values of Λ_1 , Λ_2 and Λ_3 are roughly 0.04, 0.3 and 0.3, respectively. These actual rms deviations obtained by setting the denominators in the integrals to unity in equations 63, 64 and 65 are roughly 1.0, 0.90 and 1.8 nT, respectively. The model magnetic field in the neutral sheet and the lobe is shown in Figures 55 and 56. The model field is the sum of a terrestrial dipole field and that due to the model cross-tail, ring and Chapman-Ferraro currents.

There is one striking feature on the plot of the model magnetic field in the neutral sheet along the sun-Earth line (Figure 55a). This is the large model B_z relative to the function of *Rostoker and Skone* [1993] in the region between roughly $X_{\text{gsm}} = -15 R_E$ and $X_{\text{gsm}} = -20 R_E$. The data to which *Rostoker and Skone* [1993] fit their empirical function show the same trend. Their Figure 3b, comparing their data with the best fit function clearly illustrates that for X_{gsm} values between -15 R_E and -20 R_E , the average data is larger than their function by about 2 nT. This is not as great a difference as that between my model and their function. A possible explanation for the B_z values is that, during active times, it has been suggested that a current “blade” forms in the near Earth magnetotail [*Kaufmann*, 1987; *McIlwain*, 1992]. This intensification of the cross-tail current sheet around $X_{\text{gsm}} = -10 R_E$ is thought to be necessary to explain magnetic field perturbations

in the near Earth magnetotail during substorm growth phase [Kaufmann, 1987]. This additional current would provide positive B_z tailward of the blade location.

There are differences between my model current system and the actual nightside magnetospheric current system. One of these is the lack of pressure gradient (or diamagnetic) currents that flow at the high-latitude edge of the plasma sheet. These would serve to decrease the X_{gsm} component of the magnetic field in the plasma sheet. To obtain a specified lobe magnetic field intensity, the total model cross-tail current strength would be essentially the same as if only a model neutral sheet current were used. Thus, the inclusion of diamagnetic currents would lead to both lower model neutral sheet current strengths and model CPS magnetic field strengths.

A second major difference between my model current system and the actual magnetospheric current system is the lack of field-aligned currents in my model. In chapter 3, I outlined a method that I developed to model the magnetic effects of field-aligned currents. I have added a set of model field-aligned currents to the magnetic field model described in this section. The currents I added were closed in the same way as were the current systems used to produce the shifts of magnetic field lines towards the flanks illustrated in Figures 53 and 54. What I find is that, for field lines that cross the equatorial plane twenty or so Earth radii down the magnetotail, the effect of flaring towards the flanks is far less pronounced than when the currents were added to the T87 model. This is due to the fact that the cross-tail current in my model is much thinner than that in the T87 model. As discussed above, this representation of the entire cross-tail current by a thin current sheet leads to larger CPS magnetic field strengths. The addition of the same azimuthal component to my model field will therefore have less effect. In

any event, due to the lack of inclusion of the magnetic effects of the high latitude currents and our present lack of understanding about how the field-aligned current system is closed in the magnetosphere, it is just as reasonable not to include these effects in the present version of the model as to include them: I have decided not to include these effects at this stage of development.

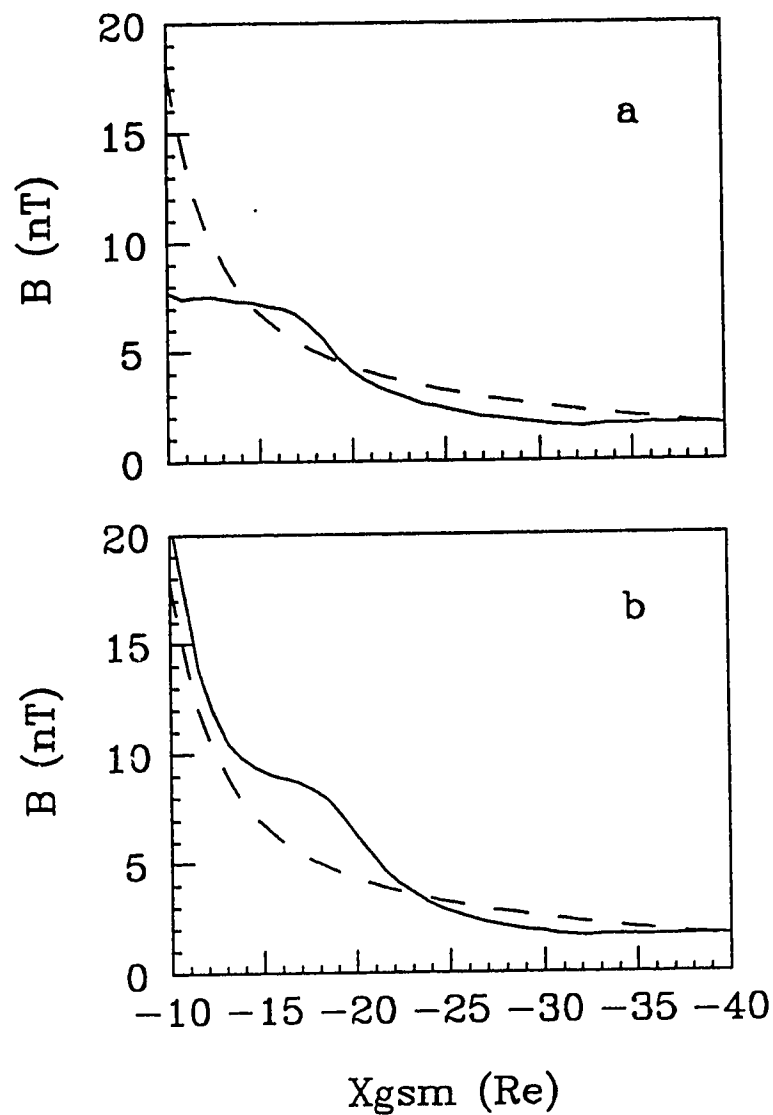


Figure 55. Magnetic field values in the neutral sheet according to the global model (solid curve) and the empirical function of *Rostoker and Skone* [1993] (dashed curve). Values of the model field at $Y_{gsm} = 10$ and $Y_{gsm} = 0 R_E$ are shown in panels a and b, respectively.

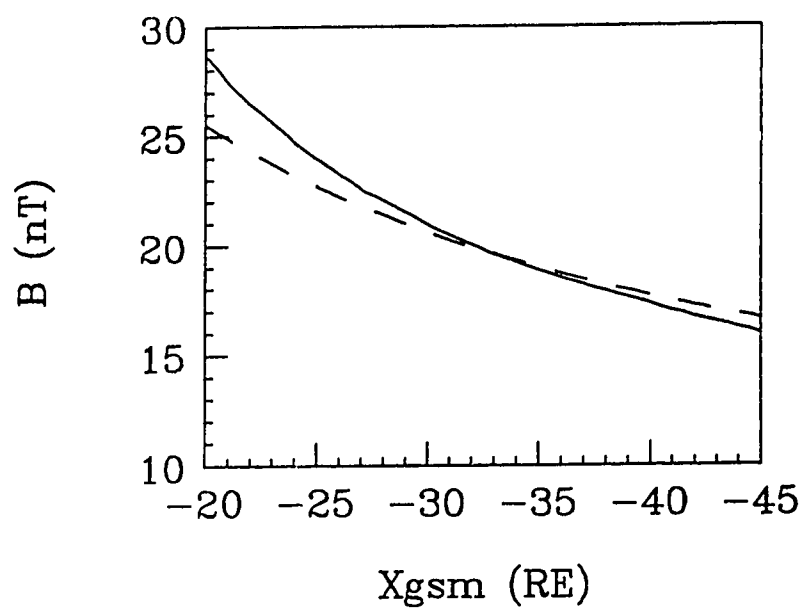


Figure 56. Lobe field strength according to the global model (solid curve) and the empirical function of *Slavin et al.* [1993] (dashed curve).

Mapping During an Individual Event

In this section, I present the results of “mappings” obtained using my model. This involves the tracing of field lines from the auroral oval out to the equatorial plane of the magnetosphere. The ionospheric footpoints of the field lines are located in three features of the auroral oval. These features are obtained from two Viking satellite UV images [*Anger et al*, 1987] taken at 0114:47 UT and 0116:07 UT on April 3, 1986. These images are shown in Figures 57 and 58. Also on the images is the outline of the continents and five MLT meridians. My choice of this date and time is based on three considerations. First, my model does not presently allow for dipole tilt effects and at this time on this day, the dipole direction was very nearly perpendicular (within 1.5°) to the sun-Earth line. Second, the images were taken during a time of enhanced steady driven activity. Third, during the time after the first image and before the second image (the time interval between the first and second images is only two minutes) a bright feature in the poleward portion of the auroral oval forms (This bright spot is located at 2100 MLT just east of Hudson Bay).

The brightening feature indicates a local enhancement of energetic electron precipitation and, therefore, of upward field aligned current. At the same time, the clear magnetic signature of a current wedge (see introduction) was recorded by a ground based magnetometer located at Poste-de-la-Baleine on the east coast of Hudson Bay. This substorm wedge is almost certainly very localized in latitude, as the magnetic signature of this wedge is not observed by any other auroral or mid-latitude magnetic field observatory [*S. Skone, personnel communication, 1993*]. The magnetospheric source region for high-latitude auroral features such as the newly formed bright spot in Figure 58 are not known. One of the primary uses of magnetic

field models is in attempts to identify, by field line tracing, the magnetospheric source regions for auroral precipitation [e.g., *Elphinstone et al.*, 1991].

As an illustration of the use of my model, I shall present the results of field line tracings from points in the auroral oval at the time the images were taken. I trace field lines from three loci of points in the auroral oval. These loci are the equatorward and poleward borders of the oval and a set of points that roughly trace the boundary of the bright spot. The loci of points defining the poleward and equatorward borders extend along those borders from roughly 1900 hours MLT to 2400 hours MLT. For the purpose of comparison I also trace field lines from the same loci of points using the T87 and T89 model magnetic fields. The $L_n = 4$ Tsyganenko models are appropriate for the activity level at the time the images were taken. The model of terrestrial magnetic field that I use for these mappings is the complete IGRF model discussed in chapter 2.

The results of the mappings of the equatorward and poleward borders of the auroral oval using the T87, T89 and my model are shown in Figures 59, 60 and 61, respectively. The mapping of the equatorward border is essentially the same in each case, as would be expected: the magnetic field in the near-Earth region is almost completely dominated by that of the Earth. The mapping of the poleward border by the T87 model (Figure 59) extends from near midnight out towards the flank at roughly $40 R_E$ down the magnetotail. The mapping of the poleward border by the T89 model (Figure 60) also extends to over $40 R_E$ down the magnetotail; however, this mapping extends out more towards the flank and along the flank to $X = -10 R_E$. In an earlier study of this event [*Donovan et al.*, 1992], we argued that T89 mapping is more reasonable than that of the T87 model, *if* the high-latitude edge of the auroral oval maps to the LLBL through the PSBL as

is the contention of *Rostoker and Eastman* [1987]. On the other hand, according to *Vasyliunas* [1979] it is possible that the PSBL (technically, in this paper, he is referring to the plasma boundary layer separating the CPS and the lobe) and LLBL are not threaded by common magnetic field lines. This view, if true, would indicate that the T87 mapping is the more reasonable. The mapping by my model is, roughly, to the same downtail range but extends further towards the flank than that of the T87 model.

The mappings of the auroral bright spot all fall into roughly the same range of X_{gsm} . The T89 mapping is further to the flank than that of the T87 model, which is consistent with the fact that the T89 model field is more flared than that of the T87 model (chapter 2). My model mapping falls between the two others and is slightly further from the Earth. According to these three mappings, the particles precipitating onto this bright spot originate in the CPS. The mappings are all well inside of where the magnetopause is likely to be at $25 R_E$ down the magnetotail. In fact, my model magnetopause is roughly $24 R_E$ in radius at $X_{\text{gsm}} = -25 R_E$.

There are difficulties with drawing conclusions from this type of mapping. One source of difficulty is that I am looking at an individual event. There is a range of real activity levels that correspond to a given value of Kp . Consequently, there is a wide range of magnetospheric configurations that can occur during a period over which the Kp index does not change. Even if the Tsyganenko models, or any own, do reflect a reasonable “average” magnetic field configuration, then, it is possible that a field line starting at a point in the ionosphere might map significantly further from the Earth or closer to it than these models would indicate. A second source of difficulty is that there are differences between the model currents and the actual currents. This is true for each of the models. I pointed out discrepancies between

the real currents and those in the Tsyganenko models and my own in chapter 2 and the previous section in this chapter, respectively.

The most surprising result of the mappings is that those from my model are as close as they are to those due to the Tsyganenko models appropriate for $Kp = 4$. As I described above, I fit the model to empirical functions representing the lobe and neutral sheet magnetic fields. These functions, in turn, are representative of average conditions (i.e., $Kp=2$). At higher activity levels, a magnetic field line passing through a point in the ionosphere will, on average, cross the plane of the neutral sheet further from the Earth than it will at quiet times. The T87 and T89 model magnetic fields also show this trend [Tsyganenko 1987, 1989]. From these mappings, I must conclude that either my magnetic field model is too stretched to be representative of average conditions or the Tsyganenko models are not stretched enough.

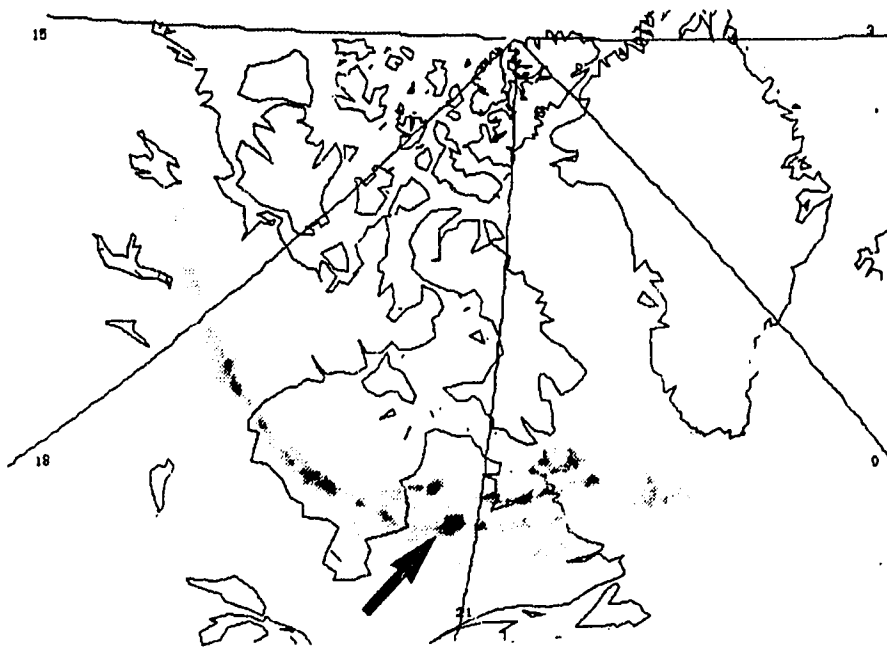


Figure 57. Viking satellite image of auroral oval at 0114:47 UT on April 3, 1976.

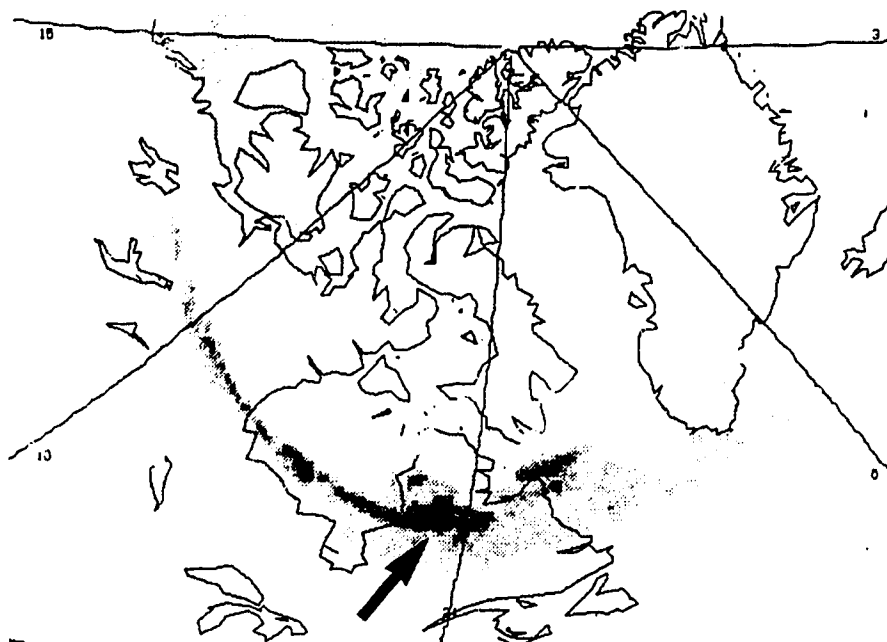


Figure 58. Viking satellite image of auroral oval at 0116:07 UT on April 3, 1976. The arrow indicates the location of a "bright spot". A locus of points roughly forming the boundary of this bright spot are the ionospheric footpoints of the field lines with equatorial crossing points shown in Figure 62.

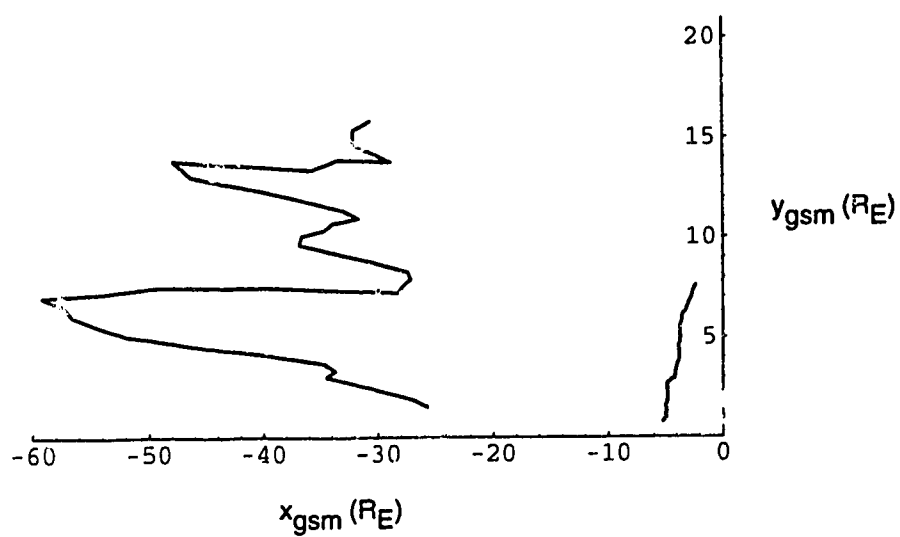


Figure 59. Poleward and equatorward boundaries of the evening sector auroral oval mapped to the equatorial plane using the T87 $Kp = 4$ model.

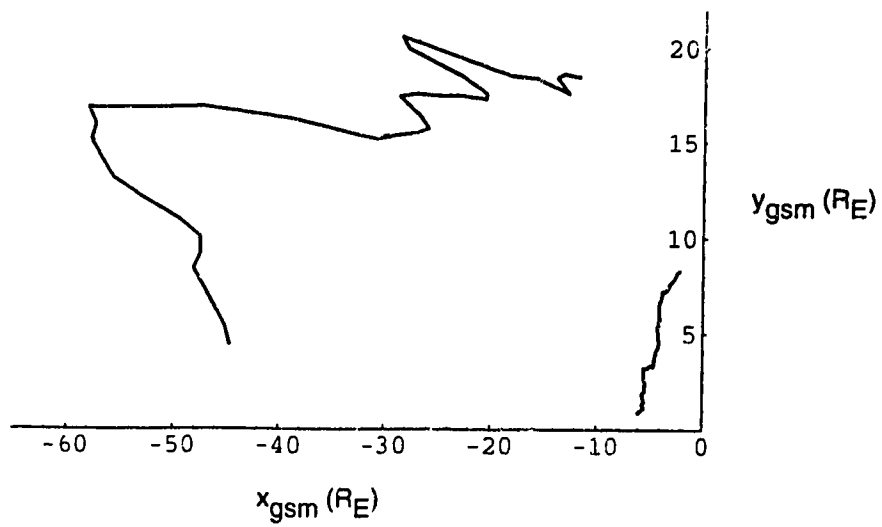


Figure 60. Poleward and equatorward boundaries of the evening sector auroral oval mapped to the equatorial plane using the T89 $Kp = 4$ model.

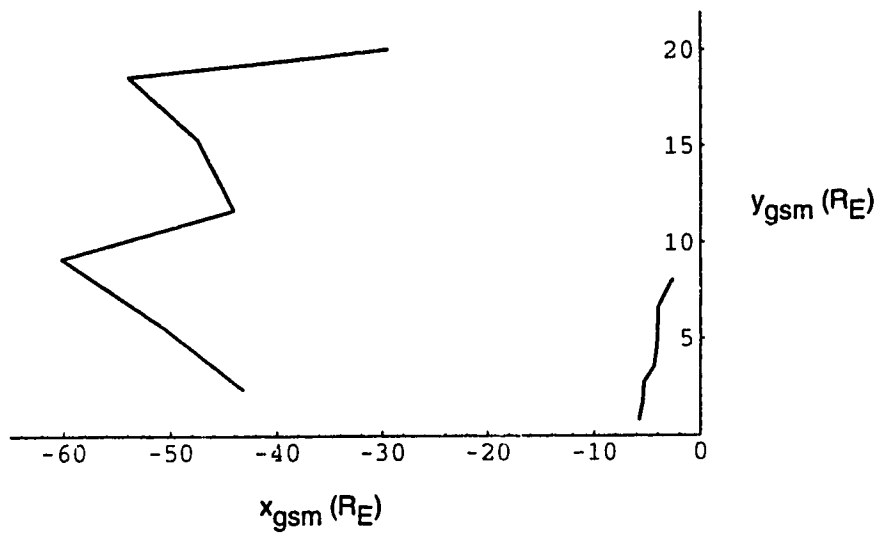


Figure 61. Poleward and equatorward boundaries of the evening sector auroral oval mapped to the equatorial plane using the new model described in the text.

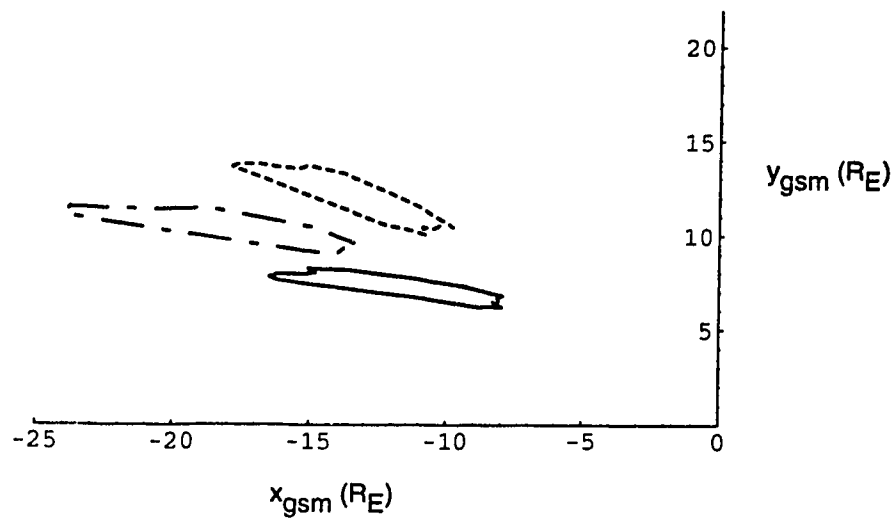


Figure 62. Locus of points from the border of the bright feature in Figure 58 (indicated by arrow) mapped to the equatorial plane using the T87 (solid curve), T89 (dashed curve) and the new model described in the text (dot-dashed curve).

5. Discussion

There have been a number of studies aimed at testing the validity of global magnetospheric magnetic field models. Generally, these fall into one of two categories. One involves determining whether the models in question satisfy certain simple physical criteria, such as the current and magnetic field being divergence free and the magnetic field being consistent with a simple momentum balance condition such as $\vec{J} \times \vec{B} = \vec{\nabla}G$, where G is an unspecified scalar function [e.g., *Walker and Southwood*, 1982]. The other involves comparing the model magnetic field with *in situ* measurements of the magnetic field [e.g., *Fairfield*, 1991; *Jordan et al.*, 1992]. Such tests are important, although it is not entirely clear whether the momentum balance condition mentioned above is satisfied in the real magnetosphere (i.e. assuming this momentum balance condition holds amounts to assuming that the pressure is isotropic and that $\vec{\nabla} \times (\vec{V} \cdot \vec{\nabla}\vec{V})$) or whether the average magnetic field configuration is representative of any instantaneous magnetic field.

In chapter 2, I presented the results of my work aimed at testing the validity of the Tsyganenko magnetic field models. I feel that, in particular, one of these tests falls into a third category of testing magnetic field models. The test I am speaking about is the use of inferred magnetospheric plasma convection patterns to assess the mapping capabilities of the Tsyganenko models. In general, this category of tests involves the use of the model to infer some observable quantity that is not the magnetic field or the current, and the comparison of that result with measurements of the same quantity. This is a way of assessing the mapping capabilities of global models and is important since these models are used extensively for the purpose of mapping, along magnetic field lines, between the ionosphere and the magnetosphere and vice versa. As well, systematic differences between the model field and the

actual field are likely to be more readily identified in this way. There are two reasons for this. The first is that the effect of these differences, integrated along an entire field line, will often be more pronounced than is the difference between the model and average magnetic field at a given point in space. The second is that, as I discussed in chapter 2, it is possible that contributions to the real magnetic field that are important for mapping are not even present in the averaged data upon which the model is based. The example I discussed in chapter 2 is the possibility that the motion of a thin current sheet could cause the average magnetic effects in a region of space due to that current sheet to be close to zero.

The results of the tests I applied to the Tsyganenko models in chapter 2 led me to conclude that there are important differences between the current systems in the Tsyganenko models and the actual magnetospheric current system. This, in turn, was my motivation to try to develop new methods of modelling the magnetic effects of magnetospheric currents. I based my approach to this problem on that of *Olson and Pfitzer* [1974]. One of my contributions has been the use of a different current element to build up the model current systems. The element I use is a cylinder of finite radius and length. The advantage of this approach is that the magnetic effects of currents following any specified path through the magnetosphere can be modelled. As well, although the currents are both finite and volume filling and the resulting magnetic field is also finite, the particular choice of current element allows me to circumvent direct calculation of the magnetic field via the Biot-Savart law. In fact, it is the magnetic field that is specified: the current is found afterwards by using Ampere's law. In chapter 3, I outlined the use of this method to model the magnetic effects of the large scale field-aligned currents and those of the ring and cross-tail currents.

Using the field-aligned current model, I showed that the field-aligned currents can have a significant effect on mappings between the magnetosphere and the ionosphere. As well, I showed that the effects of the field-aligned current distribution depend markedly on how those currents are closed in the magnetosphere. One interesting result was that the field-aligned current system, including the closure currents in the magnetosphere, could actually decrease the neutral sheet magnetic field strength near midnight. Overall, this technique is valuable because it allows for the modelling of realistic field-aligned current distributions and for the closure of those currents along any specified path. Although I have used this technique to model the magnetic effects of a simple night-side Region I and II current system in generating the results presented in this thesis, there is no reason why the magnetic effects of any field-aligned current system could not be modelled in this way (computer power permitting). An example of another use for this method is as follows. It is possible, based on satellite images of the aurora and simultaneous measurements of the electric potential along the trajectory of one or more satellites passing across the auroral oval and polar cap, to infer "instantaneous" distributions of field-aligned currents [e.g., *Marklund et al.*, 1987]. Modelling the magnetic effects of these inferred currents would be useful in individual event (i.e., substorm) studies.

The global nightside magnetospheric magnetic field model I presented in chapter 4 includes the magnetic field contributions of the Earth, as well as the neutral sheet, ring and Chapman-Ferraro currents. This model represents a step forward for several reasons. The neutral sheet current closure around the magnetospheric lobes is realistic: the current both contains the magnetospheric lobe field and allows for a realistically flaring magnetotail. As well, the model lobe magnetic

field is curl free. These are properties that the most widely used magnetic field models do not have; however, more work can and should be done to make the global nightside magnetospheric model that I have developed more realistic and any future studies done with the model more conclusive. For instance, the mapping results I presented at the end of chapter 4 would indicate that the bright feature in the auroral image (Figure 62) indicates particle precipitation from the near-Earth CPS, well away from the LLBL. This conclusion may, however, change after the model current systems are further improved. In the following paragraphs, I discuss the improvements that I consider to be the most important. In each case, I briefly describe how I intend to implement these improvements.

The model cross-tail current does not presently include the magnetic effects of the diamagnetic currents that flow through the high-latitude portion of the CPS. These currents flow from dawn to dusk (or east to west) above and below the neutral sheet. Together with the neutral sheet current, they comprise the cross-tail current. I would include the effects of these currents as follows. Using type I current elements, I would construct a current loop that goes across the magnetotail and encloses the region of space that corresponds to the high-latitude CPS and closes around the lobe. The current closure would be along the same path as the closure of the neutral sheet current. A second current loop would be included on the other side of the neutral sheet, enclosing the other lobe. These two current loops form a theta current configuration. Using a large number of these theta shaped current elements, I would build up a model of the diamagnetic current layer in both the northern and southern parts of the CPS.

I stated in chapter 4 that it would be inappropriate to include the field-aligned currents in a model that does not include the diamagnetic currents. The converse

is also true: the field-aligned (Region I) and diamagnetic currents together make up the high-latitude current system. Once the diamagnetic currents are included in the model, I would also include the field-aligned currents. Of course, a caveat on any results produced with this model will still be that we do not yet know how these currents should be closed.

It is also important to allow for a range of magnetospheric activity levels. I would give some degree of “activity dependence” to the model by simply varying the empirical functions representing the average magnetic field in the lobe and neutral sheet to reflect how these quantities change with changes in magnetospheric activity. One difficulty with this is that while it is well understood how, on average, the lobe size and field strength vary with activity [e.g., *Sibeck et al.*, 1991], it is not clear how the neutral sheet magnetic field strength behaves. As I point out below, however, studies are presently being carried out that are aimed at determining the behavior of the magnetic field strength in the neutral sheet. An activity dependent model must incorporate an activity dependent contribution due to the Chapman-Ferraro currents: solar wind variations that lead to changes in magnetospheric activity level also cause changes in the size and shape of the magnetopause and, therefore, in the Chapman-Ferraro currents. As I stated in chapter 4, *Olson and Pfitzer* [1982] have developed a method of scaling the magnetic effects of their Chapman-Ferraro current model based on the assumption that a change in solar wind parameters will cause the magnetopause to change from one shape to another, self-similar one. I also stated that there are difficulties with using this approach, particularly near the flanks of the magnetosphere. One alternative to this approach is to use the approach of *Olson* [1969] to obtain models of the magnetic effects of the Chapman-Ferraro currents on a number of different magnetopause surfaces,

each one corresponding to some specified solar wind parameters. These models would consist of values of the magnetic field at a large number of locations through the magnetosphere.

I feel that with the implementation of most of these improvements, the model will be useful in a number of important ways. Of course, one important application will be in studying the connection, along magnetic field lines, between the high-latitude auroral ionosphere and the magnetosphere. In particular, the capacity to model the magnetic effects of both the field-aligned currents and the realistic closure of the cross-tail current around the lobes will make this model particularly well suited to studying the topologies of field lines that cross the equatorial plane near the flanks of the magnetosphere. Hopefully, this will help in determining, for instance, how significant a role the LLBL plays in the dynamics of the nightside auroral oval and whether or not the nightside Region I currents are generated in the LLBL.

In conclusion, I point out three open research questions in magnetospheric physics which my model may be able to address. First, where are field-aligned currents generated and how do they close through the magnetosphere? Second, what is the distribution of cross-tail current with respect to the neutral sheet? That is, how much of the cross-tail current is concentrated near the neutral sheet and how much of it is diamagnetic current in the higher-latitude portion of the CPS? Third, what is the typical distribution of B_z in the neutral sheet region? Only recently have efforts to answer this last question been undertaken. A study by *Rostoker and Skone* [1993] has shown that B_z in the near-Earth neutral sheet is significantly larger than was previously thought based on measurements in the CPS near the *statistical* location of the neutral sheet [e.g., *Fairfield*, 1979;1986]. These

new results then suggest that some of the well accepted “rules of thumb” about B_z in the neutral sheet, which are also based on measurements not necessarily in the neutral sheet, may not be correct. The answers to these questions are important for the development of realistic models of the large scale magnetospheric current system. It is also true that sophisticated models of the magnetospheric magnetic field, including the realistic effects of field-aligned and cross-tail currents, will help to answer these questions. Thus, the effectiveness of one of the tools that is used to explore magnetosphere-ionosphere coupling depends on knowledge of that coupling and progress in this field is an iterative process.

Bibliography

- Akasofu, S.-I. and S. Chapman, The ring current, geomagnetic disturbance and the Van Allen radiation belts, *J. Geophys. Res.*, *66*, 1321, 1961.
- Akasofu, S.-I., J. C. Cain and S. Chapman, The magnetic field of a model radiation belt, numerically computed, *J. Geophys. Res.*, *66*, 4013, 1961.
- Akasofu, S.-I., The development of the auroral substorm, *Planet. Space Sci.*, *12*, 273, 1964.
- Arfken, G., *Mathematical Methods for Physicists*, Academic Press, San Diego, 1985.
- Axford, W. I. and C. O. Hines, A unifying theory of high latitude geophysical phenomena and geomagnetic storms, *Can. J. Phys.*, *39*, 1433, 1961.
- Axford, W. I., Magnetospheric convection, *Rev. Geophys.*, *7*, 421, 1969.
- Baumjohann, W., G. Paschmann and C. A. Cattell, Average plasma properties in the central plasma sheet, *J. Geophys. Res.*, *94*, 6597, 1989.
- Baumjohann, W. and G. Paschmann, Pressure balance between lobe and plasma sheet, *Geophys. Res. Lett.*, *17*, 45, 1990.
- Behannon, K. W., Mapping the Earth's bow shock and magnetic tail by Explorer 33, *J. Geophys. Res.*, *73*, 907, 1968.
- Birn, J. and E. W. Hones, Jr., Three-dimensional computer modeling of dynamic reconnection in the geomagnetic tail, *J. Geophys. Res.*, *86*, 6802, 1981.
- Birn, J., E. W. Hones, Jr., J. D. Craven, L. A. Frank, R. D. Elphinstone and D. P. Stern, On open and closed field line regions in Tsyganenko's field model and their possible associations with horse collar auroras, *J. Geophys. Res.*, *96*, 3811, 1991.
- Boström, R., The magnetic field of three-dimensional magnetospheric model current systems and currents induced in the ground, *Acta. Poly. Scand.*, *77*, 1, 1971.
- Chapman, S. and V. C. A. Ferraro, A new theory of magnetic storms, *Nature*, *126*, 129, 1930.
- Clauer, C. R. and R. L. McPherron, Mapping the local time-universal time development of magnetospheric substorms using mid-latitude magnetic observations, *J. Geophys. Res.*, *79*, 2811, 1974.

- Coroniti, F. V. and C. F. Kennel, Changes in magnetospheric configuration during the substorm growth phase, *J. Geophys. Res.*, **77**, 3361, 1972.
- DeCoster, R. J. and L. A. Frank, Observations pertaining to the dynamics of the plasma sheet, *J. Geophys. Res.*, **84**, 5099, 1979.
- Donovan, E. F., G. Rostoker and C. Y. Huang, Regions of negative B_z in the Tsyganenko 1989 model neutral sheet, *J. Geophys. Res.*, **97**, 8697, 1992.
- Donovan, E. F., G. Rostoker and B. Jackel, The effects of field-aligned currents on mapping from the ionosphere to the magnetosphere, in *Proceedings of the International Conference on Substorms (ICS-1)*, Kiruna, Sweden, 23-27 March 1992, ESA SP-335, p. 19, 1992.
- Doyle, M. A. and W. J. Burke, S3-2 Measurements of the Polar Cap Potential, *J. Geophys. Res.*, **88**, 9125, 1983.
- Dungey, J. W., Interplanetary magnetic field and the auroral zones, *Phys. Rev. Lett.*, **6**, 47, 1961.
- Eastman, T. E., E. W. Hones, Jr., S. J. Bame, J. R. Ashbridge, The magnetospheric boundary layer: site of plasma, momentum and energy transfer from the magnetosheath into the magnetosphere, *Geophys. Res. Lett.*, **3**, 685, 1976.
- Elphinstone, R. D., D. Hearn, J. S. Murphree and L. L. Cogger, Mapping using the Tsyganenko long magnetospheric model and its relationship to Viking auroral images, *J. Geophys. Res.*, **96**, 1467, 1991.
- Erickson, G. M. and R. A. Wolf, Is steady convection possible in the earth's magnetotail, *Geophys. Res. Lett.*, **7**, 897, 1980.
- Fairfield, D. H., Magnetic field signatures of substorms on high-latitude field lines in the nighttime magnetosphere, *J. Geophys. Res.*, **78**, 1553, 1973.
- Fairfield, D. H., On the average configuration of the geomagnetic tail, *J. Geophys. Res.*, **84**, 1950, 1979.
- Fairfield, D. H., The magnetic field of the equatorial magnetotail from 10 to 40 R_E , *J. Geophys. Res.*, **91**, 4238, 1986.
- Fairfield, D. H., An evaluation of the Tsyganenko magnetic field model, *J. Geophys. Res.*, **96**, 1481, 1991.
- Formisano, V., V. Domingo and K.-P. Wenzel, The three-dimensional shape of the magnetopause, *Planet. Space Sci.*, **27**, 1137, 1979.

- Frank, L. A., Relationship of the sheet, ring current, trapping boundary and plasmopause near the magnetic equator and local midnight, *J. Geophys. Res.*, *76*, 2265, 1971.
- Frank, L. A., Plasmas in the Earth's magnetotail, *Space Sci. Rev.*, *42*, 211, 1985.
- Fung, S. F. and R. A. Hoffman, Finite geometry effects of field-aligned currents, *J. Geophys. Res.*, *97*, 8569, 1992.
- Goertz, C. K. and R. A. Smith, The thermal catastrophe model of substorms, *J. Geophys. Res.*, *94*, 6581, 1989.
- Gold, T., Motions in the magnetosphere of the earth, *J. Geophys. Res.*, *64*, 1219, 1959.
- Hapgood, M. A., Space physics coordinate transformations: a user's guide, *Planet. Space Sci.*, *40*, 711, 1992.
- Hasegawa, A. and T. Sato, Generation of field-aligned current during substorm, in *Dynamics of the Magnetosphere*, edited by S.-I. Akasofu, p. 529, D. Reidel, Hingham, Mass., 1979.
- Heinemann, M. and D. H. Pontius, Jr., Representation of currents and magnetic fields in isotropic magneto-hydrostatic plasma, *J. Geophys. Res.*, *95*, 251, 1990.
- Heppner, J. P., The Harang discontinuity in auroral belt ionospheric currents, *Geofysiske Publikasjoner*, *29*, 105, 1972.
- Heppner, J. P. and N. C. Maynard, Empirical high-latitude electric field models, *J. Geophys. Res.*, *92*, 4467, 1987.
- Hill, T. W. and G.-H. Voigt, Limits on plasma anisotropy in a tail-like magnetic field, *Geophys. Res. Lett.*, *12*, 2441, 1992.
- Hones, E. W. Jr., Motion of charged particles trapped in the Earth's magnetosphere, *J. Geophys. Res.*, *68*, 1209, 1963.
- Hones, E. W. Jr., J. R. Ashbridge, S. J. Bame, M. D. Montgomery, S. Singer, and S.-I. Akasofu, Measurements of magnetotail plasma flow made with Vela 4B, *J. Geophys. Res.*, *77*, 5503, 1972.
- Huang, C. Y. and L. A. Frank, A statistical study of the central plasma sheet: Implications for substorm models, *Geophys. Res. Lett.*, *13*, 652, 1986.
- IAGA Commission 2 Working Group 4, International geomagnetic reference field 1965.0, *J. Geophys. Res.*, *74*, 4407, 1969.

- IAGA Division V Working Group 8, international geomagnetic reference field, 1991 revision, *J. Geomag. Geoelectr.*, *43*, 1007, 1991.
- Iijima, T. and T. A. Potemra, The amplitude distribution of field-aligned currents at northern high latitudes observed by TRIAD, *J. Geophys. Res.*, *81*, 5971, 1976.
- Iijima, T. and T. A. Potemra, Large scale characteristics of field-aligned currents associated with substorms, *J. Geophys. Res.*, *83*, 599, 1978.
- Jordan, C. E., J. N. Bass, M. S. Gussenhoven, H. J. Singer and R. V. Hilmer, Comparison of magnetospheric magnetic field models with CRRES observations during the August 26, 1990, storm, *J. Geophys. Res.*, *97*, 16907-16920, 1992.
- Kamide, Y., S.-I. Akasofu and G. Rostoker, Field-aligned currents and the auroral electrojet in the morning sector, *J. Geophys. Res.*, *81*, 6141, 1976.
- Kaufmann, R. L., Substorm currents: growth phase and onset, *J. Geophys. Res.*, *92*, 7471, 1987.
- Kaufmann, R. L. and D. J. Larson, Electric field mapping and auroral Birkeland currents, *J. Geophys. Res.*, *94*, 15307, 1989.
- Kavenagh, L. D., Jr., A revised (B,L) coordinate system to allow for distortion of the magnetosphere by a symmetric ring current, *J. Geophys. Res.*, *73*, 185, 1968.
- Kelley, T. J., C. T. Russell, R. J. Walker, G. K. Parks and J. T. Gosling, ISEE 1 and 2 observations of Birkeland currents in the earth's inner magnetosphere, *J. Geophys. Res.*, *91*, 6945, 1986.
- Kisabeth, J. L. and G. Rostoker, The expansive phase of magnetospheric substorms 1. Development of the auroral electrojets and auroral arc configuration during a substorm, *J. Geophys. Res.*, *79*, 972, 1974.
- Kisabeth, J. L., On calculating magnetic and vector potential fields due to large-scale magnetospheric current systems and induced currents in an infinitely conducting Earth, in *Quantitative Modeling of Magnetospheric Processes*, edited by W. P. Olson, Geophysical Monograph 21, AGU, p. 473, 1979.
- Kivelson, M. G. and H. E. Spence, On the possibility of quasi-static convection in the quiet magnetotail, *Geophys. Res. Lett.*, *15*, 1541, 1988.
- Langel, R. A., The main field, in *Geomagnetism*, edited by J. A. Jacobs, volume 1, p. 249, Academic Press, London, 1987.

- Lin, C. S. and J. N. Earfield, Magnetic field inclination angle at geosynchronous orbit, *Planet Space Sci.*, *32*, 1283, 1984.
- Lopez, R. E., H. Luhr, B. J. Anderson, P. T. Newell and R. W. McEntire, Multi-point observations of a small substorm, *J. Geophys. Res.*, *95*, 18897, 1990.
- Lui, A. T. Y., E. W. Hones, Jr., F. Yasuhara, S.-I. Akasofu and S. J. Bame, Magnetotail plasma flow during plasma sheet expansions: Vela 5 and 6 and Imp 6 observations. *J. Geophys. Res.*, *82*, 1235, 1977.
- Lui, A. T. Y., Estimates of current changes in the geomagnetotail associated with a substorm, *Geophys. Res. Lett.*, *5*, 853, 1978.
- Lui, A. T. Y. and S. M. Krimigis, Association between energetic particle bursts and Birkeland currents in the geomagnetic tail, *J. Geophys. Res.*, *89*, 10741, 1984.
- Lui, A. T. Y., R. W. McEntire and S. M. Krimigis, Evolution of the ring current during two geomagnetic storms, *J. Geophys. Res.*, *92*, 7459, 1987.
- Lui, A. T. Y., A. Mankofsky, C.-L. Chang, K. Papadopoulos and C. S. Wu., A current disruption mechanism in the neutral sheet: A possible trigger for substorm expansions, *Geophys. Res. Lett.*, *17*, 745, 1990.
- Lui, A. T. Y., A synthesis of magnetic substorm models, *J. Geophys. Res.*, *96*, 1849, 1991.
- Lundin, R., On the Magnetospheric Boundary Layer and Solar Wind Energy Transfer Into the Magnetosphere, *Space Sci. Rev.*, *48*, 263, 1988.
- Lyons, L. R. and D. J. Williams, *Quantitative Aspects of Magnetospheric Physics*, D. Reidel Publishing Company, Boston, MA., 1984.
- Manuel, J. R., The spatial development of the magnetospheric low-latitude boundary layer, Ph.D. Thesis, University of Alberta, 1992.
- Marklund, G. T., L. G. Blomberg, T. A. Potemra, J. S. Murphree, F. J. Rich and K. Staciewicz, A new method to derive "instantaneous" high-latitude potential distributions from satellite instruments including auroral imager data, *Geophys. Res. Lett.*, *14*, 439, 1987.
- McIlwain, C. E., Auroral mapping during substorms, in *Proceedings of the International Conference on Substorms (ICS-1)*, Kiruna, Sweden, 23-27 March 1992, ESA SP-335, p. 65, 1992.
- McPherron, R. L., Growth phase of magnetospheric substorm, *J. Geophys. Res.*, *75*, 5592, 1970.

- McPherron, R. L., Physical processes producing magnetospheric substorms and magnetic storms, in *Geomagnetism*, 4, edited by J. A. Jacobs, Academic, London, 1991.
- Mead, G. D. and D. B. Beard, Shape of the geomagnetic field solar wind boundary, *J. Geophys. Res.*, 69, 1169, 1964.
- Mead, G. D. and D. H. Fairfield, A quantitative magnetospheric model derived from spacecraft magnetometer data, *J. Geophys. Res.*, 80, 535, 1975.
- Miura, A., Anomalous transport of magnetohydrodynamic Kelvin-Helmholtz instabilities in the solar wind-magnetosphere interaction, *J. Geophys. res.*, 89, 801, 1984.
- Mezer, F. S., Power spectra of the magnetospheric electric field, *J. Geophys. Res.*, 76, 3651, 1971.
- Nakai, H., Y. Kamide and C. T. Russell, Influences of solar wind parameters and geomagnetic activity on the tail lobe magnetic field: a statistical study, *J. Geophys. Res.*, 96, 5511, 1991.
- Ness, N. F., C. S. Scarce and J. B. Seck, Initial results of the IMP 1 magnetic field experiment, *J. Geophys. Res.*, 69, 3531, 1964.
- Ness, N. F., The Earth's magnetic tail, *J. Geophys. Res.*, 70, 2989, 1965.
- Ohtani, S., S. Kokubun, R. C. Elphic and C. T. Russell, Field-aligned current signatures in the near-tail region 1. ISEE observations in the plasma sheet boundary layer, *J. Geophys. Res.*, 93, 9709, 1988.
- Ohtani, S., S. Kokubun, R. Nakamura, R. C. Elphic, C. T. Russell and D. N. Baker, Field-aligned current signatures in the near-tail region 2. coupling between the region 1 and the region 2 systems, *J. Geophys. Res.*, 95, 18913, 1990.
- Olson, W. P., The shape of the tilted magnetopause, *J. Geophys. Res.*, 74, 5642, 1969.
- Olson, W. P., A model of the distributed magnetospheric currents, *J. Geophys. Res.*, 79, 3731, 1974.
- Olson, W. P. and K. A. Pfitzer, A quantitative model of the magnetospheric magnetic field, *J. Geophys. Res.*, 79, 3739, 1974.
- Olson, W. P. and K. A. Pfitzer, A dynamic model of the magnetospheric magnetic and electric fields for July 29, 1977, *J. Geophys. Res.*, 87, 5943, 1982.

- Onsager, T. G., M. F. Thomsen, R. C. Elphic and J. T. Gosling, Model of electron and ion distributions in the plasma sheet boundary layer, *J. Geophys. Res.*, *96*, 20999, 1991.
- Orsini, S., M. Candidi, V. Formisano, H. Balsiger, A. Ghielmetti and K. W. Ogilvie, The structure of the plasma sheet - lobe boundary in the earth's magnetotail, *J. Geophys. Res.*, *89*, 1573, 1984.
- Parks, G. K., *Physics of Space Plasmas, An Introduction* Addison Wesley Publishing Company, Redwood City, Ca., 1991.
- Parker, E. N., Newtonian development of the dynamical properties of ionized gases of low density, *Phys. Rev.*, *107*, 924, 1957.
- Parker, E. N., Interaction of the solar wind with the geomagnetic field, *Phys. Fluids*, *1*, 171, 1958.
- Peterson, W. K., R. D. Sharp, E. G. Shelley, R. G. Johnson and H. Balsinger, Energetic ion composition of the plasma sheet, *J. Geophys. Res.*, *86*, 761, 1981.
- Peterson, W. K. and E. G. Shelley, Origin of the plasma in the cross-polar cap auroral feature, *J. Geophys. Res.*, *89*, 6729, 1984.
- Press, W. H., B. P. Flannery, S. A. Teukolsky and W. T. Vetterling, *Numerical Recipes*, Cambridge University Press, New York, 1986.
- Pulkkinen, T. I., A study of magnetic field and current configurations in the magnetotail at the time of substorm onset, *Planet. Space Sci.*, *39*, 833, 1991.
- Pulkkinen, T. I., R. J. Pellinen, H. E. J. Koskinen, H. J. Opgenoorth, J. S. Murphy, V. Petrov, A. Zaitzev and E. Friis-Christensen, Auroral signatures of substorm recovery phase: a case study, in *Magnetospheric Substorms*, edited by J. R. Kan, T. A. Potemra and T. Iijima, Geophysical Monograph 64, p. 333. AGU, Washington D.C., 1991.
- Reiff, P. H., R. W. Spiro and T. W. Hill, Dependence of polar cap potential drop on interplanetary parameters, *J. Geophys. Res.*, *86*, 7639, 1981.
- Rich, F. J. and N. C. Maynard, Consequences of using simple analytical functions for the high-latitude convection electric field, *J. Geophys. Res.*, *94*, 3687, 1989.
- Rishbeth, H. and O. K. Garriott, *Introduction to ionospheric physics*, Academic Press, New York, 1969.
- Roelof, E. C., Remote sensing of the ring current using energetic neutral atoms, *Adv. Space Res.*, *9*, (12)195, 1989.

- Rosenbauer, H., H. Grünwaldt, M. D. Montgomery, G. Paschmann and N. Sckopke, HEOS 2 Plasma observations in the distant polar magnetosphere, *J. Geophys. Res.*, *80*, 2723, 1975.
- Rostoker, G., Geomagnetic Indices, *Rev. Geophys. and Space Phys.*, *10*, 935, 1972.
- Rostoker, G. and R. Boström, A mechanism for driving the gross Birkeland current configuration in the auroral oval, *J. Geophys. Res.*, *81*, 235, 1976.
- Rostoker, G. and T. Eastman, A boundary layer model for magnetospheric substorms, *J. Geophys. Res.*, *92*, 12187, 1987.
- Rostoker, G., S.-I. Akasofu, W. Baumjohann, Y. Kamide and R. L. McPherron, The roles of direct input of energy from the solar wind and unloading of stored magnetotail energy in driving magnetospheric substorms, *Space Sci. Rev.*, *46*, 93, 1987.
- Rostoker, G, C. Y. Huang and L. A. Frank, Response of the plasma sheet to the various components of magnetospheric substorm activity, *Cospar Abstracts*, p. 132, Helsinki, Finland, 1988.
- Rostoker, G., Magnetospheric substorms as a signature of the solar terrestrial interaction, in *Ionospheric Structure and Variability on a Global Scale and Interactions with Atmosphere and Magnetosphere*, edited by L. Bossy and R. W. Schunk, p. 2, AGARD - CP - 441, Neury Sur Seine, France, 1989.
- Rostoker, G., Some observational constraints for substorm models, in *Magnetospheric Substorms*, edited by J. R. Kan, T. A. Potemra, S. Kokubun and T. Iijima, Geophysical Monograph 64, p. 61, AGU, Washington D.C., 1991.
- Rostoker, G. and S. Skone, Magnetic flux mapping considerations in the auroral oval and the Earth's magnetotail, *J. Geophys. Res.*, *98*, 1377, 1993.
- Russell, C. T., Geophysical coordinate transformations, *Cosmic Electrodynamics*, *2*, 184, 1971.
- Russell, C. T. and R. C. Elphic, Initial ISEE magnetometer results: magnetopause observations, *Space Sci. Rev.*, *22*, 681, 1978.
- Samson, J. C., L. R. Lyons, P. T. Newell, F. Creutzberg and B. Xu., Proton aurora and substorm intensifications, *Geophys. Res. Lett.*, *19*, 2167, 1992.
- Sato, T., Auroral Physics, in *Magnetospheric Plasma Physics*, Edited by A. Nishida, p. 197, D. Reidel, Dordrecht, 1982.
- Schild, M. A., Pressure balance between the solar wind and the magnetosphere, *J. Geophys. Res.*, *74*, 1275, 1969.

- Schindler, K. and J. Birn, Magnetospheric Physics, *Physics Reports*, *47*, 11, 1978.
- Senior, C., R. M. Robinson and T. A. Potemra, Relationship between field-aligned currents, diffuse auroral precipitation and the westward electrojet in the early morning sector, *J. Geophys. Res.*, *87*, 10469, 1982.
- Sergeev, V. A. and W. Lennartsson, Plasma sheet at $X \approx -20R_E$ during steady magnetospheric convection, *Planet. Space Sci.*, *36*, 353, 1988.
- Sibeck, D. G., R. E. Lopez and E. C. Roelof, Solar wind control of the magnetopause shape, location and motion, *J. Geophys. Res.*, *96*, 5489, 1991.
- Siscoe, G. L., Solar system magnetohydrodynamics, in *Solar-Terrestrial Physics*, edited by R. L. Carovillano and J. M. Forbes, p. 11, D. Reidel, 1983.
- Siscoe, G. L., The magnetospheric boundary, in *Physics of Space Plasmas (1987)*, edited by T. Chang, G. B. Crew and J. R. Jasperse, p. 3, Scientific Publishers, Cambridge, MA, 1987.
- Slavin, J. A., E. J. Smith, D. G. Sibeck, D. N. Baker, R. D. Zwickl and S.-I. Akasofu, An ISEE 3 study of average and substorm conditions in the distant magnetotail, *J. Geophys. Res.*, *90*, 10875, 1985.
- Smiddy, M., W. J. Burke, M. C. Kelley, N. A. Saffekos, M. S. Gussenhoven, D. A. Hardy, Effects of high-latitude conductivity on observed convection electric fields and Birkeland currents, *J. Geophys. Res.*, *85*, 6811, 1980.
- Smith, E. J., P. J. Coleman, D. L. Judge and C. P. Sonett, Characteristics of the extraterrestrial current system, *J. Geophys. Res.*, *65*, 1858, 1960.
- Sonnerup, B. U. Ö, Magnetic field reconnection, in *Solar System Plasma Physics*, edited by L. T. Lanzerotti, C. F. Kennel and E. N. Parker, volume 3, p. 45, North Holland Publishing Company, Amsterdam, 1979.
- Speiser, T. W., Conductivity without collisions or noise, *Planet. Space Sci.*, *18*, 613, 1970.
- Spence, H. E., Kivelson, M. G. and R. J. Walker, Comparison of field-aligned currents at ionospheric and magnetospheric altitudes, *Adv. Space Res.*, *8*, (9)343, 1988.
- Spreiter, J. R. and A. Y. Alksne, Plasma flow around the magnetosphere, *Rev. Geophys.*, *7*, 11, 1969.
- Spreiter, J. R., A. L. Summers and A. Y. Alksne, Hydromagnetic flow around the magnetosphere, *Planet. Space Sci.*, *14*, 223, 1966.

- Stern, D. P., The origins of Birkeland currents, *Rev. Geophys.*, *21*, 125, 1983.
- Stern, D. P., Parabolic harmonics in magnetospheric modeling: the main dipole and the ring current, *J. Geophys. Res.*, *90*, 10851-10863, 1985.
- Stern, D. P., Magnetospheric Models Using a Distorted Dipole, in *Physics of Space Plasmas, SPI Conference Proceedings and Reprint Series*, *7*, edited by T. Chang, G. Crew and J. R. Jasperse, Scientific Publishers, Inc., Cambridge, MA, p. 309, 1988.
- Stern, D. P. and I. I. Alexeev, Where do field lines go in the quiet magnetosphere, *Rev. Geophys. Space Phys.*, *26*, 782, 1988.
- Stern, D. P., A brief history of magnetospheric physics before the spaceflight era, *Rev. Geophys.*, *27*, 103, 1989.
- Stern, D. P., A simple model of Birkeland currents, *J. Geophys. Res.*, *98*, 5691, 1993.
- Toffoletto, F. R. and T. W. Hill, Quantitative model of magnetic coupling between the solar wind and magnetosphere, in *Solar Wind-Magnetosphere Coupling*, ed. by Y. Kamide and J. A. Slavin, p. 275, Terra Scientific, Tokyo, 1986.
- Tsyganenko, N. A., Global quantitative models of geomagnetic field in the cislunar magnetosphere for different disturbance levels, *Planet. Space Sci.*, *35*, 1347, 1987.
- Tsyganenko, N. A., A magnetospheric magnetic field model with a warped tail current sheet, *Planet. Space Sci.*, *37*, 5, 1989.
- Tsyganenko, N. A., Quantitative models of the magnetospheric magnetic field: methods and results, *Space Sci. Rev.*, *54*, 75, 1990.
- Tsyganenko, N. A., Methods for quantitative modeling of the magnetic field from Birkeland currents, *Planet. Space Sci.*, *39*, 641, 1991.
- Tsyganenko, N. A. and A. V. Usmanov, Determination of the magnetospheric current system parameters and development of experimental geomagnetic field models based on data from IMP and HEOS satellites, *Planet. Space Sci.*, *30*, 985, 1982.
- Vasyliunas, V. M., Mathematical models of magnetospheric convection and its coupling to the ionosphere, in *Particles and Fields in the Magnetosphere*, edited by B. M. McCormac, p. 60, D. Reidel, Hingham, Mass., 1970.

- Vasyliunas, V. M., Fundamentals of current description, in *Magnetospheric Currents*, Geophysical Monograph 28, edited by T. A. Potemra, p. 63, AGU, Washington, D. C., 1984.
- Voigt, G.-H., A mathematical magnetospheric field model with independent physical parameters, *Planet. Space Sci.*, 29, 1, 1981.
- Voigt, G.-H., Magnetospheric equilibrium configurations and slow adiabatic convection, in *Solar Wind - Magnetosphere Coupling*, edited by Y. Kamide and J. A. Slavin, p. 233, Terra Scientific Publishing Company, Tokyo, 1986.
- Voigt, G.-H. and R. A. Wolf., Quasi-static magnetospheric processes and the "ground state" of the magnetosphere, *Rev. Geophys.*, 26, 823, 1988.
- Walker, R. J., An evaluation of recent quantitative magnetospheric magnetic field models, *Rev. Geophys. Space Phys.*, 14, 411, 1976.
- Walker, R. J. and D. J. Southwood, Momentum balance and flux conservation in model magnetospheric magnetic fields, *J. Geophys. Res.*, 87, 7460, 1982.
- Williams, D. J. and G. D. Mead, Night side magnetosphere configuration as obtained from trapped electrons at 1100 kilometers, *J. Geophys. Res.*, 70, 3017, 1965.
- Williams, D. J., Dynamics of the Earth's ring current: theory and observation, *Space Sci. Rev.*, 42, 375, 1985.
- Wolf, R. A., S.-I. Akasofu, S. W. H. Cowley, R. L. McPherron, G. Rostoker, G. L. Siscoe and B. U. Ö. Sommerup, Coupling between the solar wind and the Earth's magnetosphere: Summary comments, in *Solar Wind-Magnetosphere Coupling*, ed. by Y. Kamide and J. A. Slavin, p. 769, Terra Scientific, Tokyo, 1986.
- Yasuhara, F., Y. Kamide and S.-I. Akasofu, Field-aligned and ionospheric currents, *Planet. Space Sci.*, 23, 1355, 1975.
- Zanetti, L. J., T. A. Potemra, T. Iijima and W. Baumjohann, Equatorial, Birke-land and ionospheric currents of the magnetospheric storm circuit, in *Magnetospheric Substorms*, edited by J. R. Kan, T. A. Potemra, S. Kokubun and T. Iijima, Geophysical Monograph 64, p. 111, AGU, Washington D.C., 1991.
- Zmuda, A. J. and J. C. Armstrong, The diurnal flow pattern of field-aligned currents, *J. Geophys. Res.*, 79, 4611, 1974.